

Structural Studies of the Aminoglycoside Modifying Enzyme  
APH(2'')-IVa and Its Inhibitors

Kun Shi

Department of Biochemistry

McGill University

Montreal, Quebec

May 2015

A thesis submitted to McGill University in partial fulfillment  
of the requirements of the degree of Doctor of Philosophy

© Copyright by Kun Shi, 2015

## Acknowledgements

No work of relevance can be completed by an individual without the help and support of many others, and this thesis is no different. Over the years I have incurred debts of gratitude to many friends and colleagues, who have all come together to create an experience that has enriched me beyond all expectations.

Let me begin by thanking my supervisor and mentor, Albert Berghuis. I am deeply grateful for your guidance, your trust, and your unwavering dedication to the academic spirit. Your leadership has been an inspiration and I thank you for helping me realize my passion for science, but also for steadfastly supporting me in the pursuit of myriad other activities. Finally, I thank you for involving me in such a fascinating area of research. The struggle against antibiotic resistance is a never-ending one. I feel humbled to have played a tiny part in it, for it is a struggle that none of us can afford to lose.

My sincere thanks to members of my research advisory committee, Bhushan Nagar, Tony Mittermeier, and Nicolas Moitessier, as well as Jason Young, who first introduced me to academic research. Many thanks also to the faculty, staff, and all of my friends from the Departments of Biochemistry and Chemistry for your enthusiasm and willingness to lend a hand. At the graduate level, much of the learning occurs through interaction with peers, and I am grateful to have been a part of an exceptional research group. In particular, I would like to thank Oliver Baettig, Jonathan Blanchet, David Burk, Shane Caldwell, Desiree Fong, Daniella Marks, Wayne Miller, Jaeok Park, Dmitry Rodionov, Pedro Romero, Barry Sleno, and Brahm Yachnin, all of whom have gone out of their way to help me in ways big and small. You are all my teachers. I would like to extend special thanks to Jonathan for helping me translating the abstract and Tara Sprules and Shuo Xing for assisting me with the NMR studies.

Over the course of my Ph.D. studies, I had the pleasure to collaborate with nine undergraduate students: Diana Czuchry, Amy Dijak-Smith, Ashley Lam, Stephen Li, Deborah Meltzer, Madhvi Nath, John Ozelik, Christopher Rouya, and Aidan Tomlinson. It has been a privilege to work with all of you, and nothing makes me happier to see that many of you have chosen to pursue graduate studies in biochemistry after your experience in the Berghuis lab.

My student life in the McGill community was much enriched by two major extracurricular initiatives, and I would like to extend my gratitude to my co-founders and all the

friends and colleagues who joined the McGill Chapter of American Association of Pharmaceutical Scientists, as well as the McGill Research Ethics Office Institutional Review Board for giving me a seat at the table.

I would also like to thank the Canadian Institutes of Health Research, the Department of Biochemistry, Faculty of Medicine, and McGill University for supporting my studies with numerous generous stipends and awards.

I leave the last words to the most important people in my life. To my parents: you have taught me the most valuable of lessons through your example, and you continue to be an inspiration for me every day. To my dear wife, Shuo: we became engaged and married during my Ph.D. studies, and you have filled my life with color and joy. Thank you for being a constant source of support in work as in life. My reservoir of appreciation and respect for your companionship is bottomless. This thesis is dedicated to you.

## Abstract

Antibiotic resistance is widely recognized as a risk to global public health. The misuse and overuse of antibiotics has promoted the emergence of multi-drug resistant bacterial strains that threaten to compromise the current repertoire of antibiotics. Among the most severely affected classes of antibiotics are the aminoglycosides. The most widely observed mechanism of resistance against aminoglycosides is inactivation through a series of detoxifying enzymes. Aminoglycoside phosphotransferases (APHs), also known as aminoglycoside kinases, are of special clinical concern due to their prevalence and broad substrate spectra.

The APHs are a large family of structurally related enzymes, all sharing a fold similar to eukaryotic protein kinases yet each having a specific set of substrate preferences. Mechanistic and structural studies have mainly focused on the ATP-specific APH(3') subfamily, with APH(3')-IIIa considered the de facto model enzyme of aminoglycoside kinases. However, it is becoming increasingly clear that APH(3')-IIIa is poorly representative of other APH subfamilies. In particular, the APH(2'') subfamily has distinguished itself with regards to nucleotide specificity as well as the scope and mode of binding of the aminoglycoside substrate. In order to overcome resistance conferred by these enzymes either by specific inhibitors or by next-generation aminoglycosides, a more comprehensive understanding of the structure and mechanism underlying these resistance factors is imperative.

This thesis focuses on the structural characterization of APH(2'')-IVa. A total of eight crystal structures of this enzyme in complex with various ligands form the foundation of our exploration of how this enzyme achieves its function. Through comparisons with crystal structures of related APH enzymes, we determined key principles that govern substrate selectivity for aminoglycoside kinases. Finally, using a fragment library screen with a combination of biophysical and functional techniques, we discovered a small molecule with early potential to become a novel competitive inhibitor specific for APH(2'') enzymes. Ultimately, the studies presented herein contribute to the ongoing efforts of combatting antibiotic resistance through structure-guided drug design.

## Abrégé

La résistance aux antibiotiques est grandement reconnue comme étant un risque pour la santé publique mondiale. L'utilisation abusive et excessive d'antibiotiques a favorisé l'émergence de souches bactériennes multirésistantes qui menacent de compromettre le répertoire actuel des antibiotiques. Les aminoglycosides sont l'une des classes d'antibiotiques les plus touchées par cette résistance. Le mécanisme de résistance aux aminoglycosides le plus abondamment observé est leur inactivation par une série d'enzymes de détoxification. Parmi ces enzymes, les aminoglycoside phosphotransférases (APHs), aussi connues comme sous le nom d'aminoglycoside kinases, sont une préoccupation clinique particulière en raison de leur prévalence et leur spectre de substrats étendu.

Les APHs font parti d'une grande famille d'enzymes liées structurellement. Elles partagent un repli similaire à des kinases eucaryotes, mais elles ont chacune des préférences spécifiques pour certains substrats. Les études mécanistiques et structurelles faites sur cette famille ont principalement porté sur une sous-famille spécifique à l'utilisation de l'ATP, les APH(3'), dont l'enzyme APH(3')-IIIa est considérée *de facto* comme le modèle principal de kinase des aminoglycosides. Cependant, il devient de plus en plus clair que APH(3')-IIIa n'est pas représentative des autres sous-familles d'APH. En particulier, la sous-famille des APH(2'') se distingue par sa spécificité aux nucléotides ainsi que par sa portée et son mode de liaison des substrats aminoglycosides. Afin de vaincre la résistance conférée par ces enzymes, soit par des inhibiteurs spécifiques ou par des aminoglycosides de nouvelle génération, il est impératif d'avoir une compréhension plus globale de la structure et du mécanisme qui sous-tend ces facteurs de résistance.

Cette thèse porte sur la caractérisation structurale de l'APH(2'')-IV. Un total de huit structures cristallines de cette enzyme, en complexe avec divers ligands, constituent le fondement de notre exploration sur la façon dont cette enzyme réalise sa fonction. Grâce aux comparaisons avec des structures cristallines connexes d'autres APHs, nous avons également déterminé les principes clés qui régissent la sélectivité de substrat pour d'autres aminoglycoside kinases. Enfin, en faisant le criblage d'une pharmacothèque de fragments en combinaison avec des techniques biophysiques et fonctionnelles, nous avons découvert une petite molécule qui pourrait avoir le potentiel de devenir un nouvel inhibiteur compétitif spécifique aux enzymes

APH(2"). Tout compte fait, les études présentées ici contribuent aux efforts en cours dans la lutte contre la résistance aux antibiotiques par la conception de médicaments basée sur la structure enzymatique.

# Table of Contents

Acknowledgements

Abstract

Abrégé

List of Tables

List of Figures

List of Abbreviations

Chapter 1 | Introduction

1.1 Antibiotic Therapeutics and Bacterial Resistance

1.1.1 The Rise of Antibiotics

1.1.2 The Threat of Antibiotic Resistance

1.1.3 Fighting Back Against Antibiotic Resistance

1.2 Aminoglycoside Antibiotics

1.2.1 Historical Overview of Aminoglycosides

1.2.2 Chemical Properties of Aminoglycosides

1.2.3 Biological Activity of Aminoglycosides

1.2.4 Clinical Applications of Aminoglycosides

1.2.5 Resistance to Aminoglycosides

1.2.6 Aminoglycoside Modifying Enzymes

1.2.7 Crystal Structures of APHs

1.3 Aminoglycoside 2''-*O*-Phosphotransferase IVa

1.3.1 Origin and Occurrence

1.3.2 Substrate Spectrum

1.3.3 Kinetic Mechanism

1.4 Thesis Objectives

## Chapter 2 | Structural Basis for Aminoglycoside Preferences of APH(2'')-IVa

### 2.1 Preface

### 2.2 Introduction

### 2.3 Materials and Methods

#### 2.3.1 Cloning, Protein Expression, and Purification

#### 2.3.2 Crystallization and Data Collection

#### 2.3.3 Structure Determination and Refinement

### 2.4 Results

#### 2.4.1 Apo Structure

#### 2.4.2 Binary Structures

#### 2.4.3 Comparison Between Apo and Binary Structures of APH(2'')-IVa

### 2.5 Discussion

#### 2.5.1 Aminoglycoside Preference of APH(2'')-IVa

#### 2.5.2 Comparison with Substrate-bound Structures of Other APHs

#### 2.5.3 Comparison of Aminoglycoside-binding Mode between APH(2'')-IVa and the Ribosome

## Chapter 3 | Nucleotide Preference of APH(2'')-IVa

### 3.1 Preface

### 3.2 Introduction

### 3.3 Materials and Methods

#### 3.3.1 Site-directed Mutagenesis

#### 3.3.2 Crystallization and Data Collection

#### 3.3.3 Structure Determination and Refinement

#### 3.3.4 Kinetic Assay

### 3.4 Results

#### 3.4.1 Overall Structural Characteristics

#### 3.4.2 Nucleoside Binding

#### 3.4.3 Structure-Function Studies

### 3.5 Discussion

#### 3.5.1 Structural Determinants of Nucleotide Specificity

#### 3.5.2 Comparison with CK2

#### 3.5.3 Implications for Inhibitor Design



## Chapter 4 | Towards the Development of an Inhibitor Against Aminoglycoside 2''-Phosphotransferases

### 4.1. Preface

### 4.2 Introduction

### 4.3 Materials and Methods

#### 4.3.1 Small Molecule Fragment Library Preparation

#### 4.3.2 Fragment Screening and Data Collection

#### 4.3.3 Structure Determination and Refinement

#### 4.3.4 NMR-STD Spectroscopy

#### 4.3.5 Inhibition Assay

### 4.4 Results

#### 4.4.1 Fragment Screening with X-ray Crystallography and Structure Determination

#### 4.4.2 Fragment Screening with NMR-STD Spectroscopy

#### 4.4.3 Inhibition Kinetic Studies

### 4.5 Discussion

#### 4.5.1 Strategies and Challenges in Inhibitor Discovery for APH(2'')

#### Enzymes

#### 4.5.2 Key Elements of Inhibitor Binding

#### 4.5.3 Potential Directions for Hit-to-Lead Development

## Chapter 5 | Conclusions

## References

## Appendix

## List of Tables

### Chapter 1

- 1 – 1 Common Aminoglycoside Antibiotics
- 1 – 2 Clinical Indications of Aminoglycosides
- 1 – 3 Crystal Structures and Substrate Profiles of Aminoglycoside *O*-phosphotransferases
- 1 – 4 Primary Sequence Comparison Among APH(2'') Enzymes
- 1 – 5 Substrate Spectrum of APH(2'') Enzymes

### Chapter 2

- 2 – 1 Data Collection and Refinement Statistics of Apo and Aminoglycoside-Bound APH(2'')-IVa

### Chapter 3

- 3 – 1 Data Collection and Refinement Statistics of Nucleoside-Bound Wild Type and Mutant APH(2'')-IVa
- 3 – 2 Steady State Kinetic Parameters for APH(2'')-IVa

### Chapter 4

- 4 – 1 Data Collection and Refinement Statistics of Ligand-Bound APH(2'')-IVa
- 4 – 2 Key Parameters of Halogen Bonds in Protein-Ligand Complexes

## List of Figures

### Chapter 1

- 1 – 1 One Hundred Years of Antibiotics
- 1 – 2 Resistance Mechanisms of Commonly Used Antibiotics
- 1 – 3 Chemical Structures of Common Aminoglycosides
- 1 – 4 Overall Crystal Structure of APHs
- 1 – 5 Putative Reaction Scheme of APH(2'')-IVa

### Chapter 2

- 2 – 1 Crystal Structures of APH(2'')-IVa
- 2 – 2 Aminoglycoside Binding Site
- 2 – 3 Tobramycin versus Kanamycin A Binding
- 2 – 4 Apo versus Aminoglycoside-Bound Structures of APH(2'')-IVa
- 2 – 5 Aminoglycoside Binding Site Comparison with APH(2'')-IIa
- 2 – 6 Aminoglycoside Binding Site Comparison with the ribosomal A-site

### Chapter 3

- 3 – 1 Key Components of Nucleoside Binding Site
- 3 – 2 Nucleoside Binding for APH(2'')-IVa
- 3 – 3 Adenosine versus Guanosine Binding
- 3 – 4 Nucleoside-Bound Structures of Mutant APH(2'')-IVa
- 3 – 5 Partial Multiple Sequence Alignment of Selected APH Enzymes and CK2
- 3 – 6 Structural Basis for ATP-Selectivity of APH(3')-IIIa
- 3 – 7 Structural Comparison Between Nucleoside-Bound Complexes of APH(2'')-IVa and CK2

### Chapter 4

- 4 – 1 Crystal Structure of APH(2'')-IVa with a Bound Fragment Molecule
- 4 – 2 Sample NMR Saturation Transfer Difference (STD) Spectra
- 4 – 3 Hits from the NMR STD Screen
- 4 – 4 Key Interactions Between APH(2'')-IVa and ABP

4 – 5 Next Step in Hit-to-Lead Development

4 – 6 Growth Potential for ABP

## **Chapter 5**

5 – 1 Active Site Architecture of APH Enzymes

5 – 2 Structure-Based Multiple Sequence Alignment of Seven APH Enzymes and the Putative APH Enzyme Rv1368

## List of Abbreviations

<b>AAC</b>	Aminoglycoside acetyltransferase
<b><i>A. baumannii</i></b>	<i>Acinetobacter baumannii</i>
<b>ABP</b>	4-Amino-3-bromopyridine
<b>ADP</b>	Adenosine diphosphate
<b>AME</b>	Aminoglycoside modifying enzyme
<b>AMPPNP</b>	Adenylyl imidodiphosphate
<b>ANT</b>	Aminoglycoside nucleotidyltransferase
<b>APH</b>	Aminoglycoside phosphotransferase
<b>A-site</b>	Aminoacyl site
<b>ATP</b>	Adenosine triphosphate
<b>B-factor</b>	Crystallographic temperature factor
<b>CCD</b>	Charge-coupled device
<b>CK2</b>	Casein kinase 2
<b>DMSO</b>	Dimethyl sulfoxide
<b>DNA</b>	Deoxyribonucleic acid
<b><i>E. coli</i></b>	<i>Escherichia coli</i>
<b>EDTA</b>	Ethylenediamine tetraacetic acid
<b>ePK</b>	Eukaryotic protein kinase
<b>F<sub>C</sub></b>	Calculated structure factor
<b>F<sub>O</sub></b>	Observed structure factor
<b>GDP</b>	Guanosine diphosphate
<b>GMPPNP</b>	Guanylyl imidodiphosphate
<b>GTP</b>	Guanosine triphosphate
<b>HEPES</b>	4-(2-hydroxyethyl)-1-piperazineethanesulfonic acid
<b>IPTG</b>	Isopropyl $\beta$ -D-thiogalactopyranoside
<b>k<sub>cat</sub></b>	Rate of catalysis
<b>K<sub>M</sub></b>	Michaelis-Menten constant
<b><i>K. pneumoniae</i></b>	<i>Klebsiella pneumoniae</i>
<b>LB</b>	Luria-Bertani broth

<b><i>M. tuberculosis</i></b>	<i>Mycobacterium tuberculosis</i>
<b>NADH</b>	Nicotinamide adenine dinucleotide
<b>NEO</b>	Neomycin
<b>NMR</b>	Nuclear magnetic resonance
<b>NTP</b>	Nucleotide triphosphate
<b>OD</b>	Optical density
<b><i>P. aeruginosa</i></b>	<i>Pseudomonas aeruginosa</i>
<b>PCR</b>	Polymerase chain reaction
<b>PDB</b>	Protein Data Bank
<b>PEG</b>	Polyethylene glycol
<b>pET</b>	Peptide expression system
<b><math>R_{\text{cryst}}</math></b>	Reliability factor
<b><math>R_{\text{free}}</math></b>	Free reliability factor
<b>RMSD</b>	Root mean square deviation
<b>RNA</b>	Ribonucleic acid
<b>rRNA</b>	Ribosomal ribonucleic acid
<b><i>S. aureus</i></b>	<i>Staphylococcus aureus</i>
<b>SDS-PAGE</b>	Sodium dodecyl sulfate polyacrylamide gel electrophoresis
<b>STD</b>	Saturation transfer difference
<b>tRNA</b>	Transfer ribonucleic acid
<b>Tris-HCl</b>	2-Amino-2-(hydroxymethyl)1,3-propanediol hydrochloride

## Chapter One

### Introduction

#### **1.1 Antibiotic Therapeutics and Bacterial Resistance**

##### **1.1.1 The Rise of Antibiotics**

The explosive growth of the world's population, from 1.7 billion roughly 100 years ago to over 7.1 billion today, can be partially ascribed to key advances in modern medicine, among them the increasingly widespread use of antibiotics. Although many antimicrobial compounds are as old as bacteria themselves, their clinical potential was only unlocked in the early 1940s, when penicillin was first introduced for general treatment of bacterial infections (Chain et al. 1940; Wainright and Swan 1986). Not only were antibiotics effective against diseases of bacterial origin, but they have also proven instrumental in a variety of other clinical contexts, such as organ transplants, surgeries, and cancer therapy (de Bruin et al. 2012; Rolston 2009). In the ensuing three decades, intensive efforts by the pharmaceutical industry led to the discovery of a plethora of different antibiotic classes, fueling the hope that once fearsome diseases such as syphilis and tuberculosis were conquered forever. The so-called "golden era" of antibiotics is now remembered with nostalgia, as no new classes of antibiotics have been discovered since the 1970s. With the decline of success rates from the traditional means of screening soil samples, the predominant approach in developing new antibiotics has been the chemical modification of existing variants (Chopra 2002, see reference in Aminov 2010). The gradual disengagement of major pharmaceutical companies from this area of research due to economic and regulatory challenges exacerbated the diminished output of new antibiotics, currently averaging one to two per year (Butler et al. 2013). The reach of antibiotics has far exceeded curing or preventing human diseases. In the US, only approximately 20% of antibiotics produced are for human use, with the remaining 80% destined for applications in animal husbandry, agriculture, and aquaculture (Hollis and Ahmed 2013; Davies 2006).

##### **1.1.2 The Threat of Antibiotic Resistance**

Alexander Fleming's serendipitous discovery of penicillin in 1928 marks a cornerstone in the annals of antimicrobial research. Yet Fleming's insight far exceeded the clinical potential of his observations, as he was also among the first who cautioned about bacterial resistance to

penicillin if the drug was used in insufficient quantities or in too short treatment periods (Aminov 2010). Clinical resistance to antibiotics routinely emerges within a few years of the introduction of a new antibiotic, and resistant bacterial strains exist for every class of antibiotics in use today (Figure 1-1). In addition to improper consumption in therapeutic settings, the promiscuous distribution of antibiotics for non-therapeutic uses on livestock and agriculture further promotes the proliferation of drug-resistant variants. Animals repeatedly treated with antibiotics in the absence of disease form an important reservoir and are a source of potentially pathogenic organisms for humans (Donabedian et al. 2003; Allen 2014; Durso and Cook 2014). The global threat of antibiotic resistance is reflected by increasingly frequent reports and discussions in both the scientific literature as well as the popular press (Grady 2013; McKay and Bauerlein 2014), with some even warning of a regression to the pre-antibiotic era (Bell 2003). The World Health Organization named antibiotic resistance the theme for World Health Day in 2011, and the World Economic Forum recently highlighted antibiotic resistance among the top global risks (WEF 2013).

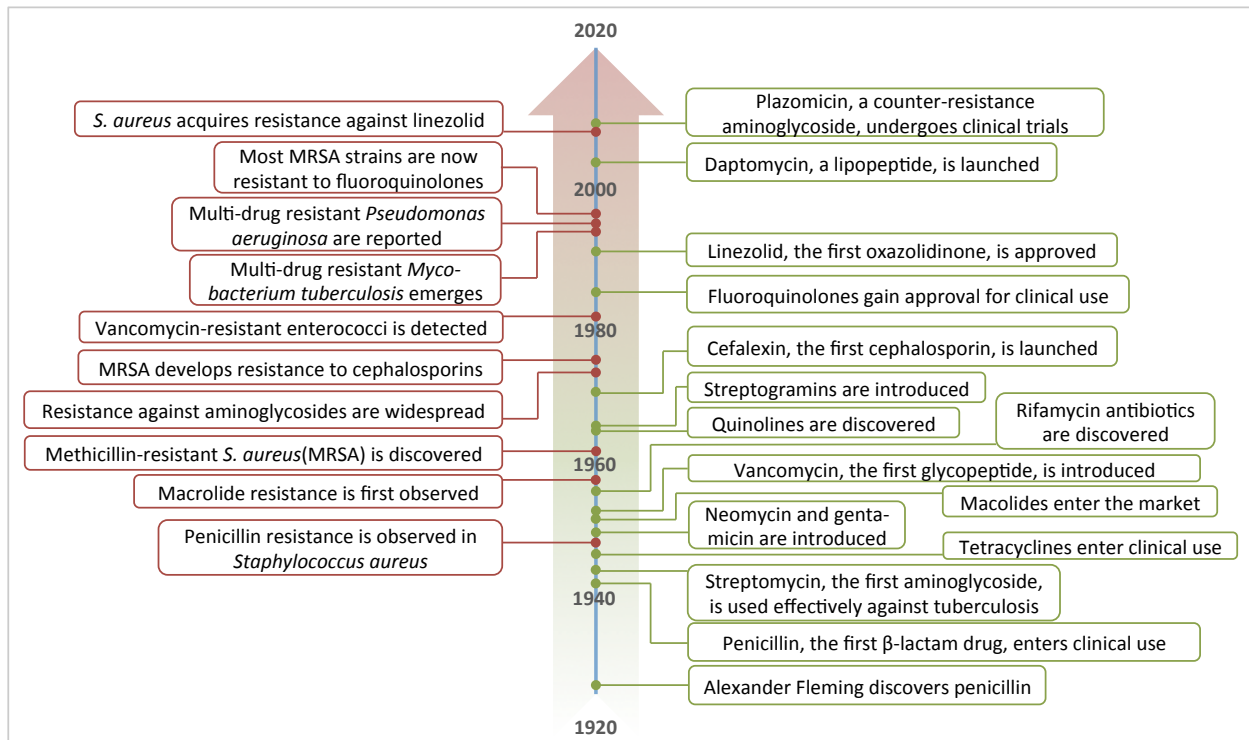


**Figure 1 – 1 | One Hundred Years of Antibiotics**

The timeline shows major milestones in antibiotic discovery (green) and landmarks in the emergence of bacterial resistance (red) from the discovery of penicillin to the present day. The so-called Golden Age of antibiotics is shaded green on the timeline. (Figure adapted from Hopwood et al. 2007.)



### 1.1.3 Fighting Back Against Antibiotic Resistance

The traditional clinical response to antibiotic resistance has been the adoption of new antibiotics that are not susceptible to resistant strains. However, with the decline of the antibiotic pipeline, it has become increasingly apparent that such evasive strategies are not sustainable. It is now clear that to effectively combat antibiotic resistance, we must first acquire a thorough understanding of the cellular and molecular mechanisms that confer resistance, and then apply that knowledge in the design of countermeasures.

Bacteria have responded to antibiotics through a multitude of evolved or acquired adaptations. Common mechanisms of antibiotic resistance are summarized in Figure 1-2 and fall under three broad categories: physically preventing the drug from reaching its target, chemically changing the drug, and altering the target itself (Walsh 2000; Davies and Davies 2010).

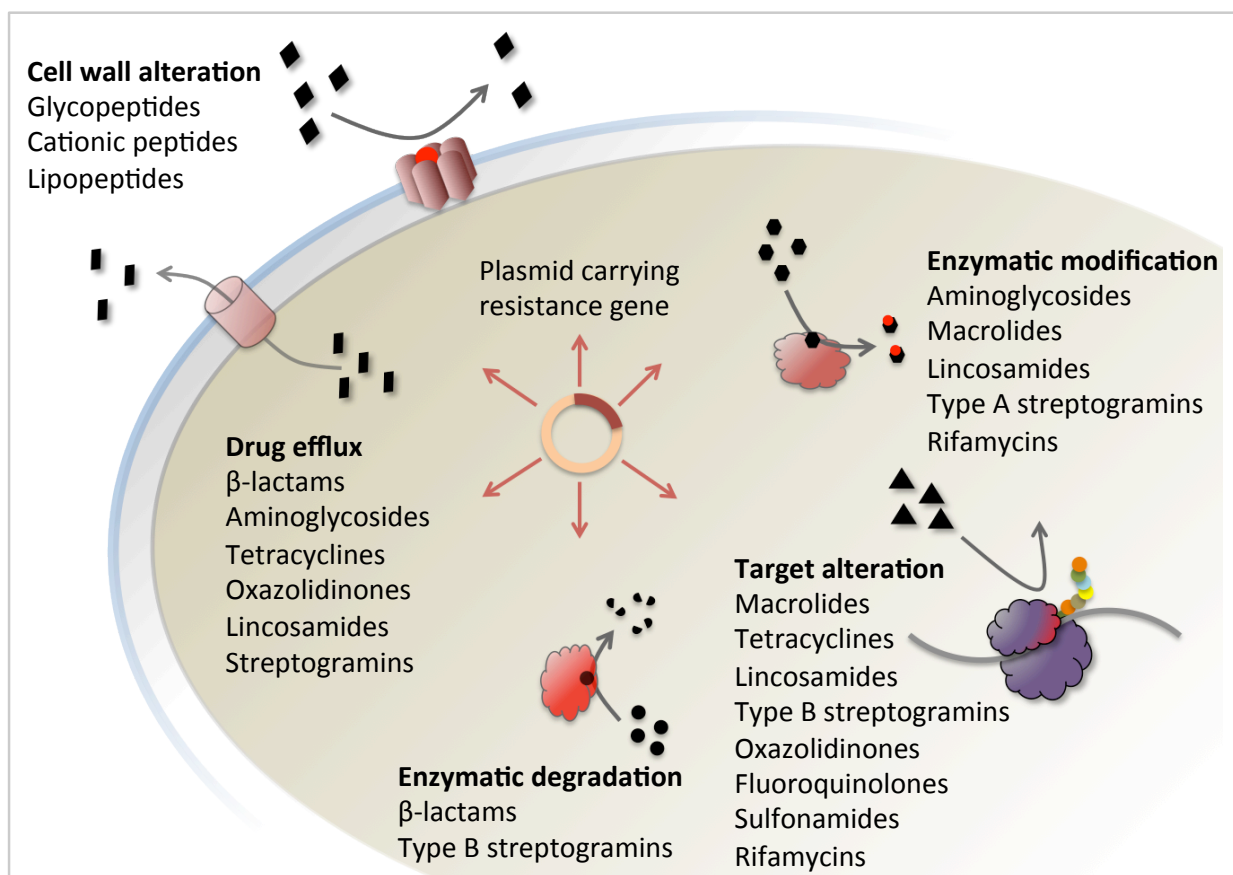


**Figure 1 – 2 | Resistance Mechanisms of Commonly Used Antibiotics**

Five common mechanisms of antibiotic resistance are illustrated. The antibiotic is denoted in black, and the various resistance mechanisms are shown in red.

## 1.2 Aminoglycoside Antibiotics

### 1.2.1 Historical Overview of Aminoglycosides

Clinical use of aminoglycosides dates back to the infancy of antibiotics, when the introduction of streptomycin in 1944 was hailed as the “silver bullet” against tuberculosis (Schatz et al. 1944; Iseman 1994). Even today, despite severe complications due to resistance, streptomycin and its derivatives remain a mainstay in chemotherapy against this disease (Böttger and Springer 2008). Similar to other types of antibiotics, naturally occurring aminoglycosides are bacterial metabolites with the ability to kill other bacteria, evolved from the incessant struggle to gain a competitive advantage in an environment of scarce resources. Early aminoglycosides were thus discovered through the systematic screening of soil actinomycetes. Subsequently, in a response to growing prevalence of resistance against aminoglycosides, new additions in this class of antibiotics have comprised of semisynthetic variants such as amikacin or dibekacin, which typically incorporate functional groups that prevent recognition by resistance factors (see Table 1-2). However, the pace of developing newer generations of aminoglycosides has markedly slowed since the mid-seventies, and most clinically relevant aminoglycosides today have been in use for several decades, allowing resistant strains to continually diminish their applicability. Plazomicin, formerly ACHN-490, is the only so-called neoglycoside currently undergoing clinical trials (Aggen et al. 2010). It displays activity against methicillin-resistant *S. aureus* and multi-drug resistant *E. coli*, *K. pneumonia* and *Enterobacter* spp. and has shown excellent promise in the treatment of urinary tract infections and pyelonephritis (Tenover et al. 2011; Galani et al. 2012).

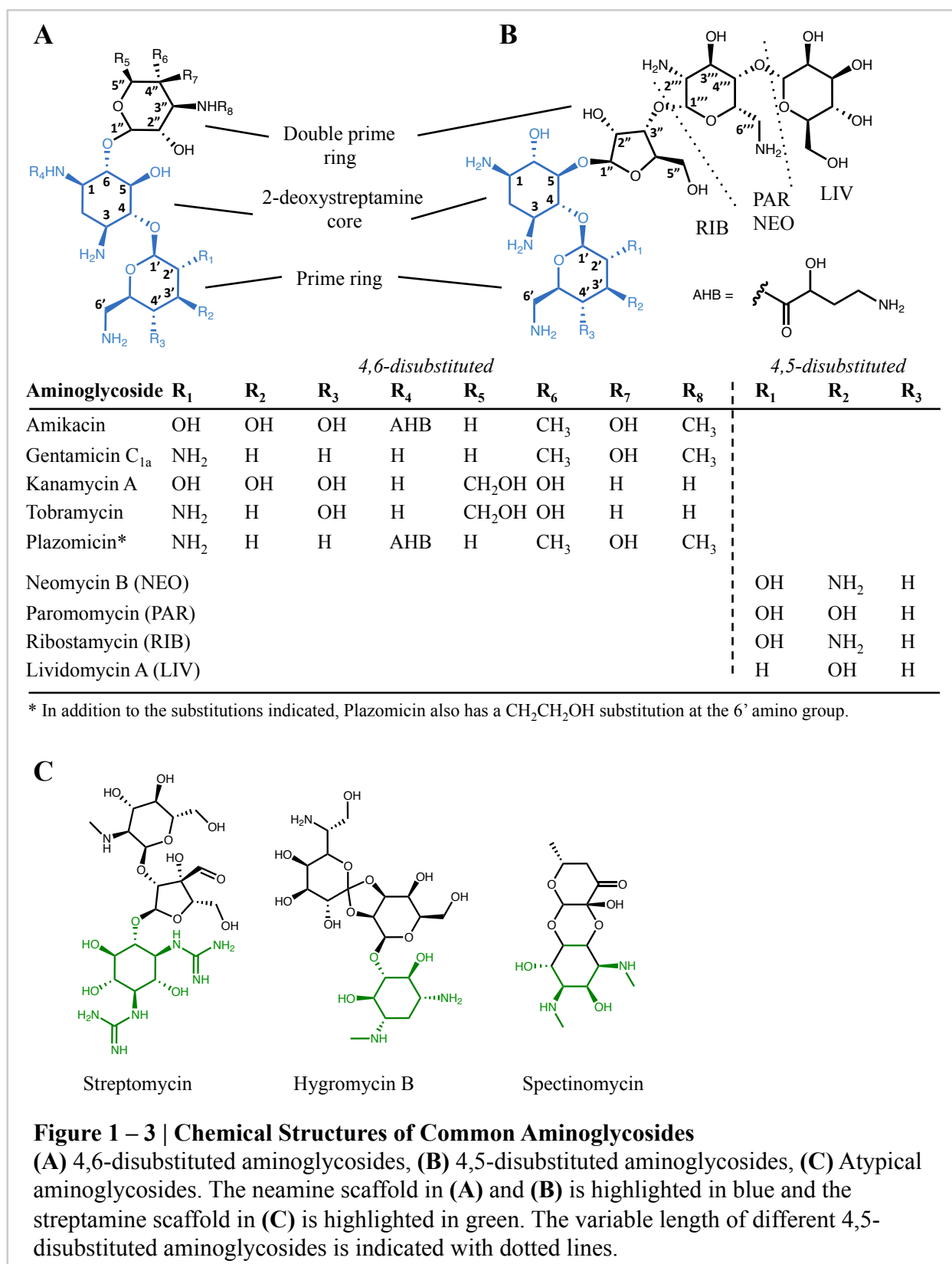
**Table 1 – 1 | Common Aminoglycoside Antibiotics**

<b>Aminoglycoside</b>	<b>Origin</b>	<b>Year discovered</b>	<b>Literature reference</b>
<i>4,6-disubstituted</i>			
Amikacin	Semi-synthetic, derived from kanamycin A	1974	Kawaguchi et al. 1976
Arbekacin	Semi-synthetic, derived from dibekacin	1973	Tanaka et al. 1983
Dibekacin	Semi-synthetic, derived from kanamycin B	1974	Noone 1984
Gentamicin	<i>Micromonospora</i>	1963	Weinstein et al. 1963

Isepamicin	<i>purpurea</i> Semi-synthetic, derived from gentamicin B	1980	Thornsberry et al. 1980
Kanamycin	<i>Streptomyces kanamyceticus</i>	1957	Umezawa 1958
Neomycin	<i>Streptomyces griseus</i>	1949	Waksman and Lechevalier 1949
Netilmicin	Semi-synthetic, derived from sisomicin	1976	Noone 1984
Plazomicin	Semi-synthetic	2009	Endimiani et al 2009
Sagamicin	<i>Micromonospora sagamiensis</i>	1974	Okachi et al 1974
Sisomicin	<i>Micromonospora inyoensis</i>	1971	Noone 1984
Tobramycin	<i>Streptomyces tenebrarius</i>	1971	Dienstag and Neu 1972
Verdamycin	<i>Micromonospora grisea</i>	1975	Weinstein et al 1975
<hr/>			
<b><i>4,5-disubstituted</i></b>			
Butirosin	<i>Bacillus circulans</i>	1972	Howells et al. 1972
Lividomycin	<i>Streptomyces lividus</i>	1971	Oda et al. 1971
Paromomycin	<i>Streptomyces krestomuceticus</i>	1956	Davidson et al. 2009
Ribostamycin	<i>Streptomyces ribosidificus</i>	1970	Omoto et al. 1973
<hr/>			
<b><i>Atypical</i></b>			
Apramycin	<i>Streptomyces tenebrarius</i>	1976	O'Connor et al. 1976
Hygromycin	<i>Streptomyces hygroscopicus</i>	1953	Pettinger et al. 1953
Kasugamycin	<i>Streptomyces kasugaensis</i>	1965	Schuwirth et al. 2006
Spectinomycin	<i>Streptomyces spectabilis</i>	1961	Davies et al 1965
Streptomycin	<i>Streptomyces griseus</i>	1943	Schatz et al 1944

### 1.2.2 Chemical Properties of Aminoglycosides

Aminoglycosides typically contain a core 2-deoxystreptamine that is extended by a variable number of five- or six-membered sugars via glycosidic linkages (Figure 1-3). Because of the conserved central aminocyclitol ring, this class of antibiotics is formally named the aminoglycoside-aminocyclitols (Davis 1980).



A prominent feature of aminoglycosides is the presence of multiple amino groups, which, in addition to a large number of hydroxyl groups on the sugar rings, confer a hydrophilic and basic chemical profile. Neamine, the smallest aminoglycoside, has a single amino hexose ring (also called the prime ring or ring A) linked to position four of the 2-deoxystreptamine core (also called the central ring or ring B). Though not clinically useful owing to its poor antibiotic activity, neamine nevertheless represents a minimal structural motif for specific ribosome binding at the aminoacyl-tRNA site and thus has served as a starting point for the synthesis of derivatives with higher specificity and potency (Fourmy et al. 1998; Xu et al. 2009).

The neamine scaffold is also common to the majority of naturally occurring aminoglycosides, which can be divided into three broad categories based on their substitution patterns:

- *4,6-disubstituted aminoglycosides* have one or more sugar rings linked to position six of the central ring, conventionally termed the double-prime rings or rings C, D, etc. Many therapeutically relevant aminoglycosides have this basic structure, and representative members of this group include gentamicin, tobramycin, kanamycin, as well as the semisynthetic variants amikacin and plazomicin.
- *4,5-disubstituted aminoglycosides* feature a variable number of pentose or hexose rings extending from position 5 of the central ring instead, and consequently adopt a less elongated and bulkier three-dimensional structure. Some of the earliest aminoglycosides isolated, neomycin and paromomycin, are members of this group.
- A third group of so-called *atypical aminoglycosides* comprises a small number of structurally diverse aminocyclitols that share a streptamine scaffold instead of a neamine scaffold. Streptomycin is the best-known example of this category. Several aminoglycosides prominent in veterinary medicine, such as apramycin and hygromycin, also belong to this group (Ryden and Moore 1977).

### 1.2.3 Biological Activity of Aminoglycosides

The hydrophilic character of aminoglycosides prevents this class of antibiotics from readily diffusing across membranes. The method by which aminoglycosides penetrate into the bacterial cytoplasm is poorly understood, and is further complicated by the possibility that uptake mechanisms diverge for different aminoglycosides. In the most widely accepted model,

aminoglycoside uptake follows a three-stage process (Taber et al. 1987). In the first step, the drug is bound to anionic lipopolysaccharides and proteins of the outer bacterial membrane through electrostatic interactions. This non-specific binding event is followed by a rate-limiting, energy-dependent step in which the antibiotic crosses the membrane, using energy from electron transport and ATP hydrolysis (Davis 1987; Bryan and Van Den Elzen 1976 and 1977). The detailed mechanism of this step remains elusive. In the last phase, aminoglycoside accumulation is autocatalytic as the first molecules begin to compromise protein translation and render the cytoplasmic membrane increasingly porous (Davis et al. 1986).

In contrast to aminoglycoside uptake, the mode of action of these antibiotics is much better understood, owing in part to the elucidation of several high-resolution crystal structures of different aminoglycosides in complex with their target. Studies on the mode of action of aminoglycosides fundamentally contributed to our understanding of protein synthesis and translation fidelity. Indeed, early studies with aminoglycosides provided the first demonstrations that the ribosome played a vital role in reading the genetic code for the determination of the protein sequence (Davies et al. 1964). Binding of a cognate tRNA normally induces conformational changes within the A-site of the 30S ribosomal subunit that enable a precise fit of the specific tRNA (Yoshizawa et al. 1999). This conformation of the A-site is also known as the decoding or “on” state (Schilling-Bartetzko et al. 1992). High resolution crystal structures of bacterial ribosomes in complex with different aminoglycosides have shown that these drugs interact with the A-site such that it is stabilized in the decoding state, which readily allows the binding of non-cognate tRNAs and thus the production of aberrant proteins (Ogle et al. 2001). The accumulation of such non-native proteins impairs both cellular functions as well as the structural integrity of the cell wall and ultimately results in the death of the bacterium. A notable exception to this mechanism is streptomycin, which binds to a different position at the 16S rRNA and interferes with initial tRNA selection (Carter et al. 2000). In addition, some aminoglycosides are also known to interfere with ribosome recycling by binding an alternative site in the 50S ribosomal subunit (Borovinskaya et al. 2007). Consequently, the crucial ribosome recycling factor is unable to interact with the 70S ribosome and separate it into its component subunits for a subsequent cycle of translation, thus protein synthesis is further compromised.

### 1.2.4 Clinical Applications of Aminoglycosides

Aminoglycosides are traditionally prescribed against a wide range of bacterial infections caused by Gram-negative and some Gram-positive organisms. Beside for use in humans, aminoglycoside antibiotics are also routinely used in veterinary medicine (Regula 2009). The highly polar character of aminoglycosides prevents them from effective adsorption. Thus, the methods of administration of choice are either topical or parenteral. Aminoglycosides are prescribed with caution due to potentially severe chronic side effects. Renal injury is observed in 10%-20% of therapeutic courses, where incomplete glomerular filtration leads to reabsorption by the proximal tube (Swan 1997). In addition, vestibular and cochlear toxicity can occur from damage to the sensory hair cells of these organs (Avent et al. 2011). The dual pressures of toxicity and antibiotic resistance have rendered a number of widely used aminoglycosides obsolete, such as kanamycin A and neomycin. Gentamicin, tobramycin, netilmycin and amikacin are some of the few aminoglycosides currently still in active clinical use (Table 1-3). In order to minimize the exposure to the development of bacterial resistance, the prescription of semi-synthetic aminoglycosides resistant against bacterial inactivation is tightly regulated and only considered when first-line drugs fall short of controlling the infection. Despite the threat of resistance, kanamycin A, along with gentamicin, amikacin, paromomycin, and spectinomycin, are included in the World Health Organization’s Model List of Essential Medicines, a collection of medication deemed most important in a basic health system (WHO 2013).

**Table 1 – 2 | Clinical Indications of Aminoglycosides**

<b>Aminoglycoside</b>	<b>Target Organisms</b>	<b>Current Clinical Indications</b>
Amikacin	<i>Pseudomonas spp.</i> , <i>E. coli</i> , <i>Klebsiella-Enterobacter- Serratia spp.</i> <i>Acinetobacter spp.</i>	Bacterial septicemia, respiratory tract infections, meningitis, postoperative infections, urinary tract infections
Arbekacin	<i>S. aureus</i>	MRSA infections
Gentamicin	<i>P. aeruginosa</i> , <i>Proteus spp.</i> , <i>E. coli</i> , <i>Klebsiella-Enterobacter- Serratia spp.</i> , <i>Citrobacter spp.</i> , <i>S. aureus</i>	Initial therapy for serious infections caused by the target organisms listed
Kanamycin	<i>M. tuberculosis</i>	Multi-drug resistant tuberculosis
Neomycin	<i>E. coli</i> , <i>Enterobacter spp.</i> ,	Superficial eye infections and infections

	<i>Proteus spp.</i>	in skin lesions, hepatic encephalopathy
Netilmicin	<i>Pseudomonas spp., E. coli, Klebsiella-Enterobacter-Serratia spp., Acinetobacter spp.</i>	Bacteremia, septicemia, respiratory tract infections, postoperative infections
Paromomycin	<i>Leishmania spp., Entamoeba histolytica</i>	Intestinal amebiasis, cutaneous leishmaniasis
Spectinomycin	<i>Neisseria gonorrhoeae</i>	Gonorrhea
Streptomycin	<i>Mycobacterium tuberculosis, S. aureus, E. faecium, E. faecalis, Yersinia pestis</i>	Tuberculosis, enterococcal endocarditis, plague
Tobramycin	<i>P. aeruginosa, E. coli, Klebsiella-Enterobacter-Serratia spp., S. aureus</i>	Bacterial septicemia, respiratory tract infections, meningitis, urinary tract infections, cystic fibrosis, ophthalmic infections

### 1.2.5 Resistance to Aminoglycosides

Similar to many other antibiotics, aminoglycosides were only in use for a short number of years before the first resistant bacterial strains began to emerge (Lebek 1963; Umezawa et al. 1967). Patients with compromised immune systems are especially vulnerable to bacterial infections, and widespread resistance has been observed in the group of pathogens nicknamed ESKAPE (*Enterococcus faecium, Staphylococcus aureus, Klebsiella pneumonia, Acinetobacter baumannii, Pseudomonas aeruginosa* and *Enterobacter* species), which is responsible for the majority of nosocomial infections in hospitals worldwide (Rice 2008). A variety of resistance mechanisms has been characterized through studying these organisms. Specifically, resistance mechanisms that affect aminoglycosides include:

- Reduced uptake of the aminoglycoside: Mutations that reduce the net negative charge of the outer membrane lipopolysaccharides in *P. aeruginosa* have been linked to reduced aminoglycoside efficacy, presumably due to diminished electrostatic interactions in the first step of uptake (Macfarlane et al. 2000). Further, congruent with the energy-dependent model of aminoglycoside transport across the membrane described above, nitric oxide-mediated impairment of the electron transport chain have also led to impermeability resistance in *S. aureus* and *P. aeruginosa* (McCollister et al. 2011).



- Multidrug efflux pumps: Efflux proteins belonging to the resistance nodulation division family or the multidrug and toxic compound extrusion family have been found to play a role in aminoglycoside resistance in a variety of Gram-negative bacteria, such as *A. baumannii* and *Enterobacter* spp., though this resistance mechanism is less prevalent and of comparatively low clinical concern (Poole 2001; Su et al. 2005).
- Target mutation: Shortly after streptomycin was adopted as a treatment for tuberculosis, resistant isolates were discovered that had mutations in the 16S rRNA and the ribosomal protein S12 (Springer et al. 2001). Similarly, high-level resistance against a broad range of 4,5- and 4,6-disubstituted aminoglycosides has been observed featuring a single base mutation of A1408 in the 16S rRNA, which is responsible for a key interaction in aminoglycoside binding (De Stasio et al. 1989).
- Ribosomal methyltransferases: Enzymatic modification of the ribosomal target can be found in aminoglycoside-producing actinomycetes, where methylation of either G1405 or A1408 in the 16S rRNA A-site renders them immune against the toxicity of their own metabolites (Doi and Arakawa 2007). While traditionally believed to be confined to actinomycetes, resistance methyltransferases have recently been found in numerous ESKAPE species and poses a rising threat due to their rapid worldwide dissemination and their ability to confer nearly complete resistance against all aminoglycosides currently in clinical use (Wachino and Arakawa 2012).
- Aminoglycoside modifying enzymes (AMEs): Notwithstanding the multitude of resistance mechanisms outlined above, the vast majority of clinical resistance against aminoglycoside antibiotics is due to the enzymatic inactivation of the drugs themselves. The abundance and ease of horizontal transfer of AMEs has been the leading driver of obsolescence for one aminoglycoside after another (Davies and Wright 1997; Ramirez and Tolmasky 2010). Given their prominence, it is no exaggeration to suppose that the threat of aminoglycoside resistance cannot be overcome without a thorough understanding of this group of enzymes.

### 1.2.6 Aminoglycoside Modifying Enzymes

There is no consensus regarding the origin of aminoglycoside modifying enzymes, but it has been suggested that some enzymes normally involved in cellular metabolism could be repurposed to confer resistance upon selective pressure from aminoglycosides (Franklin and

Clarke 2001). While some AMEs are known to be chromosomally encoded, most AMEs are found on plasmids, which permits the rapid horizontal transfer among bacteria (Costa et al. 1993; Magnet et al. 2001). Thus, it is common that pathogens exhibiting aminoglycoside resistance harbor not one but multiple AME-encoding genes.

AMEs are classified by their activity, and currently well over one hundred enzymes are known, with more additions discovered at an alarming rate (Ramirez and Tolmasky 2010). All AMEs belong to three broad families:

- ATP and/or GTP-dependent aminoglycoside *O*-phosphotransferase (APH)
- ATP-dependent aminoglycoside *O*-nucleotidyltransferase (ANT)
- Acetyl-coenzyme A-dependent aminoglycoside *N*-acetyltransferase (AAC)

Distinct subfamilies exist within each group, which phosphorylate, adenylylate, and acetylate specific hydroxyl or amino groups on compatible aminoglycosides. Collectively, the APH family can inactivate all disubstituted aminoglycosides, as well as the atypical aminoglycosides streptomycin, spectinomycin, and hygromycin. The full designation of each enzyme conventionally includes a number in parentheses that indicates the regiospecificity, followed by a roman numeral that describes a particular substrate spectrum, and finally a letter in lower case identifying genetic variants. Thus, the enzyme of interest in this thesis, APH(2'')-IVa, is an aminoglycoside *O*-phosphotransferase that specifically targets 2''-hydroxyl groups. It is the fourth APH discovered that targets this functional group and the first one bearing its particular substrate spectrum. Excluded from this nomenclature system is the tremendous diversification sometimes found at the genetic level. For example, it has been reported that over 40 similar but non-identical genetic variants all encode AAC(6')-Ib, resulting in an amalgam of resistance factors with slightly differing structural features and substrate preferences (Ramirez et al. 2013). Such extensive microheterogeneity poses a significant challenge to the development of anti-resistance therapeutics that aim to neutralize these resistance enzymes.

### 1.2.7 Crystal Structures of APHs

At the time of this thesis' writing, a total of 49 crystal structures have been reported for eight established and one putative APH enzymes (Table 1-4). The collection of available APH structures demonstrates the diverse characteristics of this family of enzymes. APH(2'') and APH(3') form the two largest subfamilies, and their broad substrate specificity coupled with

prevalence among clinical isolates renders their structural information of high potential value for combatting this type of antibiotic resistance.

**Table 1 – 3 | Crystal Structures of Aminoglycoside *O*-phosphotransferases**

<b>Enzyme</b>	<b>PDB Code</b>	<b>Ligand</b>	<b>Res. (Å)</b>	<b>Literature reference</b>
APH(3')-Ia	4EJ7	ATP	2.3	Stogios et al. 2013
APH(3')-Ia	4FEX	Tyrphostin AG1478	2.7	Stogios et al. 2013
APH(3')-Ia	4FEU	Anthrapyrazolone SP600125	2.4	Stogios et al. 2013
APH(3')-Ia	4FEV	Pyrazolopyrimidine PP1	1.9	Stogios et al. 2013
APH(3')-Ia	4FEW	Pyrazolopyrimidine PP2	2.0	Stogios et al. 2013
APH(3')-Ia	4GKH	Kanamycin A; 1-NA-PP1	1.9	Stogios et al. 2013
APH(3')-Ia	4GKI	Kanamycin A; 1-NM-PP1	1.9	Stogios et al. 2013
APH(3')-IIa	1ND4	Kanamycin A	2.1	Nurizzo et al. 2003
APH(3')-IIIa	1L8T	ADP; Kanamycin A	2.4	Fong and Berghuis 2002
APH(3')-IIIa	1J7I	-	3.2	Burk et al. 2001
APH(3')-IIIa	1J7L	ADP	2.2	Burk et al. 2001
APH(3')-IIIa	1J7U	AMPPNP	2.4	Burk et al. 2001
APH(3')-IIIa	3TM0	AMPPNP, Butirosin A	2.1	Fong and Berghuis 2009
APH(3')-IIIa	2BKK	Ar_3A	2.2	Kohl et al. 2005
APH(3')-IIIa	3Q2J	CKI-7	2.2	Fong et al. 2011
APH(3')-IIIa	2B0Q	ADP; Neomycin B	2.7	Fong and Berghuis 2002
APH(2'')-IIa	3HAM	Gentamicin C1	2.5	Young et al. 2009
APH(2'')-IIa	3HAV	ATP; Streptomycin	2.5	Young et al. 2009
APH(2'')-IIa	4DCA	ADP	1.8	N/A (CSGID)
APH(2'')-IIa	3UZR	-	2.0	N/A (CSGID)
APH(2'')-IIIa	3TDV	GDP	2.2	Smith et al. 2012
APH(2'')-IIIa (F108L)	3TDW	GDP	1.7	Smith et al. 2012
APH(2'')-IVa	3SGC	-	2.1	Shi et al. 2011 <sup>†</sup>
APH(2'')-IVa	3SG8	Tobramycin	1.8	Shi et al. 2011 <sup>†</sup>
APH(2'')-IVa	3SG9	Kanamycin A	2.2	Shi et al. 2011 <sup>†</sup>
APH(2'')-IVa	4DT8	Adenosine	2.2	Shi and Berghuis 2012 <sup>†</sup>
APH(2'')-IVa	4DT9	Guanosine	2.1	Shi and Berghuis 2012 <sup>†</sup>
APH(2'')-IVa (F95M)	4DTA	Adenosine	2.4	Shi and Berghuis 2012 <sup>†</sup>
APH(2'')-IVa	4DTB	Guanosine	2.1	Shi and Berghuis 2012 <sup>†</sup>

(F95Y)				
APH(2'')-IVa	3N4T	-	2.2	Toth et al. 2010
APH(2'')-IVa	3N4U	-	2.2	Toth et al. 2010
APH(2'')-IVa	3N4V	-	2.4	Toth et al. 2010
APH(2'')-IVa	4DBX	-	2.0	Shakya et al. 2011
APH(2'')-IVa	4DE4	HEPES	2.0	Shakya et al. 2011
APH(2'')-IVa	4DFB	Kanamycin A	2.0	Shakya et al. 2011
APH(2'')-IVa	4DFU	Quercetin	2.0	Shakya et al. 2011
<hr/>				
APH(4)-Ia	3TYK	Hygromycin B	2.0	Stogios et al. 2011
APH(4)-Ia	3W0S	AMPPNP; Hygromycin B	1.8	Iino et al. 2013
APH(4)-Ia*	3W0M	-	2.2	Iino et al. 2013
APH(4)-Ia*	3W0N	AMPPNP; Hygromycin B	1.9	Iino et al. 2013
APH(4)-Ia*	3W0O	ADP; Hygromycin B	1.5	Iino et al. 2013
APH(4)-Ia*	3W0P	ADP; Hygromycin B	2.0	Iino et al. 2013
(D198A)				
APH(4)-Ia*	3W0Q	AMPPNP; Hygromycin B	1.8	Iino et al. 2013
(N203A)				
APH(4)-Ia*	3W0R	AMPPNP; Hygromycin B	2.3	Iino et al. 2013
(N202A)				
<hr/>				
APH(9)-Ia	3I1A	-	1.7	Fong et al. 2010
APH(9)-Ia	3I0Q	AMP	2.8	Fong et al. 2010
APH(9)-Ia	3I0O	ADP; Spectinomycin	2.4	Fong et al. 2010
APH(9)-Ia	3Q2M	CKI-7	2.9	Fong et al. 2011
<hr/>				
Rv3168 (putative)	3ATT	ATP	2.0	Kim et al. 2011

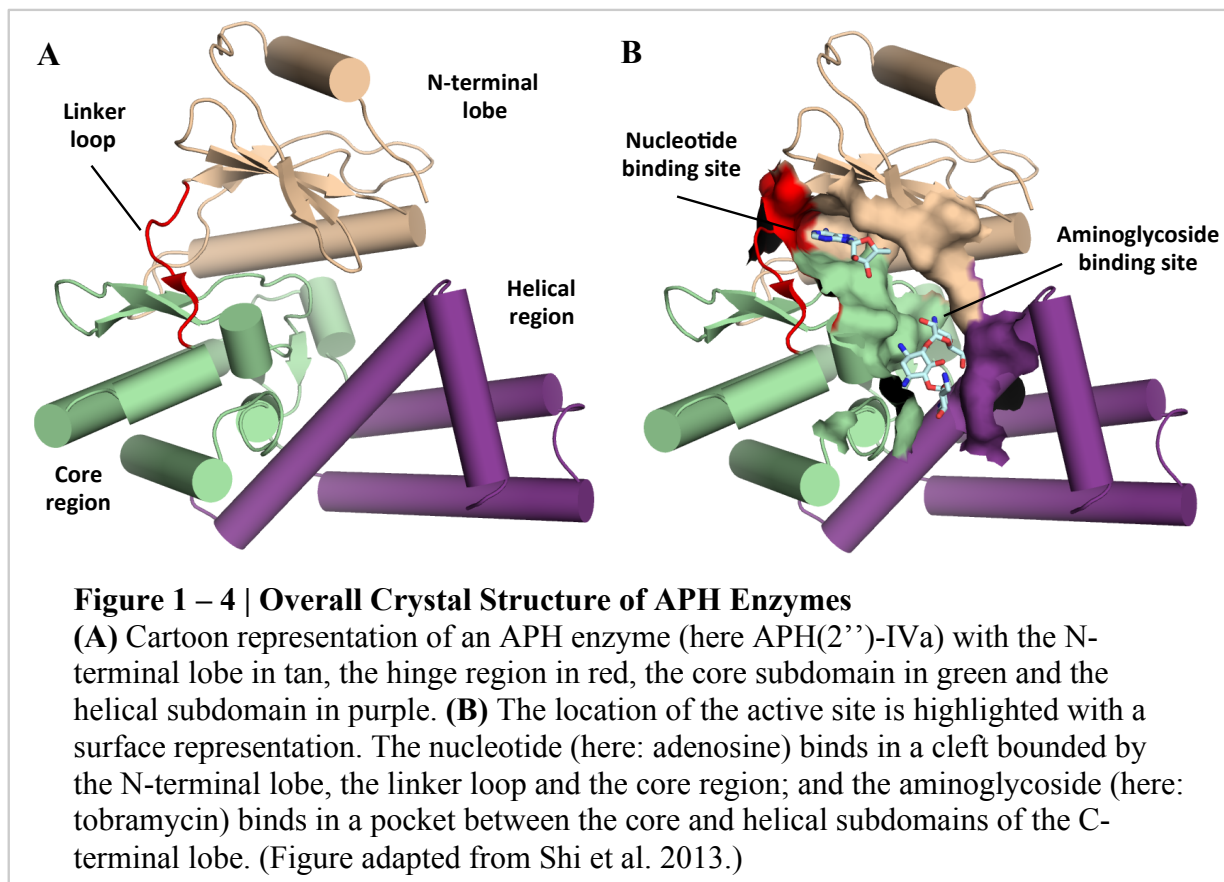
† These structures form the body of this thesis and will be discussed in detail in the ensuing chapters.

\* These structures are of a thermostable variant of APH(4)-Ia with the following set of mutations: D20G, A118V, S225P, Q226L, T246A.

The determination of the first crystal structure of an APH enzyme immediately revealed a strong resemblance to the catalytic subunit of eukaryotic protein kinases (ePKs) (Hon et al. 1997), and every subsequent structure determined has confirmed that the APHs belong to the ePK superfamily of enzymes (Hanks and Hunter 1995).

APH enzymes generally have a bilobal structure where an N-terminal lobe with a five-stranded antiparallel  $\beta$ -sheet flanked by two  $\alpha$ -helices is joined via a linker region to a much larger C-terminal lobe (Figure 1-4). The latter is in turn divided into the “core” and “helical”

subdomains. The N-terminal lobe and the core subdomain are relatively well conserved among APHs and together they form the basis for nucleotide binding and catalysis. In contrast, the helical subdomain is structurally more variable and provides the framework for aminoglycoside recognition and selectivity among different APHs (Shi et al. 2013).



## 1.3 Aminoglycoside 2''-O-Phosphotransferase IVa

### 1.3.1 Origin and Occurrence

High-level resistance to a number of aminoglycosides, most notably gentamicin, in enterococci has traditionally be ascribed to the bifunctional AAC(6')-Ie-APH(2'')-Ia enzyme. However, in the 1990's, three other *aph(2'')* genes were discovered, each exhibiting similar resistance characteristics as the APH domain of the bifunctional enzyme, though sequence similarity between any pair of *aph(2'')* genes is typically below 30% (Table 1 – 4) (Kao et al. 2000; Chow et al. 1997; Tsai et al. 1998). Historically, these genes were named *aph(2'')-Ib*, *aph(2'')-Ic*, and *aph(2'')-Id*, but their nomenclature was changed to *aph(2'')-IIa*, *aph(2'')-IIIa*, and *aph(2'')-IVa*, respectively, as differences in their substrate profiles were elucidated (Toth et al. 2009). Among them, the plasmid-encoded *aph(2'')-IVa* gene was first isolated from clinical blood isolates containing *Enterococcus casseliflavus* from a patient in Chicago (Tsai et al. 1998). Since then, other studies have reported the occurrence of this resistance factor in Asia, Europe and Africa in various enterococci species, accounting for approximately 16% of high-level gentamicin resistance in clinical isolates (Zarrilli et al. 2005; Qu et al. 2005; Abbassi et al. 2007). Although it is difficult to trace the precise origin of the *aph(2'')-IVa* gene, it has been posited that gentamicin-resistant enterococci originated from food-producing animals due to the routine administration of gentamicin on livestock (Donabedian et al. 2003). More recently, two additional *aph(2'')* genes have been characterized, encoding for the enzymes APH(2'')-Ie and APH(2'')-If (Alam et al. 2005; Toth et al. 2013). However, given their high sequence identity with APH(2'')-IVa and APH(2'')-Ia at 96% and 78%, respectively, it is debatable whether these new alleles constitute bona fide novel members of the APH(2'') family or rather derivatives of other APH(2'') proteins as a result of genetic microheterogeneity.

**Table 1 – 4 | Primary Sequence Comparison Among APH(2'') Enzymes**

	Percentage identity (lower left half) \ percentage similarity (upper right half) <sup>†</sup>				
Enzyme	APH(2'')-Ia	APH(2'')-IIa	APH(2'')-IIIa	APH(2'')-IVa	APH(2'')-Ie
APH(2'')-Ia	100	55	47	54	54
APH(2'')-IIa	29	100	47	55	55
APH(2'')-IIIa	21	24	100	50	50
APH(2'')-IVa	28	29	26	100	96
APH(2'')-Ie	28	30	26	94	100

<sup>†</sup> Percentages adapted from Alam et al. 2005.

### 1.3.2 Substrate Spectrum

APH(2'')-IVa is composed of 301 amino acids and has a molecular weight of 36.2 kDa. Although APH(2'')-IVa was first characterized as a resistance enzyme conferring high-level gentamicin resistance, it is equally capable of detoxifying a broad range of other 4,6-disubstituted aminoglycosides, including tobramycin, kanamycin, and semisynthetic derivatives amikacin and arbekacin (Table 1-4). 4,5-disubstituted aminoglycosides, on the other hand, are not compatible substrates and can in fact act as competitive inhibitors (Toth et al. 2010). This aminoglycoside substrate profile is largely similar to those of other APH(2'') enzymes, although each member in this subfamily has distinct substrate preferences. The structural basis for this divergence remains unclear.

**Table 1 – 5 | Substrate Spectrum of APH(2'') Enzymes<sup>†</sup>**

Enzyme	Nucleotide substrate(s)	Aminoglycoside substrates <sup>*</sup>
APH(2'')-Ia	GTP	Kan, Gen, Tob, Net, Dbk, Sis, Isp, Amk, Neo, Par, Liv, Rib, But
APH(2'')-IIa	ATP and GTP	Kan, Gen, Tob, Net, Dbk, Sis, Isp, Amk, Arb
APH(2'')-IIIa	GTP	Kan, Gen, Tob, Net, Dbk, Sis
APH(2'')-IVa	ATP and GTP	Kan, Gen, Tob, Net, Dbk, Sis, Isp, Amk, Arb

<sup>†</sup> Table adapted from Toth et al. 2010

<sup>\*</sup> Kan – kanamycin A; Gen – gentamicin C1; Tob – tobramycin; Net – netilmicin; Dbk – dibekacin; Sis – sisomicin; Isp – isepamicin; Amk – amikacin; Neo – neomycin B; Par – paromomycin; Liv – lividomycin A; Rib – ribostamycin; But – butirosin; Arb – arbekacin

The nucleotide specificity of the APH(2'') subfamily is noteworthy in that while other APH enzymes are generally ATP-specific, all APH(2'') enzymes can accept GTP as a phosphate donor in the phosphotransfer reaction. Furthermore, APH(2'')-Ia and APH(2'')-IIIa are GTP-specific, APH(2'')-IIa has a strong preference for ATP, whereas APH(2'')-IVa can utilize both GTP and ATP with comparable efficiencies (Toth et al. 2009). The underlying reasons for the dual nucleotide specificity of APH(2'')-IVa is unclear, but ATP is likely the preferred nucleotide in vivo given its higher intracellular concentration compared to GTP (Buckstein et al. 2008).



### 1.3.3 Kinetic Mechanism

Although no systematic analysis of the kinetic mechanism of APH(2'')-IVa has been undertaken to date, the mechanisms of APH(2'')-Ia and APH(2'')-IIa have been elucidated (Martel et al. 1983; Toth et al. 2007). Based on initial velocity patterns and dead-end inhibitor studies, it was shown that both enzymes are consistent with a random equilibrium Bi Bi mechanism. Given the structural homology among APH(2'') enzymes and their highly similar substrate profiles, it is very likely that APH(2'')-IVa also utilizes this catalytic mechanism (Figure 1-5).

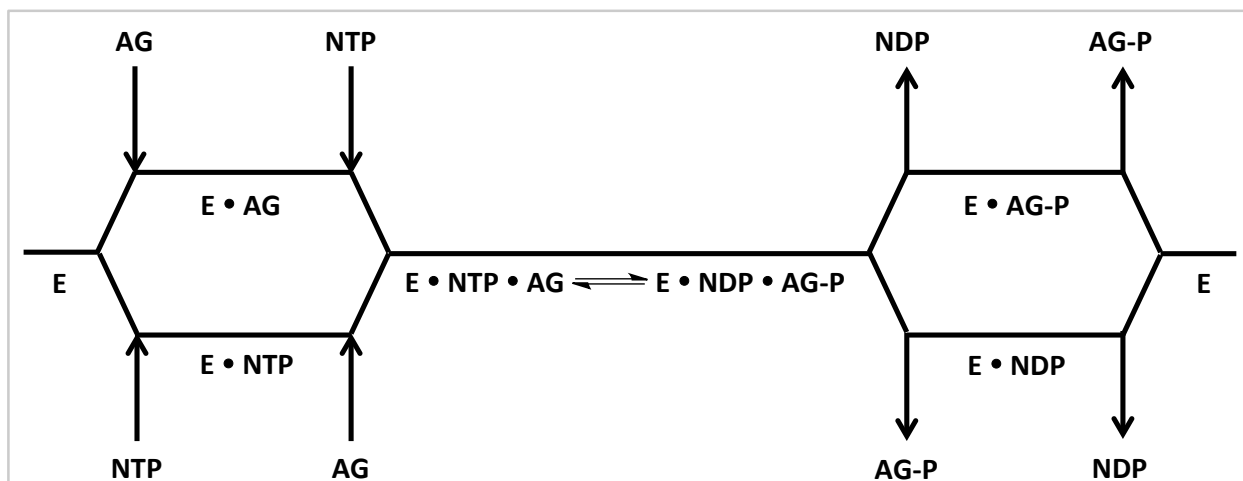


**Figure 1 – 5 | Putative Reaction Scheme of APH(2'')-IVa**

Aminoglycoside (AG) phosphorylation is accomplished via a random equilibrium Bi-Bi mechanism, where the apo enzyme (E) binds the aminoglycoside and nucleotide (NTP referring to ATP or GTP) in any order to form the catalytic complex; the phosphotransfer reaction occurs and the phosphorylated aminoglycoside (AG-P) and nucleoside diphosphate (NDP referring to ADP or GDP) are released in any order, thereby reconstituting the apo form.

It should be noted, however, that not all APH enzymes share the same mechanism. Although all APHs investigated to date follow a sequential model, it has been demonstrated that APH(3')-IIIa follows an ordered Theorell-Chance mechanism, where the nucleotide triphosphate must enter the active site first and exit last (McKay and Wright 1995).

## 1.4 Thesis Objectives

A thorough understanding of the atomic structure of aminoglycoside resistance-conferring enzymes and their precise mode of interaction with their substrates is instrumental for the rational design of novel therapeutic agents, whether in the form of next-generation aminoglycosides or specific inhibitors targeting the resistance enzymes. When initiating the research reported in this thesis (in 2008), structural information regarding the clinically important APH(2'') enzymes were scarce. In this thesis, we present a detailed analysis of how APH(2'')-IVa interacts with its native substrates, and we discuss the potential for inhibitor development using the insights gained from our structural studies.

Specifically, the second chapter focuses on the aminoglycoside-binding site and addresses the following questions:

- How does APH(2'')-IVa interact with its aminoglycoside substrates and do any conformational changes occur upon substrate binding?
- How can we rationalize the observation that APH(2'')-IVa modifies almost all 4,6-disubstituted aminoglycosides but none of the 4,5-disubstituted ones?
- What structural features of this binding site could potentiate the development of improved, next-generation aminoglycosides that can evade resistance?

The third chapter revolves around the nucleotide binding site and discusses the following points:

- How can APH(2'')-IVa use both ATP and GTP as the phosphate donor?
- Based on the structural information obtained, what can be inferred about determinants of nucleotide specificity within the APH enzyme family in general?
- What structural features of this binding site could potentiate the development of novel inhibitors that specifically target the resistance factor?

In the fourth chapter, a fragment screening approach towards the discovery of an APH(2'') inhibitor will be discussed in the context of different strategies and challenges of adjuvant development, and the following questions will be addressed:

- Why have approaches that yielded leads for other APH subfamilies not been effective in the search for an APH(2'') inhibitor?
- What are the advantages and challenges for a fragment screening method?
- How could hits from the fragment screening approach be improved?

## Chapter 2

### Structural Basis for Aminoglycoside Preferences of APH(2'')-IVa

#### 2.1 Preface

In recent years, development of novel aminoglycosides has been achieved through incremental modifications of existing variants, which thus become non-recognizable to known resistance enzymes. Evading drug resistance in this manner has seen parallel success in the  $\beta$ -lactam family of antibiotics, and to date represents the only clinically proven approach to combat aminoglycoside resistance. Semi-synthetic aminoglycosides such as amikacin, dibekacin, arbekacin, and the newest aminoglycoside undergoing clinical trials, plazomicin, are all products of this drug development method. However, the continued evolution of resistance factors has rendered second-generation aminoglycosides increasingly obsolete, and the need for continued updates to our aminoglycoside repertoire is pressing. Understanding the mode of interaction between the resistance enzyme and the aminoglycoside has become extremely constructive in further exploring this strategy.

In this chapter, we describe three crystal structures of APH(2'')-IVa, one in its apo form and two in complex with a bound antibiotic, tobramycin and kanamycin A. Comparison among the structures provides insight concerning the aminoglycoside selectivity of this enzyme. In particular, conformational changes upon substrate binding, involving rotational shifts of two distinct segments of the enzyme, are observed. These substrate induced shifts may also rationalize the altered substrate preference of APH(2'')-IVa in comparison to other members of the APH(2'') subfamily, which are structurally closely related. Finally, analysis of the interactions between enzyme and aminoglycoside reveals a distinct binding mode as compared to the intended ribosomal target, and differences in the pattern of interactions can be potentially utilized as a structural basis for the development of improved aminoglycosides.

This chapter is adapted from the following paper:

Crystal Structures of Antibiotic-bound Complexes of Aminoglycoside 2''-Phosphotransferase IVa Highlight Diversity in Substrate Binding Modes Among Aminoglycoside Kinases. Shi, K. Houston, D.R. and Berghuis, A.M. 2011. *Biochemistry*. 50, 6237-6244.

Individual author contributions are as follows, with approximate overall percent contribution in parentheses:

- Shi, K. (80%): Design of experiments; protein purification and crystallization; collection and analysis of crystallographic data; preparation of manuscript.
- Houston, D. R. (5%): Protein purification; review of manuscript.
- Berghuis, A.M. (15%): Supervisory guidance of experimental design, data collection and analysis; editing of manuscript.

## 2.2 Introduction

Bacterial resistance to antibiotics persists as a global threat to public health. Since the introduction of streptomycin against pulmonary tuberculosis some 65 years ago, aminoglycosides have remained an important class of bactericidal antibiotics (Ramirez and Tolmasky 2010; Allison et al. 2011; Burk and Berghuis 2002). Often used in combination with a  $\beta$ -lactam, aminoglycosides exert their effect by interacting with the A-site of bacterial 16S rRNA, and thereby impairing the fidelity of protein translation and leading to the production of aberrant proteins (Moazed and Noller 1987; Carter et al. 2000). Due to their extensive use both in clinical settings as well as on food-producing farm animals, resistant isolates are continually discovered, including of life-threatening species such as *Pseudomonas aeruginosa* and various pathogenic enterococci strains (Donabedian et al. 2003; Smith and Baker 2002).

Unlike streptomycin, the majority of aminoglycosides currently in clinical use are based on a 4, 5- or 4, 6-disubstituted 2-deoxystreptamine scaffold. By convention, the central 2-deoxystreptamine ring is termed ring B, with the 4-substituted aminocyclitol ring called ring A and any substituent on the 5 or 6 position called ring C. Variation among the numerous functional groups on rings A and C give rise to the large repertoire of natural and semi-synthetic aminoglycosides. Because the substituents on ring B are in equatorial positions, the resulting molecule adopts a roughly crescent-shaped conformation, where a convex and a concave side can be differentiated.

The major resistance mechanism for aminoglycoside antibiotics is the enzymatic modification of the drug, which leads to poor ribosome binding and decreased efficacy, by a series of proteins collectively referred to as the aminoglycoside modifying enzymes. Among this large and growing group of enzymes, aminoglycoside *O*-phosphotransferases (APHs) catalyze the transfer of a phosphate group to specific hydroxyl groups on a wide variety of aminoglycosides, resulting in high-level resistance (Shaw et al. 1993). Within the APH family, those members that detoxify atypical aminoglycosides, including APH(4), APH(6), APH(9), APH(3'') and APH(7''), generally have a substrate spectrum limited to one drug; whereas those members that detoxify 4, 5- or 4, 6-disubstituted aminoglycosides, including APH(3') and APH(2''), generally have a much broader substrate spectrum (Mingeot-Leclercq et al. 1999). The structural basis underlying this difference in substrate specificity is presumably that the active site architectures of the first group have evolved to specifically accommodate the unique features

of the respective atypical aminoglycoside. The second group, on the other hand, has exploited structural properties common to many 4, 5- or 4, 6-disubstituted aminoglycosides, and thus evolved more promiscuous substrate-binding sites that increase the versatility of the enzyme.

The APH(2'') subfamily currently consists of five structurally related phosphotransferases, which share limited sequence homology (~30%) and possess differences in substrate preferences (Kao et al. 2000; Badarau et al. 2008; Tsai et al. 1998; Alam et al. 2005). Among them, APH(2'')-IVa has been found in approximately 16% of gentamicin-resistant enterococci isolates around the world (Tasi et al. 1998; Abbassi et al. 2007; Zarrilli et al. 2005). Kinetic studies have shown that APH(2'')-IVa is also efficient at deactivating a number of other 4, 6-disubstituted aminoglycosides, including tobramycin and kanamycin A, but it is unable to modify any 4, 5-disubstituted aminoglycosides (Toth et al. 2010). The structure of the apo state has recently been reported, but data for substrate bound states are lacking. However, structural details have been reported on APH(2'')-IIa in its binary and ternary complexes (Young et al. 2009). In addition, various structures of four other members of the APH family, APH(4)-Ia, APH(9)-Ia, APH(3')-IIa, and APH(3')-IIIa have been determined (Nurizzo et al. 2003; Fong et al. 2010; Hon et al. 1997; Stogios et al. 2011; Fong et al. 2011). Combined, structural studies for APH enzymes reveal that despite very low sequence identity [e.g. APH(2'')-IVa shares 30% and 9% sequence identity with APH(2'')-IIa and APH(3')-IIIa, respectively] and diverse resistance profiles, they nevertheless display a remarkably similar three-dimensional fold. However, the similarity in structure and partially overlapping resistance profiles does not imply that these enzymes bind their antibiotic substrates similarly. For example, APH(2'')-IIa has been shown to bind aminoglycosides in a completely different orientation compared to APH(3') enzymes (Young et al. 2009). Even within the APH(2'') enzymes, disparate substrate profiles and preferences suggest unique structural properties for each member of the family. For instance, APH(2'')-Ia is unique in that it can detoxify both 4, 5- and 4, 6-disubstituted aminoglycosides<sup>1</sup>, and APH(2'')-IIIa prefers tobramycin as a substrate while APH(2'')-IVa is best able to phosphorylate gentamicin. Additionally, APH(2'')-IVa is the only member within its family that can utilize both ATP and GTP as a phosphate donor at comparable efficiencies (Toth et al.

---

<sup>1</sup> Note: This finding has since been disproved and APH(2'')-Ia has been shown to be specific to 4,6-disubstituted aminoglycosides (Fraser et al. 2012).

2009). Such differences impact the development of novel aminoglycosides and underline the necessity of understanding the structure of individual enzymes on an atomic level.

Here we report three crystal structures of APH(2'')-IVa, one substrate-free structure that is distinct from that previously reported, and two in complex with either tobramycin or kanamycin A. These structures shed light on the substrate specificity of APH(2'')-IVa and reveal a degree of protein flexibility not commonly seen in APH enzymes. These results inform potential strategies for the design of next-generation aminoglycoside antibiotics that are less susceptible to drug resistance.

## 2.3 Materials and Methods

### 2.3.1 Cloning, Protein Expression, and Purification

The gene of native *aph(2'')-IVa*, kindly provided by Dr. Joseph Chow (Tsai et al. 1998), was cloned into the expression vector pET22b(+) between the NdeI and HindIII restriction sites and transformed into competent *E. coli* BL21(DE3) cells. A 20-ml starter culture was used to inoculate 1L of LB medium supplemented with 100 µg/ml of ampicillin. The culture was incubated at 37°C with vigorous agitation until the optical density measured at 600 nm reached ~0.6, at which time APH(2'')-IVa expression was induced by the addition of 0.1 mM isopropyl-β-D-thiogalactopyranoside, and allowed to proceed at 15°C overnight. Cells were harvested by centrifugation (6,000 × g for 20 min at 4°C), resuspended in 40 ml of a buffer consisting of 50 mM Tris-HCl, pH 8.5, 300 mM NaCl, 1 EDTA-free protease inhibitor tablet, and lysed by sonication. The lysate was centrifuged (50,000 × g for 30 min at 4°C) and purified by Ni-NTA affinity chromatography in 50 mM Tris-HCl, pH 8.5, 300 mM NaCl. After elution with a continuous imidazole gradient (0 to 500 mM), fractions were analyzed by SDS-PAGE, and those containing the target protein were further purified by size-exclusion chromatography using a Superdex S-75 column equilibrated with 50 mM Tris-HCl, pH 8.5, 300 mM NaCl. The purity and activity of the product was verified by SDS-PAGE and a previously established enzyme activity assay (McKay et al. 1994).

### 2.3.2 Crystallization and Data Collection

Crystals of apo APH(2'')-IVa were grown at 4°C using the hanging drop vapor diffusion method by equilibrating a 4-µl solution consisting of a 2-µl protein solution at 8 mg/mL and a 2-µl buffer solution of 200 mM NaCl and 15% (w/v) polyethylene glycol 2000 in 50 mM Tris-HCl, pH 8.5, against a reservoir containing 700 µl of the buffer solution. Crystals reach a maximal size of 0.5 × 0.1 × 0.1 mm within 2 weeks. Crystals were soaked in buffer solution supplemented with 10% glycerol before data were collected under cryogenic conditions (-180°C) on a Rigaku rotating copper anode X-ray generator. A total of 360 images of oscillation angle 1° were measured.

Crystals of binary complexes were grown at 4°C using the sitting drop vapor diffusion method by combining 1.5 µl of a solution comprised of 6 mg/ml protein and 1.6 mM aminoglycoside antibiotic with 1.5 µl of 17% (w/v) polyethylene glycol 4000, 10% glycerol and



5% isopropanol in 50 mM HEPES, pH 7.5, and equilibrated against 40  $\mu$ l of the latter in an MRC crystallization plate (ProGENE). Crystals reached a maximal size of  $0.20 \times 0.15 \times 0.1$  mm within 3 weeks. All data sets were collected under cryogenic conditions. Diffraction data for APH(2'')-IVa-kanamycin A were collected on a Rigaku rotating copper anode X-ray generator. A total of 360 images of oscillation angle  $1^\circ$  were measured. Diffraction data for APH(2'')-IVa-Tobramycin were collected at the CMCF Beamline 08ID-1 at the Canadian Light Source. A total of 240 images of oscillation angle  $0.75^\circ$  were measured at  $0.9795 \text{ \AA}$ . All data sets were processed using the HKL2000 program suite (Otwinowski and Minor 1997), resulting in the statistics shown in Table 1.

### 2.3.3 Structure Determination and Refinement

The apo structure of APH(2'')-IVa was solved by molecular replacement with APH(2'')-IIa-Gentamicin (PDB code: 3HAM) as the search model using Phaser from the CCP4 suite (CCP4, 1994). A single solution was found and refined with REFMAC (Murshudov et al. 1997) when the N- and C-terminal lobes were searched for as separate ensembles. Successive cycles of maximum likelihood refinement, incorporating isotropic temperature factor and torsion-libration-screw refinement, were alternated with manual adjustments to the model in Coot (Emsley et al. 2010). TLS refinement was computed with seven subsegments per protein molecule, with all subsegments manually chosen based on secondary structural features. Solvent molecules were subsequently added until no significant improvement in model statistics could be observed. The structure of APH(2'')-IVa bound with tobramycin was solved by molecular replacement with the apo APH(2'')-IVa structure. A single solution was found and refined with REFMAC. A partially refined structure of the APH(2'')-IVa-tobramycin complex was used to solve the binary structure with kanamycin A. The aminoglycoside molecules were added to the model based on difference electron density maps ( $F_o - F_c$  and  $2F_o - F_c$ ) and refined based on stereochemical constraints obtained from the PRODRG2 server (Schuettelkopf and van Aalten 2004). Final refinement statistics are summarized in Table 1.

**Table 2 – 1 | Data Collection and Refinement Statistics of Apo and Aminoglycoside-Bound APH(2'')-IVa**

	<b>APH(2'')-IVa</b>	<b>APH(2'')-IVa– Tobramycin</b>	<b>APH(2'')-IVa– Kanamycin A</b>
Resolution range (Å) <sup>a</sup>	23.8 – 2.05 (2.10 – 2.05)	34.0 – 1.80 (1.85 – 1.80)	50.0 – 2.15 (2.21 – 2.15)
Space group	<i>P</i> 2 <sub>1</sub> 2 <sub>1</sub> 2 <sub>1</sub>	<i>P</i> 2 <sub>1</sub>	<i>P</i> 2 <sub>1</sub>
<i>a</i> (Å)	50.9	43.3	42.9
<i>b</i> (Å)	61.7	101.5	101.4
<i>c</i> (Å)	102.9	73.5	73.4
$\beta$ (deg)		100.8	100.6
No. of reflections	18,692	54,440	32,322
Completeness (%)	94.0 (97.2)	99.4 (99.7)	99.7 (98.9)
Redundancy	10.9 (7.0)	5.1 (5.1)	7.0 (5.8)
Mean <i>I</i> / $\sigma$ ( <i>I</i> )	37.1 (4.1)	27.4 (4.1)	22.6 (4.6)
<i>R</i> <sub>sym</sub> <sup>b</sup>	0.057 (0.32)	0.059 (0.35)	0.095 (0.32)
<i>R</i> <sub>cryst</sub> <sup>c</sup> / <i>R</i> <sub>free</sub> <sup>d</sup>	0.219/0.262	0.188/0.242	0.198/0.251
No. of non-hydrogen atoms			
Protein	2432	4988	4941
Substrate	–	64	66
Solvent	102	341	175
Root-mean-square deviation			
Bond length (Å)	0.022	0.023	0.021
Bond angles (deg)	1.838	1.899	1.871
Average thermal factor (Å <sup>2</sup> )			
Protein	20.99	24.4	23.1
Substrate	–	36.1	44.2
Solvent	22.36	29.0	22.0
Ramachandran statistics (%) <sup>e</sup>			
Most favored regions	89.9	90.0	91.8
Additionally allowed regions	9.7	10.0	7.5
Generously allowed regions	0.4	0.0	0.7
Disallowed regions	0.0	0.0	0.0

<sup>a</sup> Values in parentheses refer to reflections in the highest-resolution shell.

<sup>b</sup>  $R_{\text{sym}} = \sum_{hkl} \sum_i |I_i(hkl) - \langle I(hkl) \rangle| / \sum_{hkl} \sum_i I_i(hkl)$ , where  $\langle I(hkl) \rangle$  is the average intensity of equivalent reflections and the sum is extended over all measured observations for all unique reflections.

<sup>c</sup>  $R_{\text{cryst}} = \sum_{hkl} (|F_o| - |F_c|) / \sum_{hkl} |F_o|$ , where  $|F_o|$  is the observed and  $|F_c|$  the calculated structure factor amplitude of a reflection.

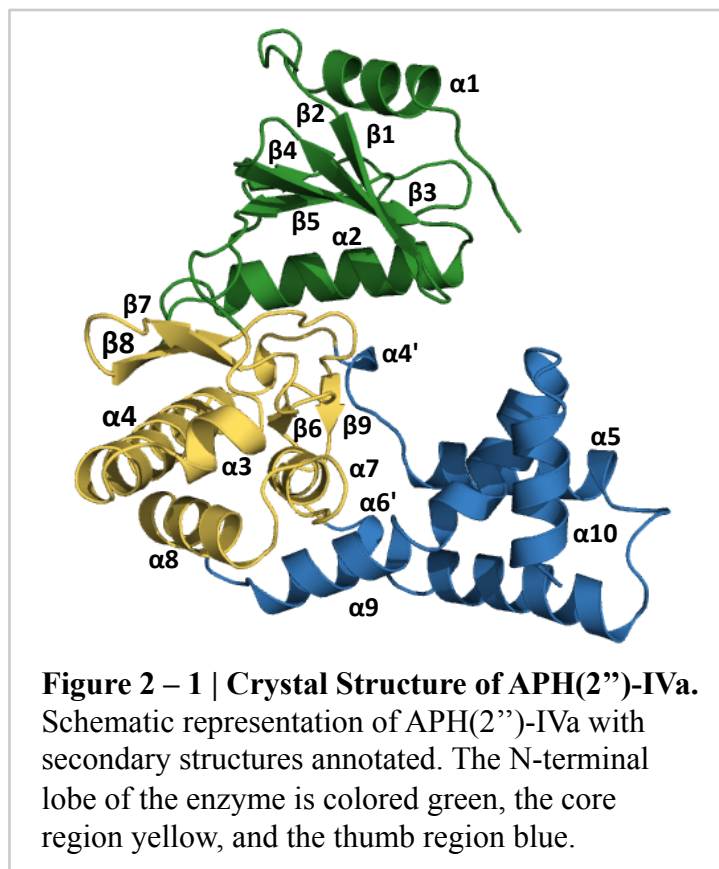
<sup>d</sup>  $R_{\text{free}}$  was calculated by randomly omitting 5% of the observed reflections from the refinement.

<sup>e</sup> According to the Ramachandran plot in PROCHECK (Laskowski et al. 1993).

## 2.4 Results

### 2.4.1 Apo Structure

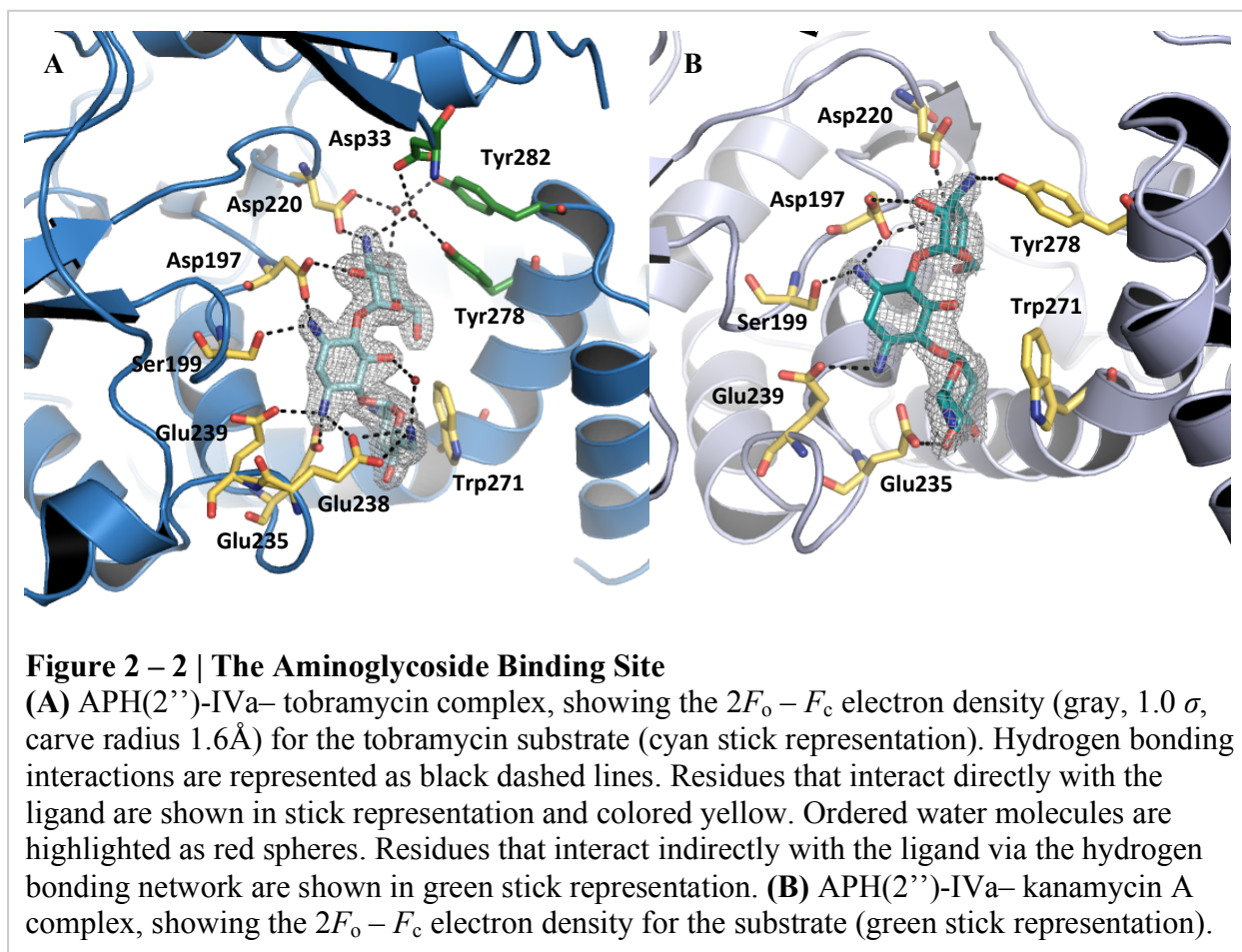
The crystal structure of apo APH(2'')-IVa was solved with one protein molecule per asymmetric unit and has been refined to 2.05 Å resolution, with an  $R_{\text{cryst}}$  of 0.219 and an  $R_{\text{free}}$  of 0.262 (Figure 2-1). The apo structure of APH(2'')-IVa has been recently reported in three crystal forms with resolutions ranging between 2.2-2.4 Å (Toth et al. 2010), superposition of which revealed that these three forms are essentially identical. The N-terminal lobe and the core subdomain are well conserved across all three structures, while several parts of the helical subdomain of one form showed small reorientations compared to the others. Comparisons of our apo structure with the three forms previously published show that it is essentially isomorphous with form I (PDB entry: 3N4T). However, while the core subdomain overlaps very well with the previous structures, both the N-terminal lobe and the helical subdomain show relative reorientations. The 5-stranded  $\beta$ -sheet in the N-terminal lobe is rotated away from the substrate-binding site, corresponding to a translation of up to 3.0 Å of the loop between  $\beta 1$  and  $\beta 2$  and up to 4 Å of the loop between  $\beta 4$  and  $\beta 5$ . In the helical subdomain, traditionally referred to as the “thumb” region, the largest structural difference is that the long helix  $\alpha 9$  bends at a less acute angle, thereby shifting helix  $\alpha 10$  and the C-terminal portion of helix  $\alpha 9$  away from the aminoglycoside-binding pocket by up to 3.0 Å.



## 2.4.2 Binary Structures

The APH(2'')-IVa-tobramycin complex has been refined to 1.8 Å with an  $R_{\text{cryst}}$  of 0.188 and an  $R_{\text{free}}$  of 0.242, while the APH(2'')-IVa-kanamycin A complex has been refined to 2.1 Å with an  $R_{\text{cryst}}$  of 0.198 and an  $R_{\text{free}}$  of 0.251. Both binary structures were solved in a monoclinic space group with two protein molecules per asymmetric unit, affording a total of four crystallographically independent APH(2'')-IVa-aminoglycoside structures. These represent the first crystal structures of APH(2'')-IVa in complex with a bound antibiotic substrate. The thermal factors for the aminoglycosides, especially for kanamycin A, are higher than those for the protein molecules. Given the inherent structural flexibility of aminoglycosides, ring C may be able to interact with the protein in slightly varying conformations, thereby causing the incomplete occupancy of some atoms of the ligands.

Consistent with other APH structures, the aminoglycoside binds in a cleft formed between the helical and the core subdomain of the C-terminal lobe of the protein. Given the abundance of positive charges on this class of antibiotics, it is not surprising that a large number



of residues located in the aminoglycoside-binding pocket are acidic in nature. The APH(2'')-IVa-tobramycin complex shows that the antibiotic molecule is positioned in its binding pocket such that the 2''-hydroxyl group of the C ring is located 2.8 Å from the O<sub>δ1</sub> atom of the putative catalytic base, Asp197 (Figure 2-2A). This residue is part of the catalytic loop widely seen in protein kinases and is conserved among all members of the APH family (Hon et al. 1997). Beside Asp197, ring C interacts with only one other side chain, namely Asp220.

The majority of interactions between protein and ligand are formed with rings A and B of the aminoglycoside. The 2-deoxystreptamine ring (ring B) is nestled against the core subdomain and interacts with Asp197, Ser199, and three glutamates from the loop between helices α7 and α8 (Glu235, Glu238, and Glu239). Ring A, which is oriented nearly perpendicularly to ring B, is stabilized by Glu238 and Glu239. In addition, ring A is stabilized by a non-polar stacking interaction with the indole ring of Trp271. It is intriguing to note that, with the exception of the non-polar interaction with Trp271, all other interactions between protein and ligand occur at the side of the ligand that faces the core subdomain, or the convex side of the molecule. Although direct interactions on the concave side with the helical subdomain are absent, two well-defined water molecules, as evidenced by below-average temperature factors, bridge the gaps between ring C and Tyr278 and Tyr282. Two other well-defined water

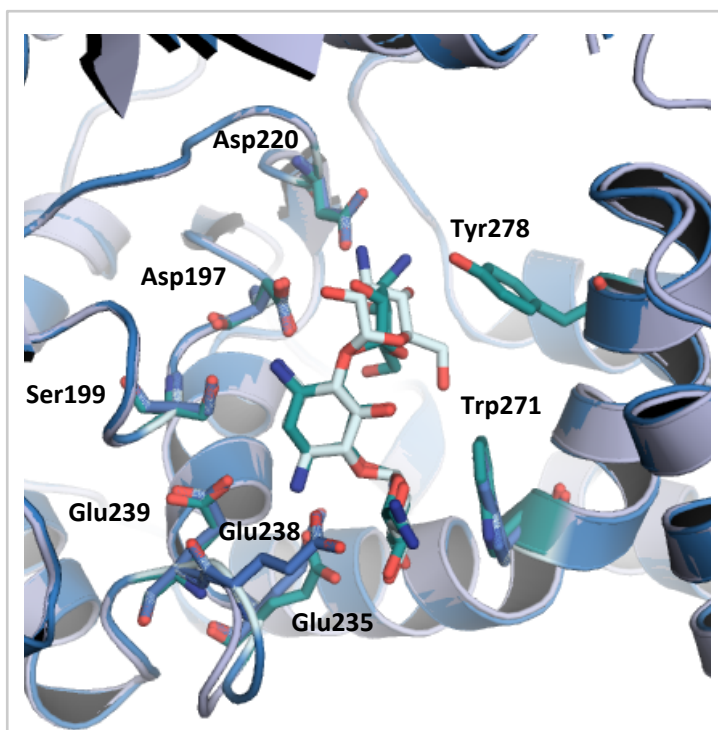


### Figure 2 – 3 | Tobramycin versus Kanamycin A Binding

Structural superposition of the APH(2'')-IVa-tobramycin complex (blue) onto the APH(2'')-IVa-kanamycin A complex (gray). Residues that form hydrogen bonds with the antibiotic show minimal conformational variation. Tobramycin (cyan) and kanamycin A (green) bind in similar conformations, with the only difference at ring C, which forms a greater angle with respect to ring B in the APH(2'')-IVa-kanamycin A complex.

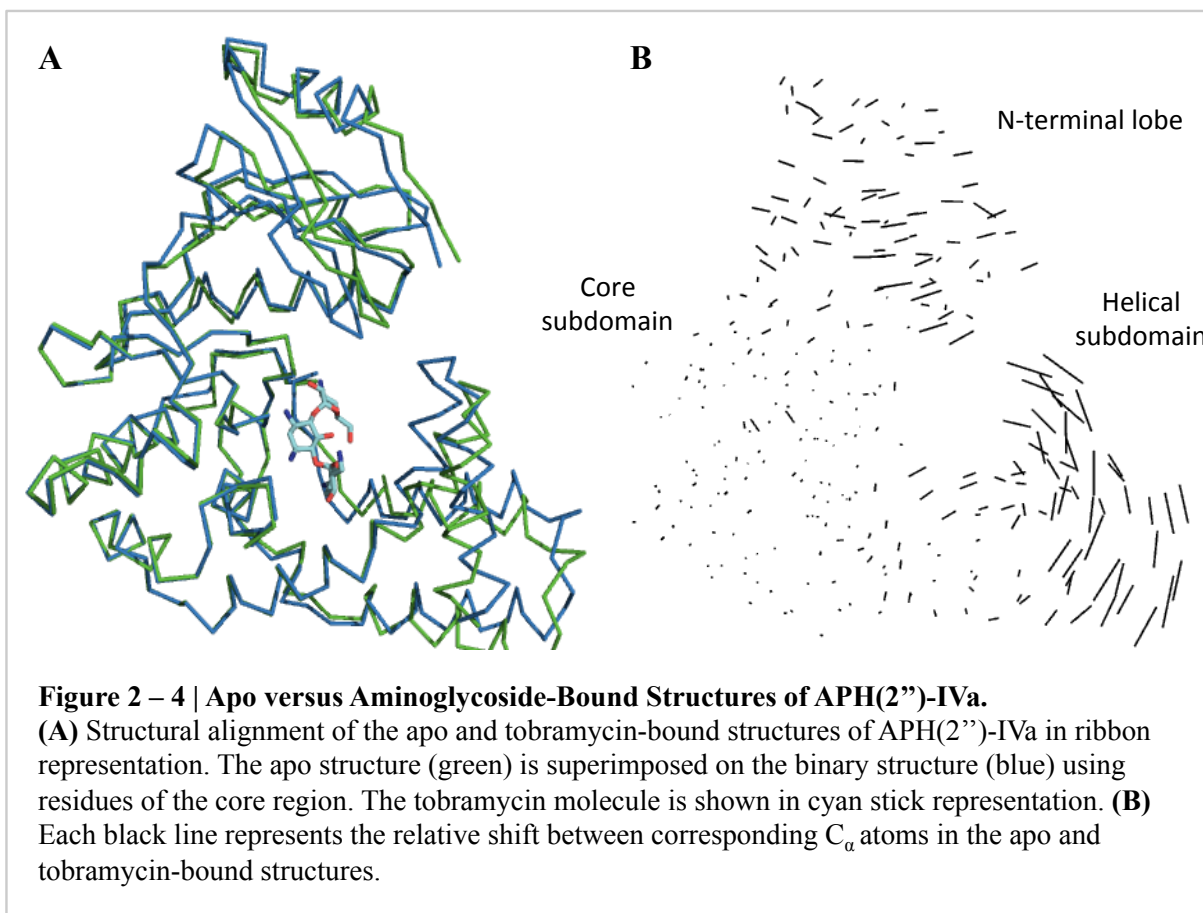
molecules interacting with the aminoglycoside are also stabilized by residues Asn32 and Asp33 from the loop between  $\beta 1$  and  $\beta 2$  of the N-terminal lobe.

Comparison between the APH(2'')-IVa-tobramycin (Figure 2-2A) and APH(2'')-IVa-kanamycin A (Figure 2-2B) complexes reveal that the aminoglycoside is bound in an almost identical conformation, with the only difference being a more pronounced twist in ring C in the APH(2'')-IVa-kanamycin A complex, bringing it nearly perpendicular to ring B and coplanar with ring A (Figure 2-3). This twist presents the 3''-amino group in sufficiently close proximity of the helical subdomain to allow a direct hydrogen bond with Tyr278 without the need for water molecules to bridge the gap. The only structural differences between tobramycin and kanamycin A lie in two functional groups on ring A. Tobramycin has an additional amino group in the 2' position, and the electrostatic interactions afforded by this group with nearby glutamate residues could explain the two-fold discrepancy in binding affinity between the two aminoglycosides (Toth et al. 2010).

#### **2.4.3 Comparison Between Apo and Binary Structures of APH(2'')-IVa**

Comparison between the apo and the binary protein structures show conformational changes in both the N-terminal lobe as well as the thumb region (Figure 2-4A). The N-terminal lobe twists towards the aminoglycoside-binding pocket, thereby presenting the loop between strands  $\beta 1$  and  $\beta 2$  in a position to interact with the bound aminoglycoside. This twist corresponds to a translation of 4.7 Å for Asn32, bringing it in proximity of ring C. The helices in the thumb region also show reorientations in the two substrate-bound structures when compared with the substrate-free structure: conformational differences for helix  $\alpha 5$  are likely a consequence of crystal packing interactions. In the binary structures, the two protein molecules forming each asymmetric unit come in close proximity. In particular, the side chain hydroxyl group of each Ser140 forms a hydrogen-bond with the amide backbone of the same residue in the other molecule, leading to a distortion of the  $3_{10}$  helix ( $\alpha 4'$ ) and the beginning of  $\alpha 5$ . Helix  $\alpha 6$  is parallel to helix  $\alpha 5$  and shows a similar displacement. This observation lends further support to an earlier reported finding that although helices  $\alpha 5$  and  $\alpha 6$  move as a rigid unit, they form an inherently flexible region of the protein (Young et al. 2009). Conformational variation for residues 277-285 is likely linked to the presence of the substrate in its binding pocket, since the difference in the binary structure sharpens the kink in helix  $\alpha 9$ , thereby bringing the C-terminal

end of this helix in a position to stabilize the 2''-ring of the aminoglycoside antibiotic. In addition to the shift of the helix, the side chain of Tyr278 is also repositioned to point towards the ligand, involving a total displacement of the terminal hydroxyl group of over 7 Å and bringing it close enough to form hydrogen bonds with Asn32 and Asp33 of the N-terminal lobe. In effect, the conformational changes described above result in a more compact aminoglycoside-binding pocket.





## 2.5 Discussion

### 2.5.1 Aminoglycoside Preference of APH(2'')-IVa

The crystal structures of the APH(2'')-IVa-Tobramycin and APH(2'')-IVa-Kanamycin A complexes represent the first binary structures for this enzyme. Together with the APH(3') subfamily, the APH(2'') enzymes form the only two subfamilies of APHs that are capable of deactivating a wide range of aminoglycoside antibiotics. The substrate specificity of APH(2'')-IVa can be explained by examining its aminoglycoside-binding site architecture, which can also serve as a point of departure for the design of next-generation aminoglycosides.

The large number of interactions and the relative rigidity of the neamine core of the aminoglycoside suggest that large-scale alterations in this portion of the ligand may be poorly tolerated by the enzyme. Amikacin, which is kanamycin A derivatized at the N1 position by a bulky 4-amino-2-hydroxybutyrate functionality, would fit poorly into the binding pocket due to potential steric clashes with nearby side chains of residues from the core subdomain, in particular Asp201, which rationalizes the 30-fold decrease in binding affinity to amikacin compared to kanamycin A (Toth et al. 2010). The observation that amikacin is nevertheless a weak substrate of APH(2'')-IVa suggests that side chains of Asp201 and His202 are capable of being displaced upon antibiotic binding. The displacement may be facilitated electrostatically due to the abundance of negatively charged residues around the aminoglycoside. Since Asp201 is not otherwise directly involved in any interactions with substrate stabilization in APH(2'')-IVa, it is conceivable that mutants featuring a less bulky residue may show more elevated resistance levels to amikacin. This potential of increasing the substrate promiscuity of APH(2'')-IVa is of clinical concern since amikacin and isepamicin are alternatives currently considered in cases where drug resistance precludes the use of gentamicin against enterococci infections (Maviglia et al. 2009). Kinetic studies have also shown that 4, 5-disubstituted aminoglycosides such as neomycin B are not substrates for APH(2'')-IVa, but instead are able to act as dead-end inhibitors (Toth et al. 2010). Structurally, this can be explained by noting that in 4, 5-disubstituted aminoglycosides, rings A-B-C form a much more acute angle, thereby shifting ring C towards the helical subdomain and away from the site of catalysis if rings A and B are bound in the same manner. The demand on space imposed by ring C and an additional ring D may be accommodated given the flexibility of the helical subdomain, and in particular helix  $\alpha 9$ .

## 2.5.2 Comparison with substrate-bound structures of other APHs

Although enzymes of the APH family share structural and topological resemblances, comparison of known binary structures reveals radically different modes of aminoglycoside binding, which can account for the diverse substrate profiles observed. Since APH(2'')-IVa has its unique substrate preference, it would not be a surprise to see key differences in its interactions with the ligand compared to even its closest relative, APH(2'')-IIa. Given the large number of interactions between the core subdomain and the aminoglycoside for the latter, it has been posited that the helical subdomain plays only a minor role in substrate binding (Young et al. 2009). The observed conformational changes in APH(2'')-IVa stand in contrast thereof, and suggest that the helical subdomain has a more active role in substrate binding.

The importance of the helical subdomain as a determinant of substrate specificity is supported by another member of the APH family, spectinomycin phosphotransferase or APH(9)-Ia. This enzyme confers resistance against one specific antibiotic, and a detailed study of the protein-ligand interactions reveals that most contacts occur with the helical subdomain (Fong et al. 2010). A remarkable feature of APH(9)-Ia is a conformational change of the N-terminal lobe and, to a smaller extent, the thumb region upon substrate binding, thereby forming a compact binding pocket. Although domain movements at the scale of APH(9)-Ia are not observed for APH(2'')-IVa, the smaller conformational changes in the N-terminal lobe and the thumb region upon substrate binding (Figure 2-3B) nevertheless represent a departure from APH(2'')-IIa and APH(3') enzymes, which rely on a less restrictive binding pocket to accommodate a wide range of substrates as opposed to flexibility of the enzyme itself (Fong and Berghuis 2002; Fong and Berghuis 2009). The interactions observed among Tyr278, Asn32 and Asp33 and their stabilizing effect on the aminoglycoside are absent in the substrate-bound structure of APH(2'')-IIa due to the greater distance between the N-terminal lobe and the aminoglycoside-binding pocket, as well as the less acute angle in helix  $\alpha 9$ , which pushes residues at the end of the helix further away from the aminoglycoside-binding site. In addition, superposition of substrate-bound forms of APH(2'')-IIa and APH(2'')-IVa shows that the ligand is shifted by approximately 2 Å in the direction of residues from the helical subdomain and the N-terminal lobe in the latter protein-ligand complex, thus facilitating interactions with these regions (Figure 2-5A). This shift is likely because the shorter side chains of aspartate residues stabilizing rings A and B are replaced by

glutamate residues in APH(2'')-IVa. Taken together, these variations result in a more compact binding pocket for APH(2'')-IVa, especially around ring C (Figures 2-5B, 2-5C). In contrast to these two APH(2'') enzymes, APH(2'')-Ia is able to deactivate 4, 5-disubstituted aminoglycosides, suggesting that it interacts with its substrate via a yet different method compared to other APH(2'') enzymes characterized thus far<sup>1</sup>. Although detailed analysis of the structural differences between APH(2'')-IVa and APH(2'')-Ia must await the elucidation of the structure of the latter enzyme, our findings thus far show that significant variability in the active site is not only present among APHs that target hydroxyl groups at different positions, but can also exist among members of the same subfamily with overlapping substrate profiles. Such variations significantly increase the difficulty of designing generic inhibitors that are potent against a large number of APHs.

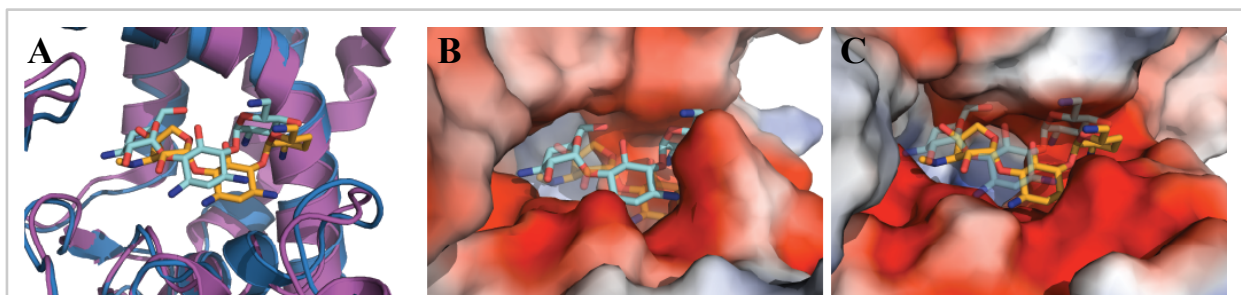


**Figure 2 – 5 | Aminoglycoside Binding Site Comparison with APH(2'')-IIa.**

(A) Structural superposition of the APH(2'')-IVa–tobramycin complex (blue with cyan substrate) onto the APH(2'')-IIa–gentamicin C complex (PDB entry 3HAM, purple with orange substrate) using residues of the core region, showing the displacement of the aminoglycoside. (B) Surface representation of the tobramycin binding site in APH(2'')-IVa with the tobramycin molecule colored cyan. The gentamicin C molecule as bound in APH(2'')-IIa is indicated in transparent orange stick representation. (C) Surface representation of the gentamicin binding site in APH(2'')-IIa, showing a less compact binding pocket on the concave side of the molecule, in particular around ring C. The tobramycin molecule as bound in APH(2'')-IVa is indicated in transparent cyan stick representation.

### 2.5.3 Comparison of aminoglycoside-binding mode between APH(2'')-IV and the ribosome

Since APH(2'')-IVa deactivates aminoglycosides that are originally meant to interact with the A-site of the bacterial ribosome, it is instructive to compare the mode of binding of the drug between the intended target and the resistance enzyme. Crystal structures of the entire 30S ribosome in complex with several aminoglycosides were solved in 2000 (Carter et al. 2000), and

<sup>1</sup> See footnote on p. 37.

subsequently the crystal structures of tobramycin and kanamycin A in complex with an oligonucleotide containing the A-site have also been determined (Vicens and Westhof 2002; Vicens and Westhof 2003). These structures show similarities as well as striking differences between the mode of binding of the aminoglycoside with the ribosome versus that of the resistance enzyme. The stereochemical conformations of the antibiotic molecules in the rRNA binding pocket are similar to those observed for APH(2'')-IVa (Figure 2-6A), and the majority of interactions between the aminoglycoside and the A-site also occur with the neamine core portion of the drug. For instance, ring A of tobramycin intercalates in the RNA helix, thus forming a non-polar stacking interaction with base G<sup>1491</sup> and a pseudo base pair with A<sup>1408</sup> (Vicens and Westhof 2002). These interactions are well-mimicked in APH(2'')-IVa, involving the indole ring of Trp271 and the side chain of Glu238, as noted above.

While the majority of functional groups utilized by the aminoglycoside to bind to the ribosome are the same that interact with the resistance enzyme, the relative orientations between the drug and its interaction partners show wide differences. In the A-site, the RNA wraps around the antibiotic and most interacting groups extend towards the top face of ring B (Figure 2-6C). In contrast, key residues from APH(2'')-IVa are mainly situated to the convex side of the molecule and interact with functional groups on the 1, 3, 5', 2'' and 3'' positions from a roughly coplanar orientation (Figure 2-6B), which represents nearly a 90 degree offset from the orientation of the RNA nucleotides. Binary structures of other members of the APH family, most notably APH(3')-IIIa, have revealed target mimicry as an effective method of drug inactivation by resistance factors (Fong and Berghuis, 2002). In the case of APH(3')-IIIa, target mimicry is achieved by the perpendicular orientation of the face of the aminoglycoside's ring structure relative to its key interacting partners, albeit the opposite face is used compared to interactions with the A-site. This type of target mimicry is not shown by APH(2'')-IVa, where the enzyme residues project towards the convex edge of the aminoglycoside rings. A necessary consequence of this difference in orientation is that the aminoglycoside is positioned deeper within the enzyme in APH(2'')-IVa. While the antibiotic binding site resembles a relatively shallow pocket in APH(3')-IIIa, it is a deeper cleft in the APH(2'') enzymes, which may explain the more limited resistance profile of the latter enzymes. The differences in aminoglycoside-binding between APH(2'')-IVa and the A-site harbor opportunities for the development of variant aminoglycoside antibiotics that can bind the ribosomal target yet are unable to be inactivated by the resistance protein.

In summary, our structural analysis of the binary complexes of APH(2'')-IVa has highlighted the importance of the helical subdomain in substrate specificity and shown important differences in the mode of aminoglycoside binding between the ribosomal A-site and the resistance factor. Together, these contributions to our general understanding of aminoglycoside phosphotransferases can help to progress the rational design of novel next-generation aminoglycoside antibiotics with reduced susceptibility to these resistance factors.

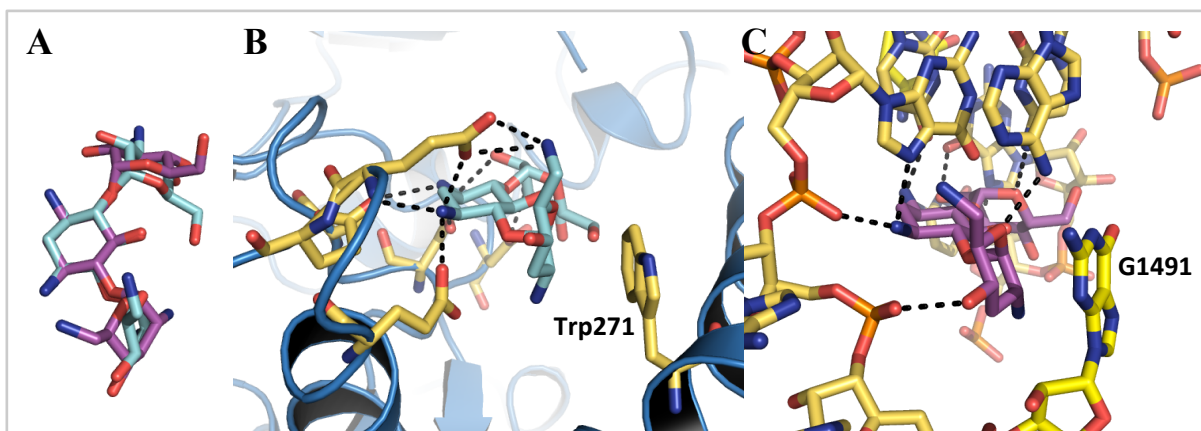


**Figure 2 – 6 | Aminoglycoside Binding Site Comparison with the Ribosomal A-site.** (A) Superposition of the tobramycin molecules in the conformations in which they bind to APH(2'')-IVa (cyan) and the ribosomal A-site (magenta; PDB entry 1LC4). (B) Aminoglycoside binding site of APH(2'')-IVa. Residues that form direct interactions with the ligand mainly interact with the aminoglycoside from the convex side of the molecule, which corresponds to the core region of the protein. (C) Crystal structure of tobramycin bound to eubacterial 16S rRNA A-site, with the tobramycin molecule in the same orientation as in Figure 2-6(B). Residues (orange) that form direct interactions with the ligand mainly interact with the aminoglycoside from the top face of the molecule.

## Chapter 3

### Nucleotide Preference of APH(2'')-IVa

#### 3.1 Preface

An alternative strategy to evading drug resistance through next-generation aminoglycosides is to directly target the resistance enzyme with specific inhibitors, which would serve as adjuvants to be administered in combination with existing aminoglycosides. Though themselves unable to kill the pathogen, such inhibitors could revive numerous obsolete aminoglycosides by weakening the bacteria's resistance mechanism. Finding an inhibitor active against not one but multiple APH enzymes simultaneously necessitates a thorough understanding of the active site architecture, and having discussed aminoglycoside binding in the previous section, this chapter centers on the second half of the active site and investigates how APH(2'')-IVa interacts with its nucleotide substrates.

We present here four crystal structures of APH(2'')-IVa, two of the wild type enzyme and two of single amino acid mutants, each in complex with either adenosine or guanosine. Together, these structures afford a detailed look at the nucleoside-binding site architecture for this enzyme and reveal key elements that confer dual nucleotide specificity, including a solvent network in the interior of the nucleoside-binding pocket and the conformation of an interdomain linker loop. Steady state kinetic studies, as well as sequence and structural comparisons with members of the APH(2'') subfamily and other aminoglycoside kinases, rationalize the different substrate preferences for these enzymes. Finally, despite poor overall sequence similarity and structural homology, analysis of the nucleoside-binding pocket of APH(2'')-IVa shows a striking resemblance to that of eukaryotic casein kinase 2 (CK2), which also exhibits dual nucleotide specificity. These results, in complement with the multitude of existing inhibitors against CK2, could serve as a structural basis for the design of nucleotide-competitive inhibitors against clinically relevant APH enzymes.

This chapter is adapted from the following paper:  
Structural Basis for Dual Nucleotide Selectivity of Aminoglycoside 2''-Phosphotransferase IVa Provides Insight on Determinants of Nucleotide Specificity of Aminoglycoside Kinases. Shi, K. and Berghuis, A.M. 2012. *J. Biol. Chem.* 287(16), 13094-13102.

Individual author contributions are as follows, with approximate overall percent contribution in parentheses:

- Shi, K. (85%): Design of experiments; collection and analysis of all crystallographic and spectrophotometric data; preparation of manuscript.
- Berghuis, A.M. (15%): Supervisory guidance of experimental design, data collection and analysis; editing of manuscript.

### 3.2 Introduction

Aminoglycosides form an important class of bactericidal antibiotics in therapeutic use today. However, bacterial resistance against nearly all known aminoglycosides persistently emerges, which poses a serious clinical threat in cases of pathogenic species (Smith and Baker 2002). A major mechanism of resistance to aminoglycoside antibiotics is the covalent addition of functional groups by a large repertoire of proteins collectively referred to as the aminoglycoside-modifying enzymes. Among them, aminoglycoside O-phosphotransferases specialize in the phosphorylation of specific hydroxyl groups and thereby prevent this class of antibiotics from effectively binding to their intended ribosomal target (Chow 2000).

Several subfamilies of APH enzymes have been discovered, and together they are capable of detoxifying aminoglycosides of diverse chemical structures. Members within the same subfamily, although generally sharing significant sequence similarity and structural homology, often exhibit distinctly different aminoglycoside preferences (Toth et al. 2009). Despite diverging antibiotic substrate profiles, all known APHs share a limited set of phosphate donors, namely ATP or GTP. Structurally, this implies that although the aminoglycoside-binding site shows wide variations among the APHs, the nucleotide-binding site is comparatively more conserved. Therefore, the latter has been considered an attractive target for the development of small molecule inhibitors that would ideally be active against a broad range of APHs and could thus serve as adjuvants in combination therapy with existing aminoglycosides (Burk and Berghuis 2002).

Although some nucleotide-competitive kinase inhibitors have also been shown to inhibit a number of APHs, the prognostic for developing a pan-APH inhibitor is poor due to significant structural divergences among different APH subfamilies (Fong et al. 2011). This does not imply, however, that a common inhibitor against a smaller subset of APHs, such as those belonging to either the APH(3') or the APH(2'') subfamily, is impossible to find. Such an inhibitor would harbor significant clinical potential because these two subfamilies, beside comprising over half of all known APH enzymes, are both characterized by a broad antibiotic substrate spectrum and contain some of the most prevalent resistance enzymes found in clinical isolates worldwide (Yagedar et al. 2009; Chandrakanth et al. 2008; Zarrilli et al. 2005).

A divide between APH(3') and APH(2'') enzymes lies in their nucleotide specificity. Members of the APH(3') subfamily are ATP-specific, whereas members of the APH(2'')



subfamily are also able to use GTP. Currently, the crystal structures of several APHs in complex with ATP-analogues have been determined (Young et al. 2009; Nurizzo et al. 2003; Fong et al. 2010), but APH structures with a bound GTP analogue remain elusive<sup>1</sup>. Among aminoglycoside phosphotransferases, APH(2'')-IVa stands out with its nearly identical catalytic efficiencies with either ATP or GTP, which presents the opportunity of contrasting ATP versus GTP binding at the same active site and elucidating key structural features that influence nucleotide specificity.

We have previously reported the apo and aminoglycoside-bound structures of APH(2'')-IVa (Shi et al. 2011), and kinetic parameters had also been established for this enzyme (Toth et al. 2010). Here, we present four nucleoside-bound crystal structures of wild type and mutant APH(2'')-IVa. These structures shed light on the detailed binding patterns of the different nucleoside substrates and explain the nucleotide specificity of this enzyme. These results, especially in complement with existing data on the nucleotide-bound structures of other APH enzymes, inform avenues for the rational design of small molecule inhibitors that can potentially target multiple subfamilies of aminoglycoside phosphotransferases.

---

<sup>1</sup> *Note: Since this paper was published several APH structures with a bound GTP analogue have been reported, including APH(2'')-IIIa and APH(2'')-Ia (Smith et al. 2012; Smith et al. 2014).*

### 3.3 Experimental Procedures

#### 3.3.1 Site-directed Mutagenesis

F95M and F95Y mutants of APH(2'')-IVa were constructed using the PCR method with the oligonucleotides 5'-GAAACGTACCAAATGTCTTTTCGCAGGTATGACAAAAA-TTAAAGGAGTACCATTG-3' and 5'-GAAACGTACCAAATGTCTTTTCGCAGGTATACAAAAATTAAAGGAGTACCATTG-3', and their appropriate reverse complements, respectively. Each 50- $\mu$ l PCR reaction contained 5  $\mu$ l of 10  $\times$  Pfu X7 buffer, 60 ng of template DNA (wild type aph(2'')-IVa in a pET 22b(+) plasmid), 0.125  $\mu$ g of each mutagenic primer, 10 mM dNTPs, and 2.5 units of Pfu X7 DNA polymerase. The PCR product was digested by DpnI restriction endonuclease for 1 h at 37  $^{\circ}$ C, and mutant plasmids were recovered by transformation of Escherichia coli DH5 $\alpha$  cells. Successful introduction of the desired mutations was verified by sequencing of plasmid DNA.

#### 3.3.2 Crystallization and Data Collection

Wild type as well as mutant APH(2'')-IVa, containing a C-terminal His<sub>6</sub> tag, were expressed and purified as previously described (Shi et al. 2011). Crystals of both binary complexes were grown at 4  $^{\circ}$ C via the sitting-drop vapor diffusion method. The reservoir solution used was composed of 100 mM HEPES at pH 7.5, 150 mM potassium nitrate, 17% (w/v) polyethylene glycol 3350, 6% 2-propanol and 10% glycerol. Initially, irregular, jagged-shaped crystals were obtained by equilibrating a 3- $\mu$ l drop against 40  $\mu$ l of reservoir solution, where the drop consisted of 50% reservoir solution and 50% protein solution, which was composed of 6 mg/ml APH(2'')-IVa and 3.2 mM nucleoside substrate in 50 mM Tris-HCl at pH 8.5 and 300 mM sodium chloride. Such crystals were transferred to 50  $\mu$ l of reservoir solution, broken up, and used as seeds. In subsequent iterations of crystallization, each 3- $\mu$ l drop was supplemented with 0.5  $\mu$ l of the seeding solution at 120-fold dilution. After four cycles of crystallization, prism-shaped crystals with approximate dimensions of 0.1  $\times$  0.1  $\times$  0.2 mm were obtained. Diffraction data were collected under cryogenic conditions ( $-180^{\circ}$ C) on a Rigaku rotating copper anode X-ray generator with a Saturn 300-mm charge-coupled device detector. For the wild type guanosine-bound structure, a data set of 180 images with an oscillation angle of 1 $^{\circ}$  was collected, and for all other structures, data sets of 360 images with an oscillation angle of 1 $^{\circ}$  were collected. All data sets were processed with the HKL2000 program suite (Otwinowski

and Minor 1997), with the results summarized in Table 3-1.

### 3.3.3 Structure Determination and Refinement

The crystal structure of adenosine-bound APH(2'')-IVa was solved by molecular replacement with Phaser from the CCP4 program suite (CCP4 1994), using protein chain A of the APH(2'')-IVa-tobramycin complex (Protein Data Bank entry 3SG8) as the search model, and difference Fourier methods were used to obtain the phases for the remaining structures. Refinement of all models consisted of successive iterations of reciprocal space refinement with REFMAC (Murshudov et al. 1997), incorporating isotropic temperature factor and torsion-libration-screw refinement, alternated with manual model building with the program Coot (Emsley et al. 2010). Torsion-libration-screw refinement was computed with seven subsegments per protein molecule, with each subsegment chosen based on secondary structural features. Adenosine and guanosine molecules were added to the respective model based on unambiguous density shown in the difference electron density maps ( $F_o - F_c$  and  $2F_o - F_c$ ) and refined on the basis of stereochemical constraints obtained from the PRODRG2 server (Schüttelkopf et al. 2004). Solvent molecules were subsequently inserted until no significant improvements could be achieved as judged by decreases in the  $R_{\text{free}}$  value. Final refinement statistics pertaining to the four models are given in Table 3-1.

**Table 3 – 1 | Data Collection and Refinement Statistics of Nucleoside-Bound Wild Type and Mutant APH(2'')-IVa**

	<b>Wild type + Adenosine</b>	<b>Wild type + Guanosine</b>	<b>Phe95Met + Adenosine</b>	<b>Phe95Tyr + Guanosine</b>
Resolution range (Å) <sup>a</sup>	41.9 – 2.15 (2.10 – 2.05)	34.0 – 2.10 (1.85 – 1.80)	30.0 – 2.35 (2.41 – 2.35)	50.0 – 2.15 (2.21 – 2.15)
Space group	<i>P2</i> <sub>1</sub>	<i>P2</i> <sub>1</sub>	<i>P2</i> <sub>1</sub>	<i>P2</i> <sub>1</sub>
<i>a</i> (Å)	42.7	42.3	42.1	42.3
<i>b</i> (Å)	101.4	101.3	101.1	101.3
<i>c</i> (Å)	73.6	73.4	73.0	73.6
$\beta$ (deg)	100.6	100.0	100.0	100.6
No. of reflections	31,670	33,433	23,821	35,596
Completeness (%)	99.9 (98.3)	99.0 (89.0)	99.9 (99.6)	99.3 (91.2)

Redundancy	7.3 (6.8)	3.3 (3.1)	6.9 (6.1)	7.3 (5.8)
Mean $I/\sigma(I)$	27.1 (5.5)	15.9 (4.1)	21.6 (4.3)	23.5 (4.7)
$R_{\text{sym}}^b$	0.075 (0.30)	0.074 (0.32)	0.089 (0.35)	0.086 (0.31)
$R_{\text{cryst}}^c/R_{\text{free}}^d$	0.190/0.245	0.185/0.242	0.198/0.257	0.195/0.246
<hr/>				
No. of non-hydrogen atoms				
Protein	4843	4819	4865	4958
Substrate	38	40	38	40
Solvent	199	200	89	185
<hr/>				
Root-mean-square deviation				
Bond length (Å)	0.017	0.017	0.014	0.023
Bond angles (deg)	1.86	1.87	1.67	1.93
<hr/>				
Average thermal factor (Å <sup>2</sup> )				
Protein	16.7	22.6	21.3	16.3
Substrate	42.4	30.1	57.0	26.4
Solvent	29.6	36.4	33.3	18.5
<hr/>				
Ramachandran statistics (%) <sup>e</sup>				
Most favored regions	91.8	91.2	89.4	90.8
Additionally allowed regions	8.2	8.6	10.4	9.2
Generously allowed regions	0.0	0.2	0.2	0.0
Disallowed regions	0.0	0.0	0.0	0.0

<sup>a</sup> Values in parentheses refer to reflections in the highest-resolution shell.

<sup>b</sup>  $R_{\text{sym}} = \sum_{hkl} \sum_i |I_i(hkl) - \langle I(hkl) \rangle| / \sum_{hkl} \sum_i I_i(hkl)$ , where  $\langle I(hkl) \rangle$  is the average intensity of equivalent reflections and the sum is extended over all measured observations for all unique reflections.

<sup>c</sup>  $R_{\text{cryst}} = \sum_{hkl} (|F_o| - |F_c|) / \sum_{hkl} |F_o|$ , where  $|F_o|$  is the observed and  $|F_c|$  the calculated structure factor amplitude of a reflection.

<sup>d</sup>  $R_{\text{free}}$  was calculated by randomly omitting 5% of the observed reflections from the refinement.

<sup>e</sup> According to the Ramachandran plot in PROCHECK (Laskowski et al. 1993).

### 3.3.4 Kinetic Assay

A continuous spectrophotometric assay that couples aminoglycoside phosphorylation with lactate production was used to measure the consumption of ATP or GTP as a function of NADH oxidation (McKay et al. 1994). Data were collected at 37 °C with a SpectraMax 190 absorbance microplate reader, where each assay was performed with a total volume of 200  $\mu$ l, containing 50 mM Tris-HCl at pH 7.5, 40 mM potassium chloride, 10 mM magnesium chloride, 3.0 mM

phosphoenolpyruvate, 3.0 mM tobramycin, 360 mM  $\beta$ -nicotinamide adenine dinucleotide (reduced), 20 units/ml pyruvate kinase, and 25 units/ml lactate dehydrogenase. Enzyme at 0.10 mg/ml (final concentration) was added to the reaction mixture 5 min before the reaction was initiated by the addition of NTP at variable concentrations. A total of 16 concentrations between 0.03 and 2.0 mM were assayed in triplicates for each nucleotide substrate. Steady state kinetic parameters were analyzed using Prism 5.0 (GraphPad Software) and are summarized in Table 3-2. Values for  $k_{cat}$ ,  $K_M$ , and  $k_{cat}/K_M$  were obtained by fitting the kinetic data nonlinearly with the Michaelis-Menten equation:

$$v = \frac{V_{max} \cdot [S]}{K_M + [S]}$$

where  $k_{cat} = V_{max}/[E]$ ,  $V_{max}$  is the maximum velocity,  $[E]$  is the enzyme concentration, and  $[S]$  and  $K_M$  are the concentration and the Michaelis-Menten constant of the nucleoside substrate.

**Table 3 – 2 | Steady State Kinetic Parameters for APH(2'')-IVa**

<b>Protein</b>	<b>NTP</b>	<b><math>k_{cat}</math> (s<sup>-1</sup>)</b>	<b><math>K_M</math> (<math>\mu</math>M)</b>	<b><math>k_{cat}/K_M</math> (M<sup>-1</sup> s<sup>-1</sup>)</b>
<b>Wild Type</b>	ATP	4.37 $\pm$ 0.04	69 $\pm$ 3	(6.3 $\pm$ 0.3) $\times$ 10 <sup>4</sup>
	GTP	5.03 $\pm$ 0.04	168 $\pm$ 5	(3.0 $\pm$ 0.2) $\times$ 10 <sup>4</sup>
<b>Phe95Met</b>	ATP	3.06 $\pm$ 0.04	55 $\pm$ 3	(5.5 $\pm$ 0.4) $\times$ 10 <sup>4</sup>
	GTP	4.35 $\pm$ 0.04	156 $\pm$ 5	(2.8 $\pm$ 0.2) $\times$ 10 <sup>4</sup>
<b>Phe95Tyr</b>	ATP	1.06 $\pm$ 0.01	72 $\pm$ 3	(1.5 $\pm$ 0.1) $\times$ 10 <sup>4</sup>
	GTP	1.15 $\pm$ 0.01	49 $\pm$ 2	(2.3 $\pm$ 0.2) $\times$ 10 <sup>4</sup>

## 3.4 Results

### 3.4.1 Overall Structural Characteristics

The wild type APH(2'')-IVa-adenosine complex has been refined to 2.15 Å with an  $R_{\text{cryst}}$  of 0.192 and an  $R_{\text{free}}$  of 0.244, whereas the guanosine-bound structure of wild type APH(2'')-IVa has been refined to 2.10 Å with an  $R_{\text{cryst}}$  of 0.187 and an  $R_{\text{free}}$  of 0.247. These represent the first nucleoside-bound structures of APH(2'')-IVa and the first crystal structure of an aminoglycoside phosphotransferase in complex with a bound GTP-like substrate. Both binary structures were solved in a monoclinic space group with two protein molecules per asymmetric unit and with cell dimensions nearly identical to the previously reported values of aminoglycoside-bound structures of APH(2'')-IVa (Shi et al. 2011). In fact, superpositions of each of the nucleoside-bound structures of APH(2'')-IVa with the tobramycin-bound structure show that the two forms of binary structures are virtually identical, with r.m.s. deviations of 0.52 and 0.25 Å for the adenosine- and guanosine-bound structures, respectively. Superposition of the two nucleoside-bound structures yielded an r.m.s. deviation of 0.43 Å, demonstrating that the protein adopts an invariable binary structure irrespective of the identity of its substrate.

### 3.4.2 Nucleoside Binding

Traditionally, structures of aminoglycoside phosphotransferases have been divided into two structural components, termed the N-terminal and C-terminal lobe, in analogy to the structurally related eukaryotic protein kinases (Hon et al. 1997). The C-terminal lobe is itself further divided into the core region and the thumb region. The two lobes are joined by a linker loop of 10 amino acids, and the interface between the two lobes forms the nucleotide-binding pocket, with the linker loop serving as the base of the binding site. The nucleoside-binding pocket of APH(2'')-IVa is mainly described by 20 residues from the N-terminal lobe and the core subdomain. These 20 residues can be deconstructed into three main structural components (Fig. 3-1). A portion of the  $\beta$ -sheet from the N-terminal lobe forms region 1, the top face of the binding pocket. Specifically, residues Ser-28 – Gly-31 fold over the ribose moiety and are poised to interact with the triphosphate group. These residues lead into a flexible loop that has been implicated in catalysis for both APH enzymes and eukaryotic protein kinases (Burk et al. 2001). Also, residues Ile-44 – Lys-46 are positioned above the purine base and contribute to the hydrophobic character of this pocket. Region 2 is part of the linker loop that connects strand  $\beta 5$

of the N-terminal lobe with helix  $\alpha 3$  of the core subdomain. In addition to affording the only hydrogen bonds with the purine base, residues Gly-94 – Ile-98 also form the interior side of the binding cavity. Region 3 describes the bottom face of the cleft and consists of a group of five residues from two loops of the core-subdomain.

In the APH(2'')-IVa-adenosine complex, the nucleoside is buried deeply in a cleft between the two lobes (Fig. 3-2A). The adenine plane is sandwiched between hydrophobic side chains of residues from both lobes, notably Ile-44 and Ile-216. The base is stabilized by a hydrogen-bonding pattern reminiscent of Watson-Crick base pairing, consisting of two hydrogen bonds between N6 and the backbone

oxygen of Thr-96 and between N1 and the amide nitrogen of Ile-98. In addition, the ribose ring is further stabilized by a pair of interactions between the side chain carboxyl group of Asp-217 and O3' and O5' of the sugar moiety. These last interactions are also observed in the guanosine-bound structure (Fig. 3-2B), but the ribose ring there adopts a slightly different puckered conformation, thus leading to a shift in the position of the base. Atoms of the guanine base are offset by up to 2.4 Å as compared with their counterparts in adenine, such that the O6 atom of guanosine replaces not the N6 but the N1 atom of adenosine and thus interacts with the amide nitrogen of Ile-98 (Fig. 3-3). Such a dislocation, which has been

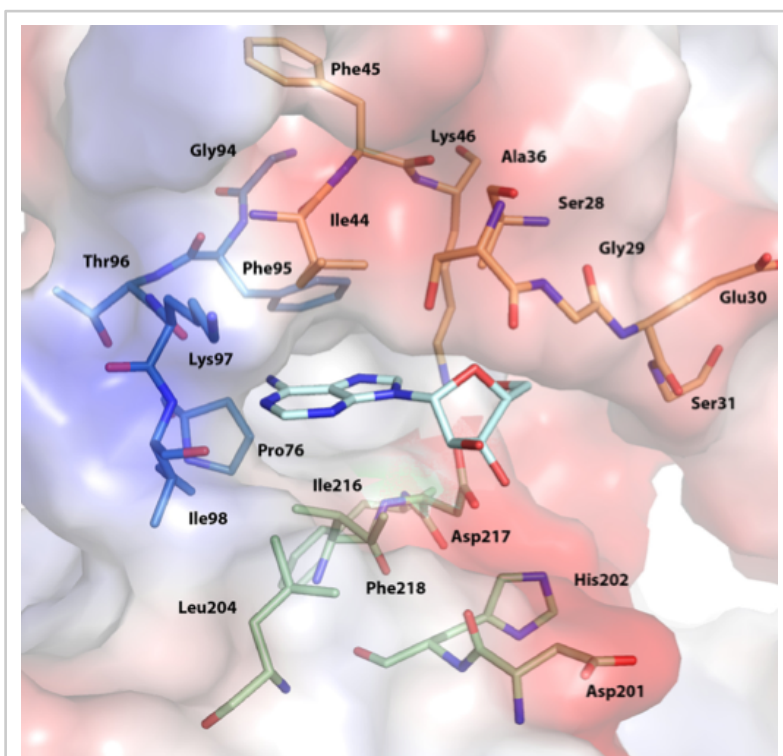


**Figure 3 – 1 | Key Components of the Nucleoside Binding Site.**

Residues forming the nucleoside binding site of APH (2'')-IVa are shown in stick and semi-transparent surface representations. A bound adenosine molecule is shown in cyan. Key residues are divided into three regions based on secondary structure elements and color-coded as follows: the N-terminal  $\beta$ -strands forming the top face of the cleft are shown in orange, the linker loop is shown in blue, and the loops from the core subdomain forming the bottom face of the cleft are shown in green.

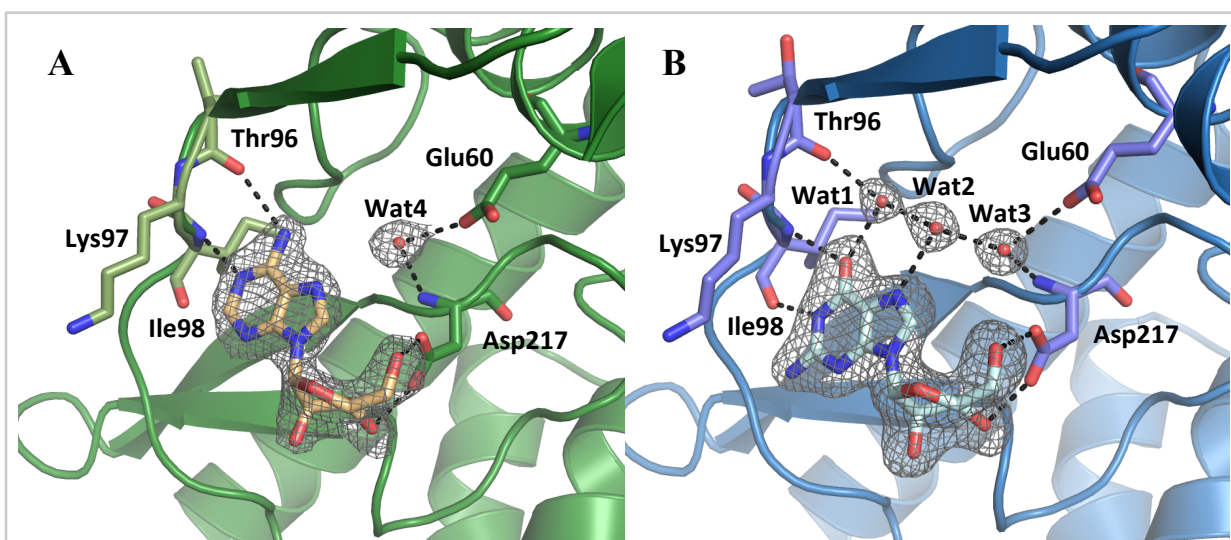


**Figure 3 – 2 | Nucleoside Binding for APH(2'')-IVa**

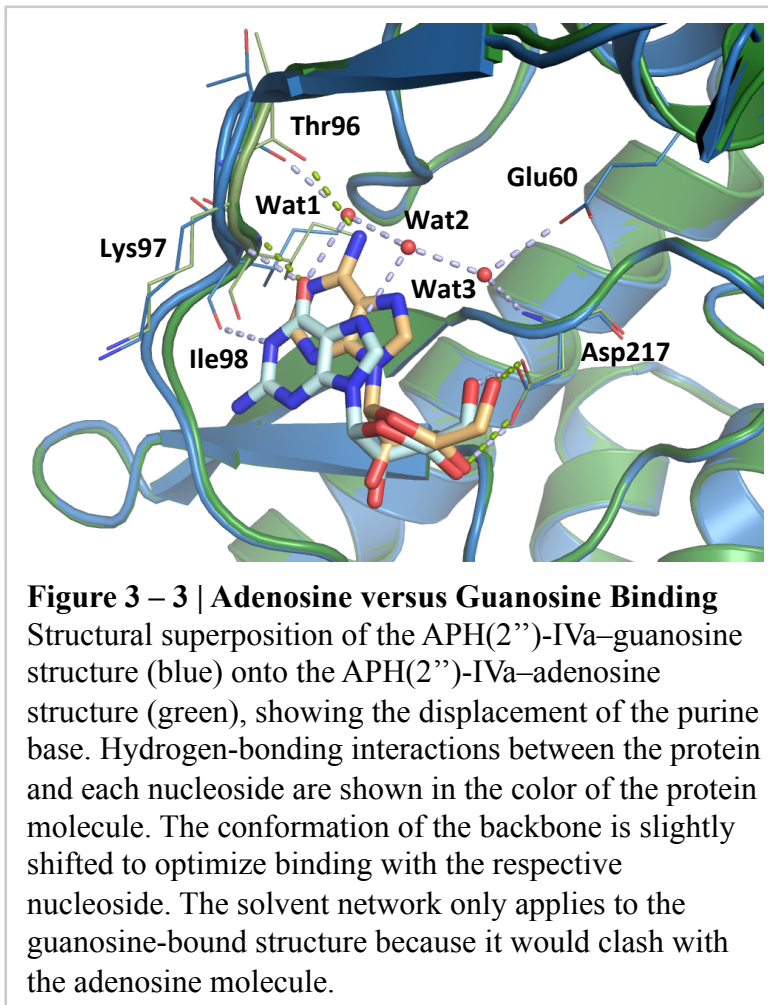
(A) APH(2'')-IVa–adenosine complex, showing the  $2F_o - F_c$  electron density (gray,  $1.0 \sigma$ , carve radius  $1.6 \text{ \AA}$ ) for the adenosine molecule (orange stick representation). Hydrogen-bonding interactions are represented as black dashed lines. Residues that directly interact with the substrate are shown in green stick representation. (B) APH(2'')-IVa–guanosine complex, showing the  $2F_o - F_c$  electron density for the guanosine molecule (cyan stick representation). Ordered water molecules (Wat1–Wat4) forming a solvent network are highlighted as red spheres. Residues involved in interacting with the substrate are shown in purple stick representation.

previously termed a “hydrogen-bonding frameshift” (Niefind et al. 1999), is necessary because the N6 atom of adenine acts as a hydrogen donor, whereas the O6 atom of guanine is a hydrogen acceptor. Thus, the guanine base must shift along the linker loop until it can favorably interact with the appropriate hydrogen-bonding partners, resulting in a lack of interaction with Thr-96, which is energetically compensated by a new hydrogen bond observed between the N1 atom of guanosine and the carbonyl oxygen of Ile-98. This shift along the linker region has previously been predicted by *in silico* modeling (Toth et al. 2010). The Watson-Crick base pairing-like bonding pattern observed for adenine is incomplete for guanine because no interaction partner is in position to accept a hydrogen from N2. The linker loop itself shows minimal differences between the two nucleoside-bound structures, with a total displacement of about  $0.6 - 0.8 \text{ \AA}$  for the key residues that form the base of the binding site, likely an adaptation to more favorably interact with the altered position of the purine base.

Globally, the displacement observed for guanosine positions the base less deeply in the nucleotide-binding cleft as compared with adenosine and thus vacates a pocket at the inside of



the cleft. Fascinatingly, this pocket is occupied by a network of three clearly defined water molecules (Wat1, Wat2, and Wat3 in Fig. 3-2B) that serve as bridges between the guanine base and the residues lining the interior of the binding cleft. One of these water molecules (Wat1) is less than 1 Å away from the position occupied by the N6 atom in the adenosine structure, thereby acting as an intermediary that connects the O6 atom of guanosine with the carbonyl group of Thr-96. Similarly, the other two water molecules indirectly connect the N7 atom of guanosine with the backbone amide of Asp-217 and the side chain carboxyl group of



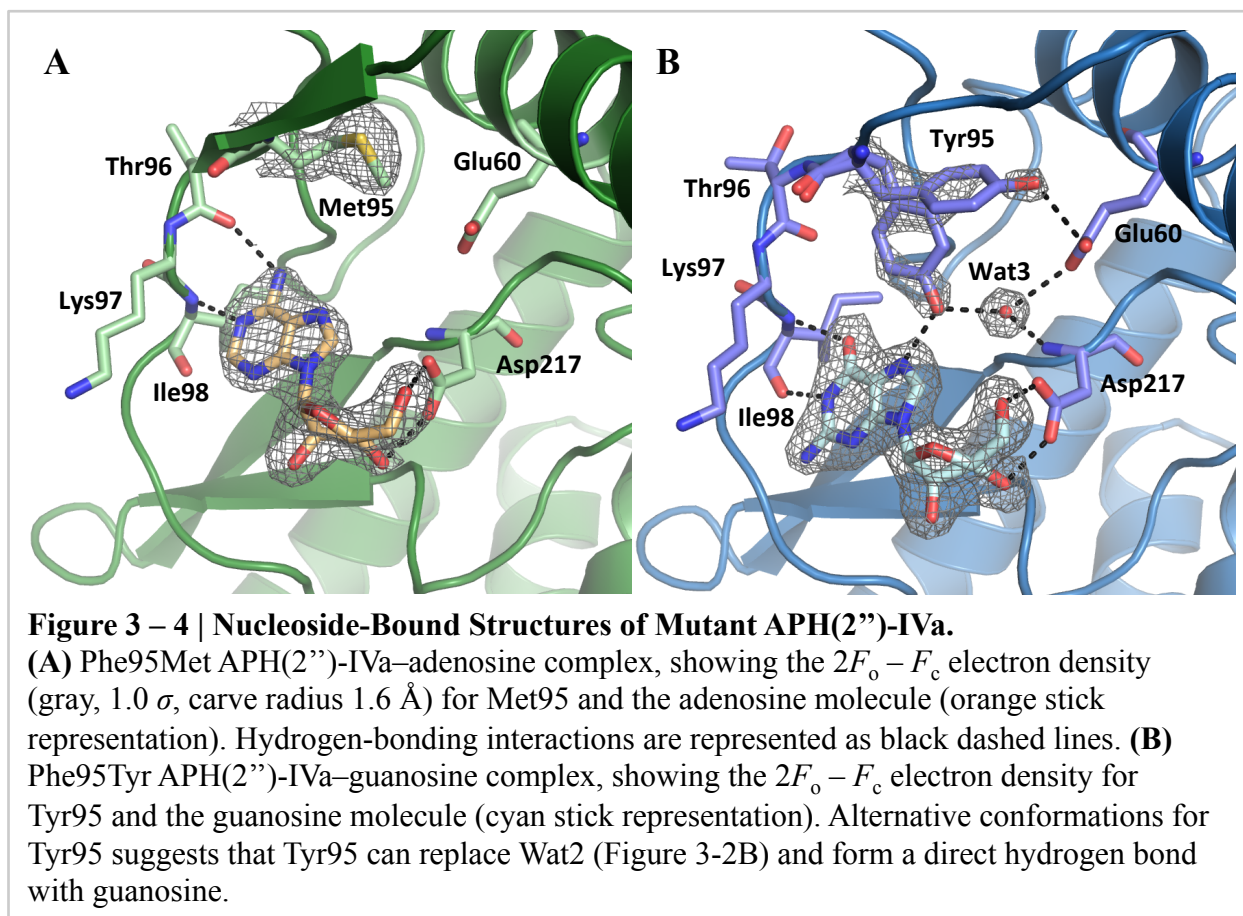
Glu-60. In contrast, because of the deeper insertion of the adenine plane into the nucleotide-binding cleft, there is insufficient space for the formation of an effective solvent network. Although a water molecule linking the amide nitrogen of Asp-17 and the terminal carboxyl oxygen of Glu-60 is clearly visible (Wat4 in Fig. 3-2A), it is too far removed from the N7 atom of adenosine to form a hydrogen bond. Also, no water molecules occupying the equivalent positions of guanine atoms such as N1 were evident in the APH(2'')-IVa-adenosine structure at the given resolution.

### 3.4.3 Structure-Function Studies

As detailed below, the mutants F95M and F95Y were created based on our structural analysis of the nucleoside-binding pocket and a sequence comparison with related APH enzymes to explore the influence of this key residue on nucleotide specificity, and kinetic data were

collected on the wild type as well as the mutant variants. The steady state kinetic parameters of wild type APH(2'')-IVa confirm that its activity is comparable in the presence of either ATP or GTP (Table 2). The  $k_{cat}/K_M$  values determined here deviate somewhat from previously reported parameters that range between  $3 \times 10^3$  and  $8 \times 10^3 \text{ M}^{-1} \text{ s}^{-1}$  (Toth et al. 2009; Toth et al. 2010). This is likely due to small differences in the experimental conditions. In general, F95M and F95Y mutations both result in a small decrease in catalytic efficiency. The F95M mutant does not show significantly different binding affinities as compared with the wild type, whereas the F95Y mutation shifts the nucleotide selectivity from a 2.5-fold preference for ATP to a 1.5-fold preference for GTP.

To complement kinetic studies, crystal structures of both mutants were determined. The F95M APH(2'')-IVa-adenosine complex has been refined to 2.4 Å with an  $R_{\text{cryst}}$  of 0.198 and an  $R_{\text{free}}$  of 0.257, and the guanosine-bound structure of F95Y APH(2'')-IVa has been refined to 2.10 Å with an  $R_{\text{cryst}}$  of 0.195 and an  $R_{\text{free}}$  of 0.246. No global changes in conformation are brought about by either mutation, and the overall r.m.s. deviations for both mutants are less than 0.4 Å as compared with the wild type enzyme. For the F95M mutant, electron density of the side chain of Met-95 is not clearly defined, suggesting that it is flexible and may partially project toward the nucleotide-binding pocket, thereby impacting the formation of an ordered solvent network (Figure 3-4A). For F95Y, the two protein molecules in the asymmetric unit show varying conformations for the mutated residue. In one instance, the mutated residue adopts an identical conformation as compared with the wild type phenylalanine, with the additional hydroxyl group forming a new hydrogen bond with the side chain carboxyl group of Glu-60. Although this conformation does not result in a direct interaction with the substrate, the increased hydrophilicity change to the local environment could favor the formation of an ordered solvent network. For the second protein molecule, the electron density for Tyr-95 is poorly defined, and an alternative conformation of the side chain can be modeled, where the terminal hydroxyl group replaces a water molecule and forms a hydrogen bond with the N7 atom of the guanine moiety. The solvent network is absent, and only one water molecule (Wat3) could be modeled (Figure 3-4B).



## 3.5 Discussion

### 3.5.1 Structural Determinants for Nucleotide Specificity

The crystal structure of APH(2'')-IVa bound to guanosine represents the first instance where an aminoglycoside resistance enzyme was successfully co-crystallized with a GTP analogue. Together with the APH(2'')-IVa-adenosine structure, it offers a detailed perspective of the nucleoside-binding site architecture of this enzyme. The number and nature of hydrogen bonds between each nucleoside and the protein are quite similar. Adenosine, being more deeply inserted in the binding cleft, likely benefits from more significant van der Waals interactions with hydrophobic residues found in the interior of the binding cavity, but guanosine compensates by having a stabilizing hydrogen-bonding network despite incurring the entropy cost of at least three localized water molecules. These results rationalize the kinetic data showing that ATP and GTP can bind with comparable efficiencies.

Previous studies have shown that nucleotide preference deviates among the four main APH(2'') enzymes, with APH(2'')-Ia and APH(2'')-IIIa being GTP-specific, APH(2'')-IIa capable of binding GTP but preferring ATP, and APH(2'')-IVa willing to accept both nucleotides to a near equal extent (Toth et al. 2009). It is instructive to consider the structural elements that give rise to this incongruity, especially because they may also help explain the nucleotide specificity of more distantly related APH enzymes. Based on a multiple amino acid sequence alignment, it is clear that the overall sequence similarity among this subfamily of enzymes is relatively low (all below 30%). However, the three major regions that form the nucleotide-binding site show conspicuous conservation, with 16 out of 20 residues either perfectly conserved or strongly similar (Fig. 3-5). The only region that shows considerable divergence is region two despite its essential role in stabilizing both the adenine and the guanine ring. The strong conservation of the other regions and the lack of conservation in this loop are suggestive of the presence of key residues that differ among the four enzymes and thus act as determinants of nucleotide specificity. This area of the binding pocket is outlined mainly by the curvature of the backbone of residues Gly-94 – Ile-98, with the majority of side chains pointing away from the nucleotide. A notable exception is Phe-95, the phenyl group of which is a major constituent of the hydrophobic interior wall of the cleft. This amino acid is replaced by a methionine residue in APH(2'')-IIa (Met-85) and by tyrosine residues in both APH(2'')-Ia and APH(2'')-IIIa (Tyr-100 and Tyr-92, respectively). To assess the impact of this amino acid, we created the F95M and

F95Y mutants, determined their kinetic parameters, and solved their crystal structures in complex with adenosine or guanosine in the same conditions as with the wild type enzyme. Kinetic parameters of the F95M mutant do not deviate significantly from wild type APH(2'')-IVa. The F95Y mutant, on the other hand, shows an increase in affinity for GTP and a decrease in affinity for ATP, such that the ratio between  $K_{M(ATP)}$  and  $K_{M(GTP)}$  is 1.4 as opposed to 0.4 for the wild type enzyme. The additional hydroxyl group of F95Y increases the polar character of a largely hydrophobic pocket and stabilizes Glu-60, a residue important for interacting with the water network.

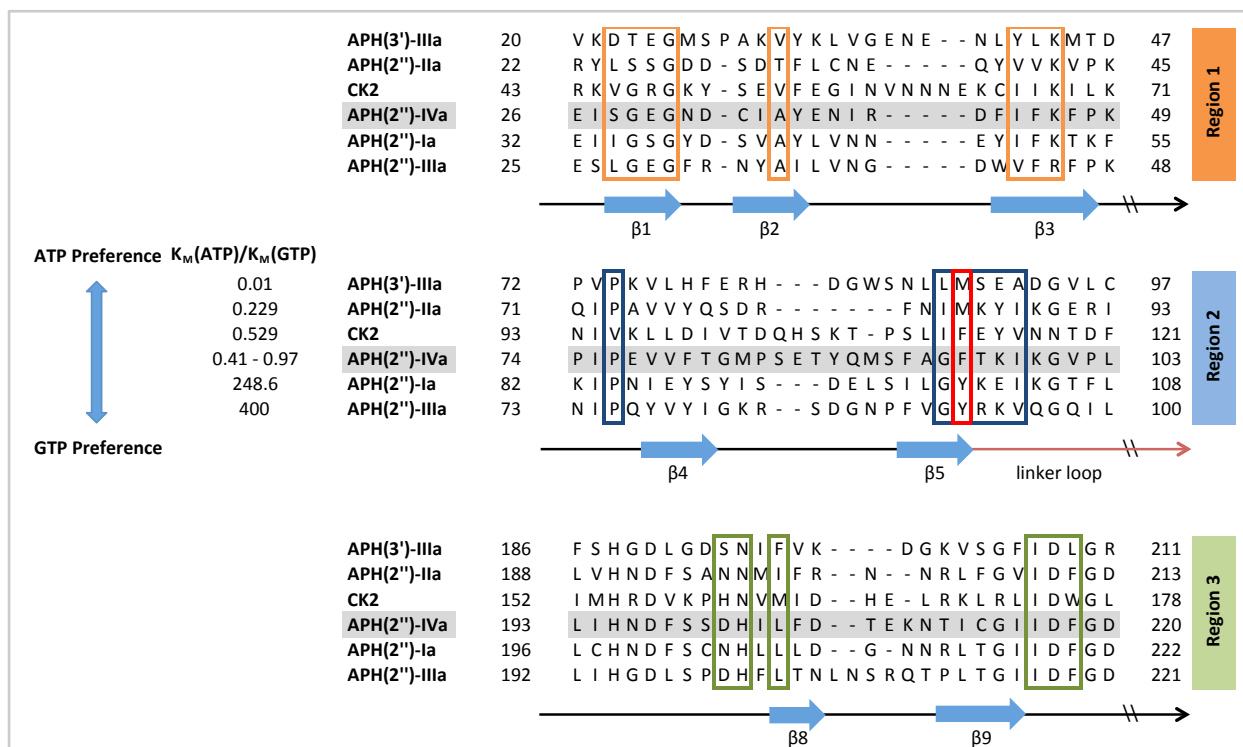


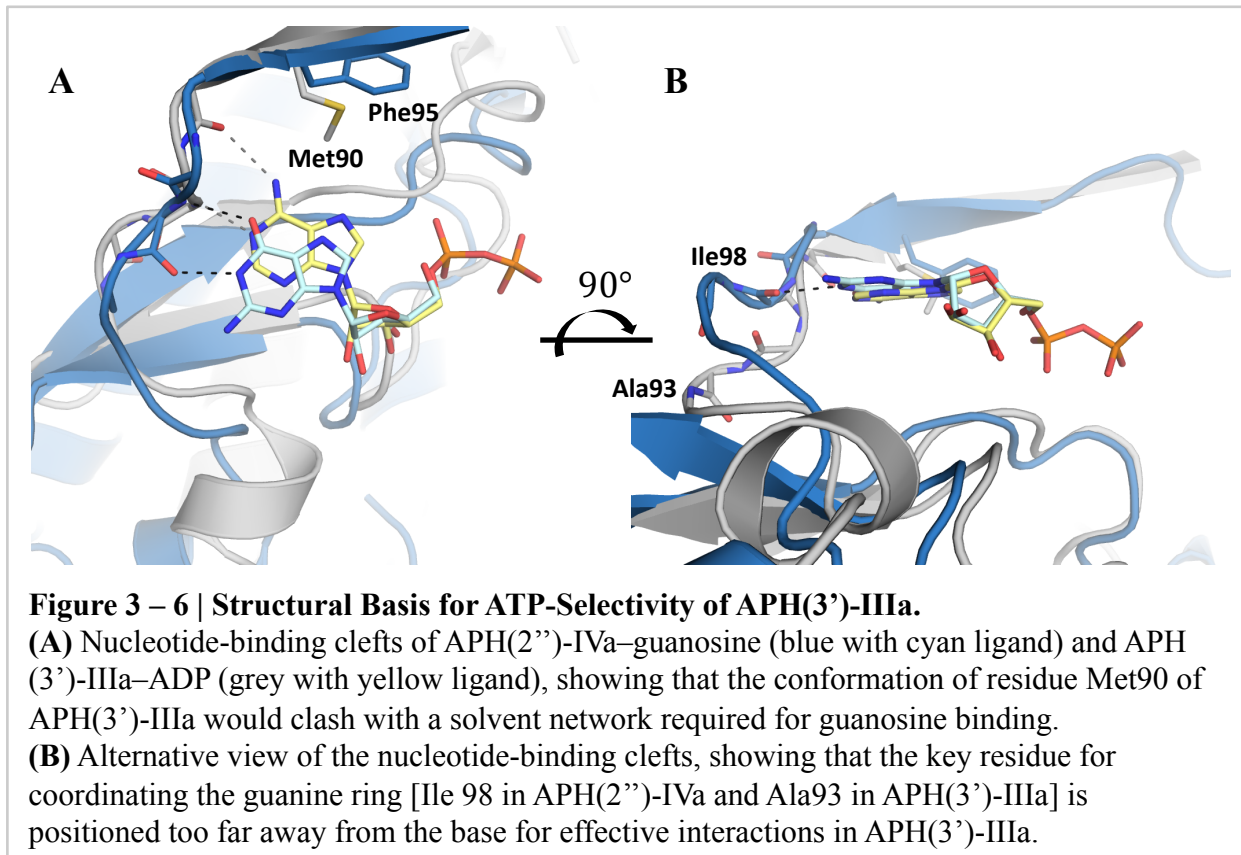
**Figure 3 – 5 | Partial Multiple Sequence Alignment of Selected APH Enzymes and CK2.**

The aligned enzymes are ordered based on increasing preference for GTP as the nucleotide substrate. Secondary structural elements are indicated below the alignment. Residues forming the nucleoside-binding site in APH(2'')-IVa are separated into three regions. Phe95 of APH(2'')-IVa and its corresponding amino acids in the other enzymes are highlighted by the red box. The alignment for APH(2'') enzymes was created with Clustal Omega (Sievers et al. 2011). APH(3')-IIIa and CK2 were aligned based on a manual structural alignment between representative structures (PDB entry 1L8T and 1LP4) and the APH(2'')-IVa–adenosine complex. The kinetic parameters for the six enzymes were taken from literature (Toth et al. 2009; Shakya and Wright, 2010; Gatica et al. 1993). The  $K_{M(ATP)}/K_{M(GTP)}$  ratio for APH(2'')-IVa varies among three independent studies due to small differences in specific experimental conditions (Toth et al. 2009; Toth et al. 2010).

More importantly, the crystal structure shows that the conformation of Tyr-95 is flexible and that its side chain hydroxyl group is able to replace a water molecule from the solvent network. In this conformation, guanosine binding is favored because of the additional hydrogen bond, and adenosine binding would be discouraged due to steric hindrance. Guanosine selectivity would be enhanced if the tyrosine residue could be trapped in this conformation, and the partial occupancy observed in the model is evidence that the surrounding residues in the binding pocket could impact nucleotide selectivity through their effect on residue 95.

Therefore, despite the effects of Phe-95 upon nucleotide specificity among APH(2'')

enzymes as indicated by these mutagenesis studies, the complete picture is clearly more complex, and nucleotide specificity is not dictated by a single amino acid. It is probable that the composite of residues around the nucleotide-binding site collectively forms a space that is adapted for the specific substrate preference of the given APH and that although individual residues such as Phe-95 play a critical role, other differences around the binding pocket also have a crucial complementary function. This is highlighted when comparing the nucleoside-binding site of APH(2'')-IVa with more distantly related enzymes, such as the ATP-specific APH(3')-IIIa. When the ADP-bound structure of APH(3')-IIIa (PDB code 1L8T) is superimposed onto the adenosine-bound and guanosine-bound structures of APH(2'')-IVa, most residues around the binding site show relatively strong positional conservation given the limited overall structural homology. However, two discrepancies are noteworthy. A substantial difference is the conformation of the interdomain linker. Although the beginning of this loop, including Ser-91 (equivalent to Thr-96 in APH(2'')-IVa) that interacts with the adenine base, is well conserved, the loop makes a sharp turn in APH(3')-IIIa thereafter, such that the backbone oxygen of residue Ala-93 (equivalent to Ile-98 in APH(2'')-IVa) is over 4 Å away from the N1 atom of the guanine moiety and therefore unavailable for hydrogen bonding (Fig. 3-6A). Secondly, the aforementioned Phe-95 of APH(2'')-IVa is replaced by a methionine residue (Met-90) in APH(3')-IIIa, which adopts a conformation such that the terminal thiomethyl group is directed toward the nucleotide and would sterically hinder the formation of a solvent network in this pocket (Fig. 3-6B). The finding that a similar orientation is not adopted by the F95M mutant of APH(2'')-IVa indicates that although residue 95 has the potential to control nucleoside binding, its effect is dependent on its conformation, which is in turn dictated by the surrounding residues forming the local microenvironment. Taken together, the inability to form an ordered solvent network and the lack of sufficient hydrogen-bonding interactions due to an altered conformation of the linker loop act synergistically to prohibit APH(3'')-IIIa from binding GTP, and neither contributing factor is controlled by individual amino acids. That other ATP-selective APHs cannot bind GTP for similar reasons is substantiated by comparisons with available structural data, such as the nucleotide-bound structure of APH(9)-Ia (Fong et al. 2010).



### 3.5.2 Comparison with CK2

Structural parallels between aminoglycoside phosphotransferases and eukaryotic protein kinases have been described since the solution of the first APH crystal structure (Hon et al. 1997). The ability to accept different types of nucleotides as a phosphate source is uncommon among protein kinases, and only very few examples have been reported to date (Gschwendt et al. 1995; Schinkmann and Blenis 1997). The best studied case is CK2 (formerly casein kinase 2), which distinguishes itself from other eukaryotic protein kinases by its dual nucleotide specificity as well as its constitutive activity, in both counts similar to APH(2'')-IVa (Niefind et al. 1999, Niefind et al. 2009). A structural comparison between adenosine-bound APH(2'')-IVa and the AMPPNP-bound catalytic subunit of CK2 from *Zea mays* (PDB code 1LP4), which is regarded as a reference structure among the over 40 deposited structures of CK2 to date (Niefind et al. 2009; Yde et al. 2005), shows clear structural divergence. However, the nucleoside-binding site is remarkably well conserved (r.m.s. deviation 0.96 Å), with almost every one of the 20 relevant residues in APH(2'')-IVa having a counterpart in CK2 (Fig. 3-7A).



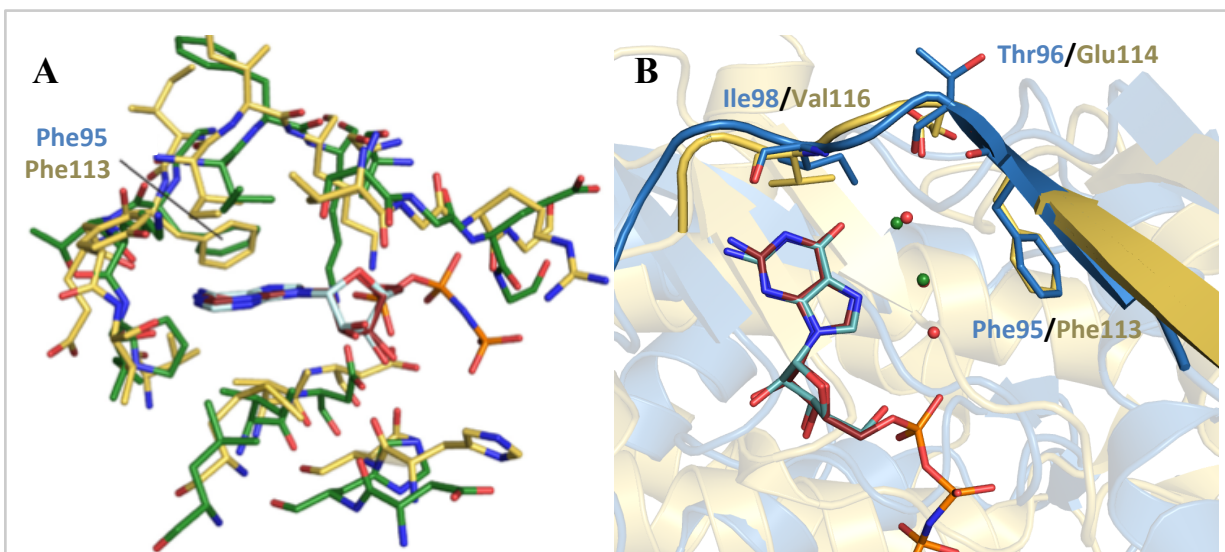


**Figure 3 – 7 | Structural Comparison Between Nucleoside-Bound Complexes of APH (2'')-IVa and CK2.**

(A) Structural superposition of residues forming the nucleoside-binding pocket of AMPPNP-bound CK2 $\alpha$  (yellow with red ligand) onto those of adenosine-bound APH(2'')-IVa (green with light cyan ligand). Despite significant discrepancies in the overall protein structure, this region shows strong structural conservation. (B) Structural superposition of GMPPNP-bound CK2 $\alpha$  onto guanosine-bound APH(2'')-IVa (blue with dark cyan ligand). The conformation of the interdomain linker, highlighted in graphic representation, and the position of key residues, shown in stick representation, are conserved. Also conserved is a solvent network, consisting of two water molecules for CK2 (green spheres) and three water molecules for APH(2'')-IVa (red spheres, with one overlapping and occluded by a green sphere).

Notably, the conformations of the linker loop in general and Phe-95 (equivalent to Phe-113 in CK2) in particular closely resemble each other in the two proteins. In addition, the basis for dual nucleotide specificity is virtually identical between the two enzymes, as evidenced by the close resemblance of the GMPPNP-bound structure of CK2 (PDB entry 1DAY) and the APH(2'')-IVa-guanosine complex. The same hydrogen-bonding pattern between the purine moiety and the interdomain loop is present in both structures, and GMPPNP binding in CK2 is also supported by a solvent network in the interior of the binding pocket (Fig. 3-7B). One difference is that for CK2, AMPPNP and GMPPNP are each stabilized by two water molecules (Niefind et al. 1999), whereas for APH(2'')-IVa, three waters are associated with guanosine binding and none are associated with adenosine binding. Such variations are not unexpected considering the structural and sequence disparity. In fact, it is intriguing to see that nature has convergently evolved the same molecular architecture supporting dual nucleotide specificity in

two enzymes that are phylogenetically only distantly related.

### 3.5.3 Implications for Inhibitor Design

Some ATP-competitive inhibitors originally developed for eukaryotic protein kinases have been shown to inhibit several aminoglycoside phosphotransferases (Daigle et al. 1997). Notably, CKI-7, an inhibitor of the isoquinolinesulfonamide family, is able to bind APH(3')-IIIa, APH(9)-Ia, and APH(2'')-Ia (Fong et al. 2011), which sets a precedent for an inhibitor active against both ATP-specific and GTP-specific APHs. If the discrepancies of the nucleotide-binding sites between APH enzymes should be too extensive to permit the optimization of a common inhibitor, then the guanine-bound structure of APH(2'')-IVa can still serve as a point of departure for the development of inhibitors against GTP-binding APHs. A number of inhibitors against CK2, belonging to diverse chemical families such as anthraquinones, coumarins, and pyrazolotriazines (Battistutta et al. 1997; Chilin et al. 2008; Nie et al. 2007), promise improved steric and chemical complementarity for a nucleotide-binding site adapted to accommodate GTP. Such molecules provide structural frameworks for the development of adjuvants to complement broad spectrum aminoglycosides currently rendered ineffective by APH(2'') enzymes. This is corroborated by a recent inhibitor profile study of various aminoglycoside kinases, which generated similar chemical scaffolds (Shakya et al. 2011).

In summary, our structural and kinetic analyses of the adenosine- and guanosine-bound complexes of wild type and mutant APH(2'')-IVa reveal the basis for nucleotide promiscuity and highlight the importance of the integrity of a solvent network in the interior of the binding cleft and the conformation of the interdomain linker in determining nucleotide specificity. These contributions to our understanding of nucleotide binding of APH enzymes serve as the first step for the structure-guided design of competitive inhibitors derived from chemical classes that have not previously been employed in the study of aminoglycoside phosphotransferases, with the ultimate aim of developing both potent and specific inhibitors against these resistance factors.

## **Chapter 4**

# **Towards the Development of an Inhibitor Against Aminoglycoside 2''-Phosphotransferases**

### **4.1 Preface**

The structural understanding of how APH(2'')-IVa interacts with its substrates discussed in the preceding sections forms the foundation for our attempts to find a small molecule that has the potential to inhibit the APH(2'') subfamily of enzymes. To date, no APH-selective inhibitors are in therapeutic use or in advanced stages of clinical development. We believe that this represents an area of opportunity for combatting aminoglycoside resistance, given the increasingly limited success of fine-tuning existing aminoglycosides. Several strategies and their associated challenges for inhibitor discovery will be explored, with the focus on a fragment screening approach that combines X-ray crystallography, nuclear magnetic resonance, and steady state kinetics. Our efforts culminated in the identification of one compound that binds competitively to the nucleotide-binding site of APH(2'')-IVa. Structural characterization of the enzyme-ligand complex and implications for inhibitor development against APH(2'') enzymes will be at the center of this chapter.

## 4.2 Introduction

Bacterial resistance against aminoglycosides has progressively forced this important and once powerful class of antibiotics into obsolescence. Though a range of mechanisms responsible for aminoglycoside resistance have been documented, the most prevalent source is a series of aminoglycoside modifying enzymes dedicated to chemically alter the drug and thus abolish its capability to interact with its intended ribosomal target. In particular, aminoglycoside phosphotransferases are known for their clinical prevalence and broad substrate spectrum. The development of next-generation aminoglycosides that bypass such resistance enzymes has seen limited success, and ongoing discoveries of AMEs jeopardize the longevity and effectiveness of these new drugs (Shi et al. 2013). Thus far, attempts at developing a potent and specific inhibitor against APHs, which would restore the activity of existing aminoglycosides, have yet to reach the clinical level. Nonetheless, benefitting from an increasingly detailed understanding of the active site architecture and molecular mechanisms of different APHs, structure-guided drug design has become an attractive option for mitigating drug resistance.

Due to the structural homology between APHs and eukaryotic protein kinases (ePKs), a variety of ATP-competitive kinase inhibitors have proven active against APHs of the same nucleotide specificity (Daigle et al. 1997). Unfortunately, the diverse modes with which APHs interact with their ligands most likely prohibits the possibility of a universal inhibitor against all APH subfamilies (Fong et al. 2011). However, compounds targeting individual subfamilies, in particular APH(3') and APH(2'') because of their broad substrate spectra, would still have significant therapeutic potential. While screening ePK inhibitors has generated promising hits for APH(3') inhibitors, efforts by our group and others have thus far not been successful in producing a convincing inhibitor candidate against APH(2'') enzymes (Shakya et al. 2011), suggesting that other avenues of hit discovery should be explored.

Although high throughput screening remains the predominant method for hit identification in the pharmaceutical community, diminishing returns and high compound attrition rates have highlighted the need for novel platforms (Scott et al. 2012). Over the past 15 years, fragment based drug discovery has emerged as a powerful alternative to conventional high throughput screening. The term “fragment” emphasizes the relatively small size of ligands that make up a typical screen, which, at the expense of specificity, allows for a broader coverage of

chemical space (Rees et al. 2004). Owing to their structural simplicity, the expected binding affinities for hits are often in the high micromolar or even millimolar range, which often renders activity assays based on competition against the natural substrate ineffective. Therefore, hit identification is achieved through more sensitive techniques that directly assess binding, such as NMR or X-ray crystallography, and advances in these biophysical methods have in part fueled the growing popularity of fragment-based screening (Blundell et al. 2002). In practice, the size of a fragment library is generally two to three orders of magnitude smaller than high throughput screens, which permits their relatively quick and inexpensive set-up and offers a degree of flexibility that is well suited for academic facilities (Hajduk and Greer 2007).

The Hol group at University of Washington has long been active in improving the efficiency of using X-ray crystallography for hit identification (Bosch et al. 2006). The relatively intensive time and labor commitments necessary to generate crystal structures have prevented this method from wide adoption as a first-pass screening technique. However, by combining numerous fragments of disparate structures into chemically stable cocktail mixtures, the sample size is reduced to a level such that crystallography becomes a viable approach in not only identifying hits, but also simultaneously generating detailed structural data that inform the ensuing process of hit to lead development (Verlinde et al. 2009).

By utilizing such a fragment screen, we have identified a small molecule inhibitor against APH(2'')-IVa. The binding of 4-amino-2-bromopyridine (ABP) has been confirmed through X-ray crystallography, NMR, and activity assays. The co-crystal structure sheds light on key interactions that may be necessary for other nucleotide competitive inhibitors against the APH(2'') subfamily. Though a poor inhibitor owing to its small size, ABP nevertheless represents a novel molecular scaffold and serves as a potential candidate for lead development through future structure-activity relationship studies.

## 4.3 Experimental Methods

### 4.3.1. Small Molecule Fragment Library Preparation

A list of 680 small molecules grouped into 68 cocktails of 10 compounds each, kindly provided by Dr. Wim Hol, was used as a starting point for the creation of a physical in-house fragment library. Based on commercial availability, price, and solubility data, a selection of 254 compounds were purchased from the following vendors: Acros, Alfa Aesar, Sigma, and TCI America. Each compound was individually assessed for DMSO and water solubility, and a total of 34 cocktail stocks were prepared in 100% DMSO (C1 – C34), where the stock concentration of each constituent compound was standardized at 100 mM. In addition, a separate set of stock solutions was created for 148 water-soluble fragment molecules, and 15 novel cocktail recipes were developed for this subset (KS1 – KS15). For stability considerations, compounds solubilized in water are individually stored, and any cocktail mixtures are prepared immediately before use. A detailed breakdown of all available compounds by cocktail is presented in appendix A.

### 4.3.2 Fragment Screening and Data Collection

For the fragment screen, APH(2'')-IVa was expressed and purified as previously described (Shi et al. 2011). Co-crystallization experiments were set up at 4 °C via the sitting-drop vapor diffusion method. A reservoir screen of several conditions known to promote APH(2'')-IVa crystal growth was employed (Shi and Berghuis 2012). Each cocktail was diluted in reservoir solution such that the final concentration of each fragment was consistently 30-fold that of the enzyme. No aminoglycoside or nucleotide substrates were included in any co-crystallization experiments. Diffraction data was collected for all conditions where crystals of sufficient quality were observed, with priority assigned to those that morphologically resemble binary crystals described in chapters two and three. In parallel, binary crystals with tobramycin were grown and used for soaking studies with all cocktails at the above concentration. Crystals were variably soaked for 0.5 – 12 hours, and diffraction data was collected unless precipitation rendered the crystal unusable. A successful crystal was obtained when 40 µl of a reservoir buffer consisting of 160 mM HEPES at pH 7.5, 160 mM potassium nitrate, 17.5% (w/v) polyethylene glycol 3350, 7% 2-propanol and 10% glycerol was equilibrated against a 3.5-µl drop composed of 1.5 µl reservoir solution, 1.5 µl protein-ligand mix, and 0.5 µl seed solution. The protein-ligand mix

contained 6 mg/ml APH(2'')-IVa and 7 mM 4-amino-3-bromopyridine in 50 mM Tris-HCl at pH 8.5, 300 mM sodium chloride, and 0.7% DMSO. Repeated iterations of seeding resulted in triangular prism-shaped crystals. A data set of 360 images with an oscillation angle of 1° were collected under cryogenic conditions (−180 °C) on a Rigaku rotating copper anode X-ray generator with a Saturn 300-mm charge-coupled device detector. All data sets were processed with the HKL2000 program suite (14), with results summarized in Table 4-1.

**Table 4 – 1 | Data Collection and Refinement Statistics of Ligand-Bound APH(2'')-IVa**

<b>APH(2'')-IVa + 4-Amino-3-bromopyridine</b>	
Resolution range (Å) <sup>a</sup>	50.0 – 2.20 (2.26 – 2.20)
Space group	<i>P</i> 2 <sub>1</sub>
<i>a</i> (Å)	42.9
<i>b</i> (Å)	101.4
<i>c</i> (Å)	73.6
$\beta$ (deg)	100.9
No. of reflections	33,479
Completeness (%)	99.7 (96.7)
Redundancy	7.0 (4.4)
Mean <i>I</i> / $\sigma$ ( <i>I</i> )	32.1 (6.4)
<i>R</i> <sub>sym</sub> <sup>b</sup>	0.059 (0.198)
<i>R</i> <sub>cryst</sub> <sup>c</sup> / <i>R</i> <sub>free</sub> <sup>d</sup>	22.1/28.5
No. of non-hydrogen atoms	
Protein	4776
Substrate	16
Solvent	50
Root-mean-square deviation	
Bond length (Å)	0.016
Bond angles (deg)	1.86
Average thermal factor (Å <sup>2</sup> )	
Protein	14.8
Substrate	18.4
Solvent	25.6

---

Ramachandran statistics (%) <sup>e</sup>	
Preferred regions	95.0
Allowed regions	5.0
Disallowed regions	0

---

<sup>a</sup> Values in parentheses refer to reflections in the highest-resolution shell.

<sup>b</sup>  $R_{\text{sym}} = \sum_{hkl} \sum_i |I_i(hkl) - \langle I(hkl) \rangle| / \sum_{hkl} \sum_i I_i(hkl)$ , where  $\langle I(hkl) \rangle$  is the average intensity of equivalent reflections and the sum is extended over all measured observations for all unique reflections.

<sup>c</sup>  $R_{\text{cryst}} = \sum_{hkl} (|F_o| - |F_c|) / \sum_{hkl} |F_o|$ , where  $|F_o|$  is the observed and  $|F_c|$  the calculated structure factor amplitude of a reflection.

<sup>d</sup>  $R_{\text{free}}$  was calculated by randomly omitting 5% of the observed reflections from the refinement.

<sup>e</sup> According to the Ramachandran plot in PROCHECK (Laskowski et al. 1993).

### 4.3.3 Structure Determination and Refinement

The crystal structure of APH(2'')-IVa in complex with 4-amino-2-bromopyridine was solved by molecular replacement with Phaser from the CCP4 program suite (15), using protein chain A of the APH(2'')-IVa-adenosine complex (PDB entry 4DT8) as the search model. Model refinement was achieved through alternating iterations of reciprocal space refinement with REFMAC (16), incorporating isotropic temperature factor and torsion-libration-screw refinement, and manual model building with the program Coot (17). The inhibitor ABP, as well as a solvent molecule DMSO, were modeled based on unambiguous density shown in the difference electron density maps ( $F_o - F_c$  and  $2F_o - F_c$ ) and refined on the basis of stereochemical constraints obtained from the PRODRG2 server (18). Solvent molecules were subsequently inserted until no significant improvements could be obtained as judged by decreases in the  $R_{\text{free}}$  value. Final refinement statistics are summarized in Table 4-1.

### 4.3.4 STD-NMR Spectroscopy

Saturation transfer difference (STD) experiments were performed using cocktails KS1 through KS15. APH(2'')-IVa was purified using a similar protocol as above, with the exception that the equilibration buffer used in the size-exclusion chromatography step consisted of 50 mM sodium phosphate at pH 7.5 and 150 mM NaCl. Each STD experiment was carried out with a 600- $\mu$ l sample composed of 10  $\mu$ M enzyme, 1 mM of each ligand from the respective cocktail, 50 mM sodium phosphate at pH 7.5, 150 mM NaCl, and 10% D<sub>2</sub>O. For each cocktail sample, a 1D proton spectra of the sample was initially acquired as reference, followed by two sets of 1024



STD scans recorded at selective saturation of protein resonances at of -0.5 ppm and between 7.8 – 8.2 ppm using a Varian INOVA 500 MHz NMR spectrometer. Difference spectra were obtained by direct subtraction of on resonance from off resonance data, and positive STD peaks were assigned to individual ligands using 2D NOESY spectra as well as any available reference 1D proton spectra from the SDBS database (SDBS 2014).

#### 4.3.5 Inhibition Assay

A similar spectrophotometric assay described in chapter 3 was used to assess inhibitory activity of the fragment molecules. Data were collected at 37 °C, where each 200- $\mu$ l sample contained a 50 mM Tris-HCl at pH 7.5, 40 mM potassium chloride, 10 mM magnesium chloride, 3.0 mM phosphoenolpyruvate, 3.0 mM gentamicin C, 360 mM  $\beta$ -nicotinamide adenine dinucleotide (reduced), 20 units/ml pyruvate kinase, and 25 units/ml lactate dehydrogenase. Enzyme at 0.10 mg/ml (final concentration) and ligand at 0.5 – 5 mM (final concentration) was added to the reaction mixture 3 min before the reaction was initiated by the addition of GTP at variable concentrations. A total of 16 concentrations between 0.03 and 2.0 mM were assayed in triplicates. Steady state kinetic parameters were analyzed using Prism 5.0 (GraphPad Software) and are summarized in Table 4-2. Kinetic parameters were obtained by fitting the kinetic data nonlinearly with the Michaelis-Menten equation for competitive inhibition:

$$v = \frac{V_{max} \cdot [S]}{K_M \left(1 + \frac{[I]}{K_I}\right) + [S]}$$

where  $k_{cat} = V_{max}/[E]$ ,  $V_{max}$  is the maximum velocity,  $[E]$  is the enzyme concentration,  $[S]$  and  $K_M$  are the concentration and the Michaelis-Menten constant of GTP, and  $[I]$  and  $K_I$  are the concentration and the Michaelis-Menten inhibition constant of the ligand.

## 4.4 Results

### 4.4.1 Fragment Screening with X-ray Crystallography and Structure Determination

Both co-crystallization screens and soaking experiments with APH(2'')-IVa were conducted with the fragment library containing 254 small molecules in 34 cocktails. Extensive attempts at soaking pre-grown APH(2'')-IVa crystals in cocktail-containing solutions ultimately proved unsuccessful, largely due to the fragile nature of the crystal. For crystals that did not fracture during soaking and for which diffraction data were collected and analyzed, none showed convincing evidence of ligand-binding in or near the active site. Co-crystallization experiments, on the other hand, generated crystals for nearly all cocktails. Based on our previous experience in crystallizing APH(2'')-IVa, we expected elongated hexagonal rod crystals to form when the enzyme is in the apo state and triangular prism-shaped crystals to form whenever a substrate occupied the active site. This morphological trend was used to triage the results of the co-crystallization screens, and a subset of thirteen cocktails were selected for subsequent optimization screens. To verify that crystal shape is a credible and convenient triage criterium and that binding of the smaller fragments followed the morphological trends we had hitherto observed with larger substrates, we also analyzed three cocktails that resulted in hexagonal rod-shaped crystals. Diffraction data collected on crystals grown in the presence of cocktails 3, 17, and 19 revealed strong difference map peaks in a pocket at the dimerization interface instead of the nucleotide-binding site. Furthermore, data sets corresponding to rod-shaped crystals as well as co-crystals with cocktails 4, 8, 13, 15, 16, 22, 25, 32, and 34, which exhibited relatively poor diffraction as indicated by their lower resolution limits, did not show any evidence of ligand-binding, suggesting that crystals must surpass an elevated quality threshold before any difference map peaks for such low affinity ligands become discernible. This poses an additional challenge for fragment screening via X-ray crystallography and significantly increases the potential for false negative results.

A data set corresponding to cocktail 27 displayed ambiguous difference map peaks in the nucleoside binding site, and screening individual cocktail components revealed that co-crystallization with 4-amino-3-bromopyridine consistently reproduced the difference map peaks observed. Upon repeated iterations of seeding, the crystal structure of APH(2'')-IVa–4-amino-3-bromopyridine complex was solved in a monoclinic space group with two protein molecules per asymmetric unit and has been refined to 2.20 Å with an  $R_{\text{cryst}}$  of 0.221 and an  $R_{\text{free}}$  of 0.285. Unit

cell parameters and overall structural features closely mirror the nucleoside-bound structures discussed in the previous chapter. Superpositions of each of the inhibitor-bound structures of APH(2'')-IVa with the adenosine- and guanosine-bound structures show modest r.m.s. deviations of 0.57 Å and 0.26 Å, respectively.

The ABP molecule binds the nucleotide-binding cleft between the N-terminal lobe and the core subdomain of the C-terminal lobe. The flat pyridine ring is sandwiched between the hydrophobic side chains of Ile-44 and Ile-215, with the N1 nitrogen atom ideally positioned to interact with the backbone amide of Ile-98 (Figure 4-1). This represents the only enzyme-ligand hydrogen bond, since the 4-amino group on the opposite side of the molecule is in a mainly hydrophobic environment and too distant for any stable interactions with potential

hydrogen acceptors. Interestingly, difference map density shows no ambiguity that the bromine atom, despite its bulk, is directed to the spatially confined interior of the binding cleft. In fact, the bromine atom snugly fits a subpocket outlined by the side chains of Lys-46, Pro-76, and Phe-95. It should be pointed out that despite the limited size of the inhibitor, no evidence of stably bound water molecules were observed in the nucleotide binding site as previously seen for the guanosine-bound structures.

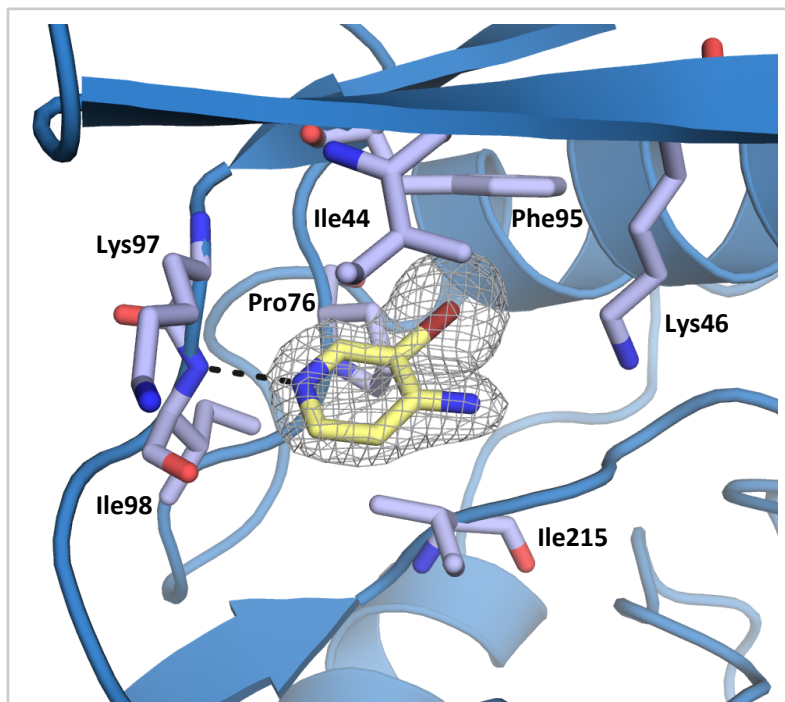


**Figure 4 – 1 | Crystal Structure of APH(2'')-IVa with a Bound Fragment Molecule.**

APH(2'')-IVa–4-amino-3-bromopyridine complex, showing the  $2F_o - F_c$  electron density (gray,  $1.0 \sigma$ , carve radius  $1.6 \text{ \AA}$ ) for the ligand (yellow stick representation). The single hydrogen-bonding interaction is represented as a black dashed line.

#### 4.4.2 Fragment Screening with NMR STD Spectroscopy

Conducted in parallel with the crystallographic screens, solution studies of APH(2'')-IVa were carried out with all compounds from the fragment library with a water solubility greater than 5 mM via NMR saturation transfer difference spectroscopy. In order to reduce the number of false-positive hits due to non-specific interactions, STD experiments were repeated at two frequencies, separately targeting aromatic and aliphatic hydrogen atoms. A representative sample of the STD spectra is shown in Figure 4-2.

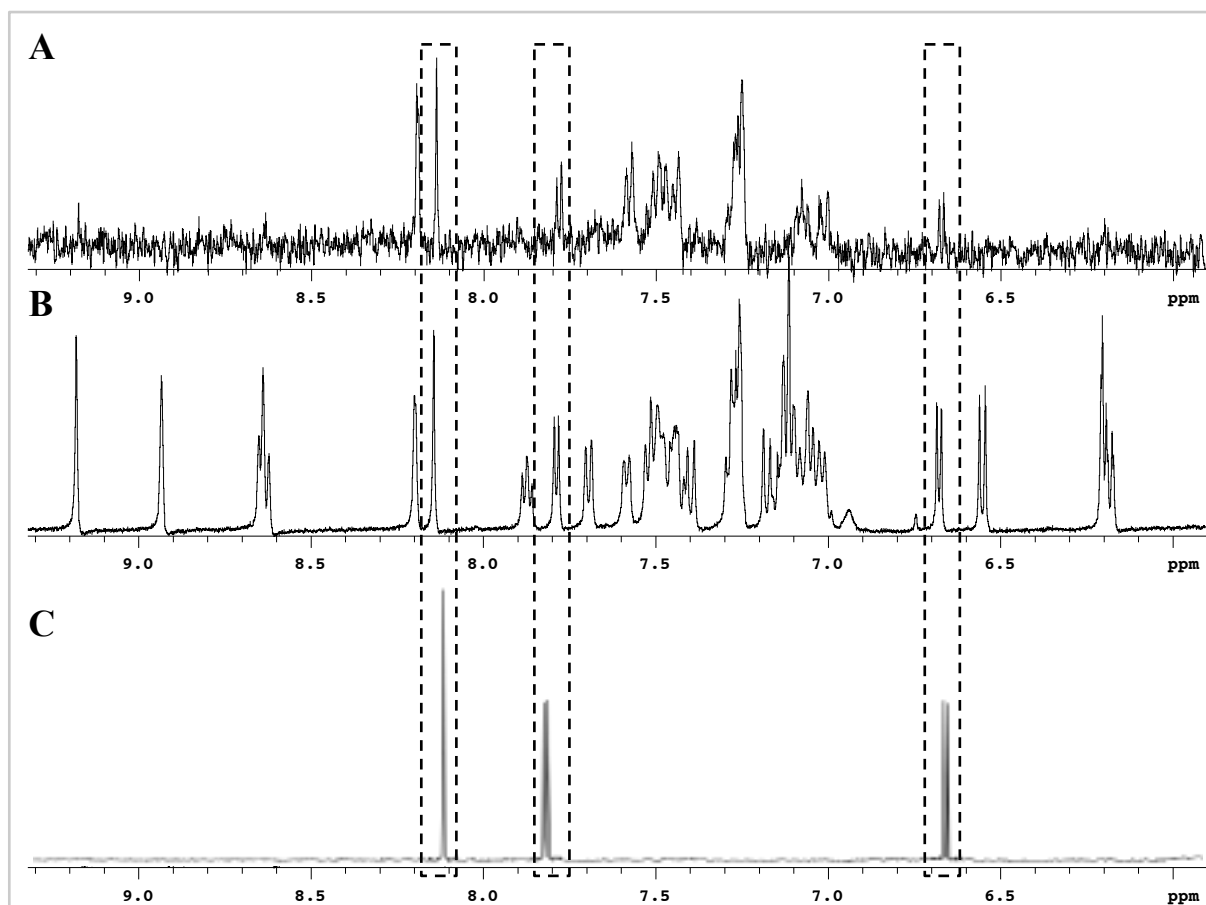
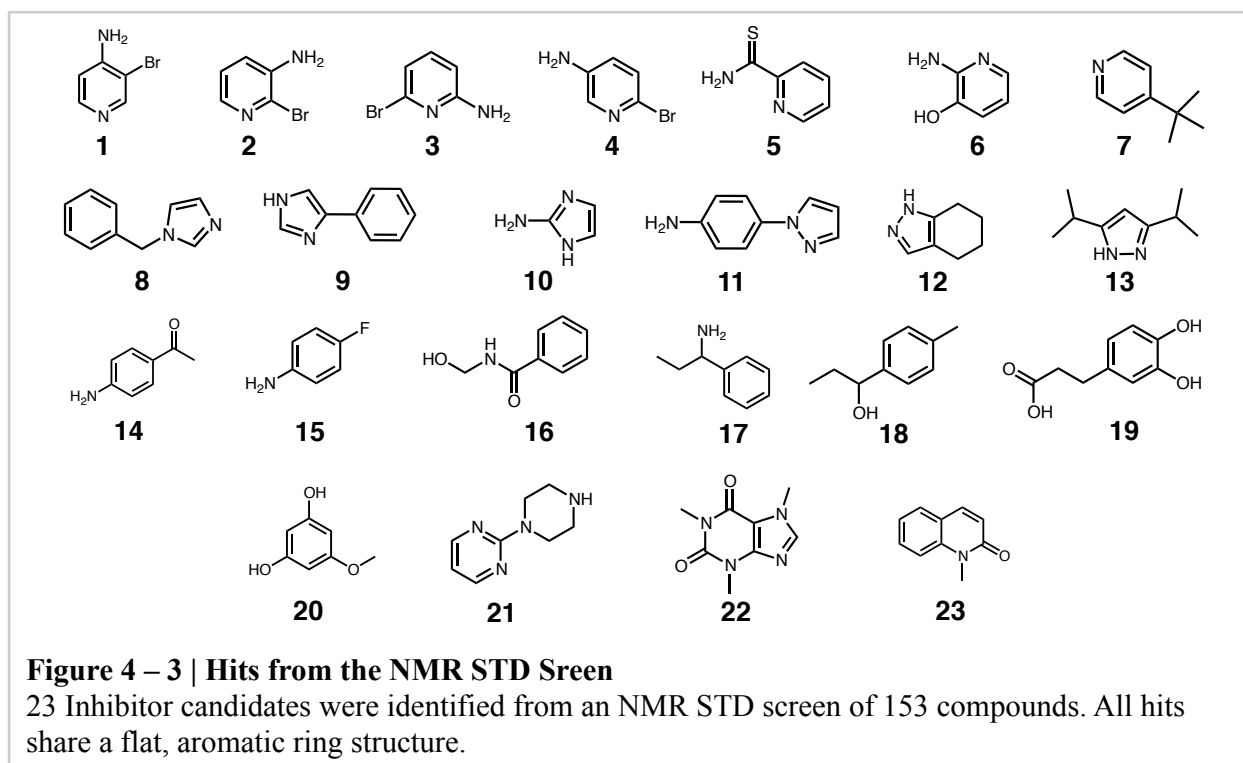


**Figure 4 – 2 | Sample NMR Saturation Transfer Difference (STD) spectra.**

(A) Aromatic region of the STD spectrum of cocktail KS3, which contains 4-amino-3-bromopyridine (ABP). (B) Corresponding chemical shift range of a 1D proton spectrum of cocktail KS3. Since peaks corresponding to ABP protons cannot be identified unambiguously, a 1D proton spectrum of ABP alone was taken (C) to confirm the chemical shifts.

With the exception of cocktail KS2, all 14 other cocktails produced at least one potential hit. In total, 23 inhibitor candidates were identified (Figure 4-3). Among these candidates, all share a flat, aromatic ring or ring system, and 74% have an aromatic nitrogen with a lone pair capable of forming a hydrogen bond with the enzyme. Twelve hits are derivatives of the heterocycles imidazole, pyrazole, or pyridine, suggesting that these moieties may serve as a good starting point to anchor the ligand in the purine binding pocket. The amino-bromopyridine scaffold is particularly well represented among the hits, with four compounds, including ABP, having this skeleton. Though sharing some structural parallels with the purines, this family of compounds does not resemble the natural substrates as much as several other candidates, such as caffeine or 2-amino-3-hydroxypyridine. However, in subsequent co-crystallization attempts with these hits, APH(2'')-IVa-ABP was the only successful enzyme-ligand complex obtained.



#### 4.4.3 Inhibition Kinetic Studies

In complement with the structural biology techniques used to screen the fragment library, steady state kinetic parameters were determined for APH(2'')-IVa in the presence of ABP. Since the activity of APH(2'')-IVa is indirectly assessed as a function of NADH consumption via a coupled reaction with pyruvate kinase and lactate dehydrogenase, and since the screen aims to

identify a nucleotide-competitive inhibitor, false positives that targeted pyruvate kinase instead of or in addition to the resistance enzyme presented a source of ambiguity. This concern was mitigated through adjusting the concentrations of the metabolic enzymes such that when GDP instead of GTP was added as a positive control, all NADH was oxidized within the first three seconds, and no measurable difference were obtained in the presence or absence of the fragment molecules. As expected, the inhibitory activity of ABP was only detectable at millimolar concentrations of the ligand, and the Michaelis-Menten inhibition constant was determined to be  $7.9 \pm 1.5$  mM. The  $k_{cat}/K_M$  value obtained for the GTP control is approximately three-fold lower than the previously reported parameters (Shi and Berghuis 2012). This is likely due to small differences in the experimental conditions. For example, gentamicin instead of tobramycin was used as the aminoglycoside in this study, and differences in the phosphate acceptor have been correlated with variations in kinetic parameters of within one order of magnitude (Toth et al. 2010). A detailed kinetic characterization of the remaining molecules from our NMR STD studies were not carried out because a preliminary assay revealed that ABP was the only compound for which inhibitory activity at low-millimolar concentrations was observed.

## 4.5 Discussion

### 4.5.1 Strategies and Challenges in Inhibitor Discovery for APH(2'') Enzymes

The search for an APH inhibitor has now persisted over two decades, and ever since the elucidation of the first APH crystal structure, intense focus has been placed on adapting known kinase inhibitors due to the structural homology of the nucleotide-binding site of APHs and eukaryotic kinases (Daigle et al. 1997; Boehr et al. 2001). Though this strategy has been validated by several promising hits, mostly of the isoquinolinesulfonamide family, ensuing structural and functional studies have made clear that a pan-APH inhibitor is unattainable given the diversity of this class of enzymes (Fong et al. 2011; Shakya et al. 2011). In particular, screening ePK inhibitors have not resulted in a convincing hit for APH(2'') enzymes. Since all APH(2'') enzymes are capable of accepting GTP as a phosphate donor whereas most ePK inhibitors tested were originally developed against ATP-specific kinases, it is tempting to ascribe the dearth of success to structural variations in the active site that also result in differences in nucleotide specificity. This hypothesis led us to investigate the potency of a number of inhibitors developed against CK2, which shares nearly identical structure and mechanism of nucleotide binding with APH(2'')-IVa, as discussed in the previous chapter. Our analyses have shown that despite these similarities, CK2 inhibitors and their analogues have not demonstrated appreciable inhibition towards APH(2'')-IVa, suggesting that structural nuances in the active site beyond the known elements that control nucleotide binding play decisive roles in inhibitor development. Further, these studies accentuate a limitation of the ePK inhibitor adaptation strategy, namely that it focuses on similarities and de-emphasizes differences between ePKs and APHs. Yet, it is through exploring those differences that ligand selectivity for APHs can be achieved and toxicities minimized. While using ePK inhibitors as a point of departure for more refined structure-activity relationship studies bypasses significant challenges of the early hit generation process, the relatively large, “drug-like” size and chemical properties of these inhibitors necessarily impose some bias that would not constrain *de novo* approaches.

Other avenues of APH inhibitor discovery, including modifying the 2-deoxystreptamine core to produce non-carbohydrate aminoglycoside analogues, and exploring uncompetitive inhibition using cationic peptides, have yet to produce a lead with sub-millimolar potency (Welch et al. 2005; Boehr et al. 2003). To our knowledge, a high-throughput screen with a broader coverage of chemical space aimed at generating new scaffolds for inhibitor development

has not yet been attempted on APH enzymes, especially those of the APH(2'') family which includes the clinically problematic bifunctional enzyme AAC(6')-Ia/APH(2'')-Ia. To circumvent the high set-up costs necessitated by a traditional high-throughput screen, we chose a fragment-based inhibitor screening approach. The small size of hits offers added flexibility in the lead optimization phase through structure-based growth of the molecule, yet simultaneously imposes a limitation of fragment-based approaches: fewer quality interactions with the target imply low initial affinity, thus presenting challenges in accurate detection during screening. In fact, we have shown that using any one screening method will likely result in a large number of false positives, and it is through a combination of structural and functional techniques that we were able to hone in on one compound.

#### 4.5.2 Key Elements of Inhibitor Binding

Hits obtained from the NMR STD screen interact with the resistance enzyme, yet little information concerning the nature and location of those interactions can be inferred from this data alone. Analyzing their chemical structures in light of the APH(2'')-IVa-ABP crystal structure sheds light on key elements that influence inhibitor binding at the desired site as opposed to non-specific interactions with the enzyme. The binding of 4-amino-2-bromopyridine involves similar protein-ligand interactions observed for the natural substrates. In particular, the hydrogen bond with Ile-98 of the linker loop is well conserved not only among all APH(2'')-IVa-nucleoside complexes, but also widely observed for ePK-inhibitor structures (La Pietra et al. 2013; Carbain et al. 2014). The prevalence of this interaction among enzyme-ligand complexes and the absence of any other stabilizing hydrogen bonds for ABP underlines the pertinence of this hydrogen bond donor in inhibitor development. Thus, it is not a surprise that compounds 14, 15, 16, 17, 18, 19, and 20 failed to bind since none of them have a suitable lone pair to support this hydrogen bond. Compounds 22 and 23 likely interact with APH(2'')-IVa non-specifically for the same reason, since the methyl substitution on the relevant nitrogen atom would sterically hinder an interaction with the lone pair, not to mention that the lone pair itself occupies a p-orbital for these molecules instead of an sp<sup>2</sup> orbital that would have the proper geometry for hydrogen bond formation. Steric hindrance is also likely the major reason compound 21 failed to crystallize with APH(2'')-IVa. Although the pyrimidine moiety has available lone pairs, the piperazine substitution at the C2 position would clash with the linker loop of the enzyme if the



aromatic ring occupied a similar region as seen for ABP. Indeed, compounds 5, 9, and 11 all feature a bulky substituent ortho to the aromatic nitrogen bearing the lone pair, and would lead to steric clashes with residues of the linker loop.

Among the imidazole and pyrazole derivatives, compounds 8, 9 and 11 feature an additional aromatic ring. Given the flat, hydrophobic nature of the subpocket, it is possible that these molecules could bind non-specifically in two opposite orientations, thus further decreasing the overall binding affinity. Of the seven pyridine derivatives, four are decorated with an amino and a bromo group (compounds 1, 2, 3 and 4). Nevertheless, crystallographic and kinetic data both point towards ABP (compound 1) as the best inhibitor candidate. This result can be rationalized by observing the tight fit of the bromo group in the interior of the binding cleft. The 3C position does not present any steric clashes, and the electronegative bromine atom has the ideal geometry to form a halogen- $\pi$  interaction with the side chain of Phe-95 (Figure 4-4 and Table 4-2).

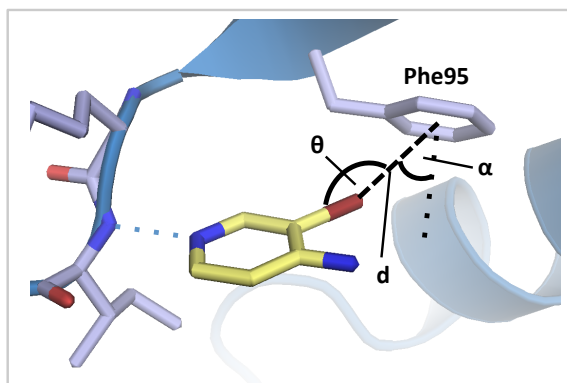


**Figure 4 – 4 | Key Interactions Between APH(2'')-IVa and ABP.**

The 4-amino-3-bromopyridine is stabilized by a hydrogen bond (blue dashed line) and a halogen bond (black dashed line). Key parameters of the halogen bond ( $d$ ,  $\alpha$ ,  $\theta$ ) between 4-amino-3-bromopyridine and the gatekeeper residue Phe95 are illustrated.

**Table 4 – 2 | Key Parameters of Halogen Bonds in Protein-Ligand Complexes**

Parameter	Empirical Mean *	Phe95 – ABP-Br
$d$ (Å)	3.9	4.1
$\alpha$ (deg)	31.5	30
$\theta$ (deg)	153.3	155

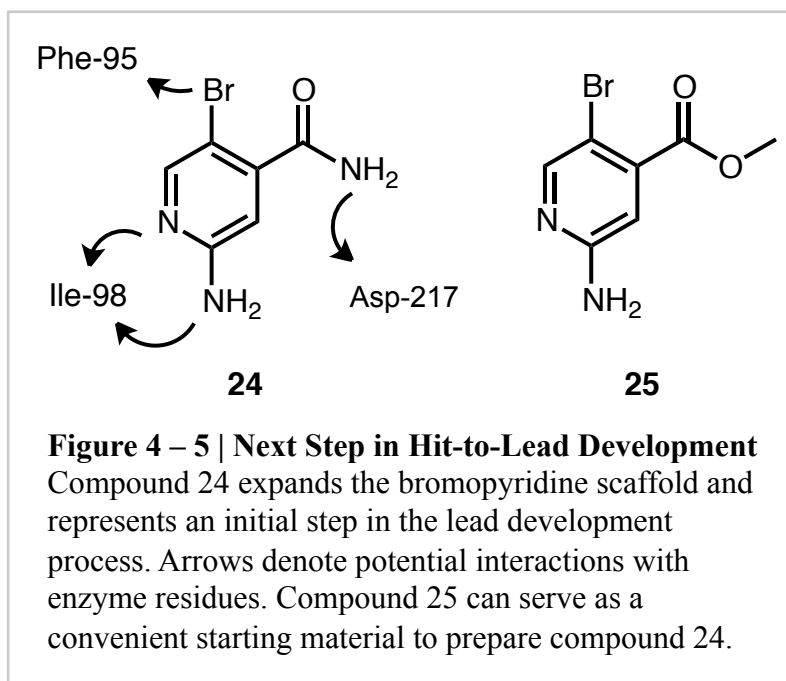
\* Statistical mean of 29 PDB entries for a total of 53 C-Br  $\cdots$   $\pi$  interactions (Lu et al. 2010).

Though traditionally of modest prominence due to the lack of robust evaluation algorithms, halogen bonds have been shown to significantly improve ligand binding to their target protein, and their growing popularity in structure-based drug discovery has even led to the inception of halogen-enriched fragment libraries (Xu et al. 2011; Wilcken et al. 2012). Intriguingly, as described in the previous chapter, Phe-95 is replaced by the aromatic tyrosine in GTP-selective APH(2'') enzymes, while ATP-selective APHs and ePKs tend to have residues

with smaller, non-aromatic side chains such as methionine or leucine, which are not capable of halogen bond formation. Thus, our crystal structure suggests that the gatekeeper residue is not only involved in influencing nucleotide specificity, but may also serve as an important element to consider in the design of APH(2'')-specific inhibitors.

#### 4.5.3 Potential Directions for Hit-to-Lead Development

Given its low molecular weight, ABP is ideally suited as an anchor for structure-guided inhibitor development. Known nucleoside-bound structures reveal that the linker loop forms at least one more interaction with the purine through either Thr-96 or Thr-98 (Shi and Berghuis, 2012). A proton donor at the C6 position of ABP would be well positioned to form such an interaction and potentially improve binding affinity. In terms of growth, ABP is already nestled against the linker loop and the hydrophilic interior of the nucleoside pocket. Thus, a natural space for expansion is presented by the positions normally occupied by the ribose and the



triphosphate moieties, the same orientation towards which the 4-amino group of ABP is directed. In our crystal structure, the 4-amino group of ABP is 4.2 Å away from the carboxyl group of the Asp-217 side chain. If the amino group were replaced by an amide instead, the nitrogen protons would be in an appropriate range to hydrogen bond with Asp-217. Having an amide group in this position would also permit further growth of the molecule in this direction with relative ease. Because of these considerations, we propose that compound 24 could be a first step in the hit-to-lead development process (Figure 4-5). Although compound 24 is currently not commercially available, there is little doubt concerning its synthetic feasibility since the preparation of the

corresponding methyl ester (compound 25) is well documented in literature (Bergeron et al. 2006).

In subsequent steps of evaluating the structure-activity relationship, groups of varying size and chemical property could be added through the amide linkage to probe for complementarity with a number of hydrophilic side chains that form this region, such as Lys-46, Asp-201 and His-202 (Fig. 4-6). Interestingly, while residues Lys-46 is well conserved among APHs and ePKs alike due to its critical roles in phosphate coordination, residues Asp-201 and His-202 are conserved only within the APH(2'') family, thus presenting an additional opportunity to achieve selectivity. This strategy of starting with an anchor at the purine binding site and expanding the molecule towards the outer areas of the nucleotide cleft to improve affinity and pharmacokinetic properties has been successfully applied in the design of several protein kinase inhibitors (Jimenez et al. 2013; Staben et al. 2014).

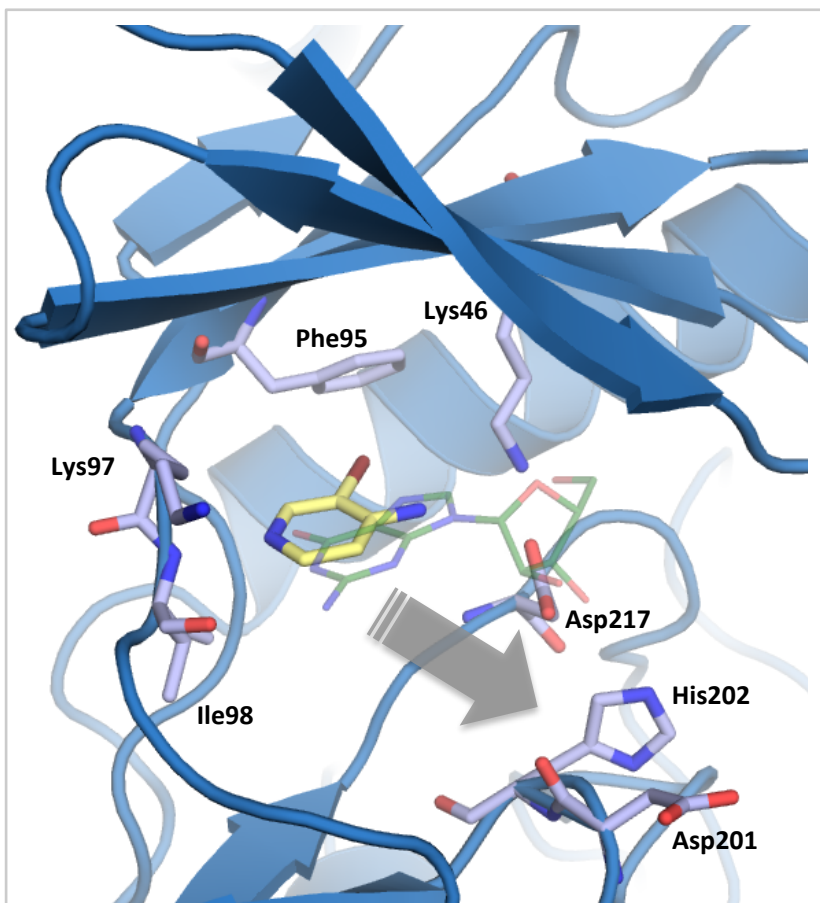


**Figure 4 – 6 | Growth Potential for ABP.**

The ABP ligand (yellow) and several residues lining the nucleotide binding cleft (light blue) are shown in stick representation. The expected position of a guanine molecule is shown in semi-transparent green. An amide linkage could be explored to extend the fragment towards outer cleft that interacts with the ribose moiety (grey arrow).

In summary, our structural and kinetic analyses of the APH(2'')-IVa-ABP have validated a novel scaffold for inhibitor development against APH(2'') enzymes. Through comparisons with

available structural data and non-productive hits from our NMR analysis, we rationalized key structural elements that anchor the fragment to the nucleotide binding site and proposed directions for expanding the molecule to achieve improved affinity and specificity. These contributions to our understanding of APH(2'')-ligand interactions advance an underexplored strategy of overcoming drug resistance and serve as an early step for the structure-guided design of inhibitor adjuvants against this family of aminoglycoside phosphotransferases.

## Chapter 5

### Conclusions

In the preceding chapters, we have undertaken a study of aminoglycoside resistance by phosphorylation from a mainly structural perspective, with the focus on one resistance enzyme, APH(2'')-IVa. This research was conducted with the aim of gaining a thorough understanding of the molecular interactions that underlie substrate binding for APH(2'')-IVa and related enzymes, and leveraging the insights obtained in the discovery of novel small molecule inhibitors targeting aminoglycoside phosphotransferases.

In chapter two, we examined the characteristics of the aminoglycoside binding pocket of APH(2'')-IVa. Using crystal structures of the apo enzyme as well as two aminoglycoside-bound forms, we were able to show that a conformational change occurs upon aminoglycoside binding, where the N-terminal lobe and the helical region of the C-terminal lobe both shift towards the core-region. These molecular movements lead to a more compact overall structure and create additional hydrogen bonding interactions that stabilize the bound aminoglycoside. Such a conformational change is not observed for APH(2'')-IIa, thus highlighting the diversity in binding modes among closely related APH enzymes. A comparison of the special orientation of the enzyme-substrate interactions versus rRNA-aminoglycoside interactions reveal that target mimicry is not an evident strategy used by this enzyme to achieve resistance, as opposed to other well-studied APHs, such as APH(3'')-IIIa. Specific differences near positions 1 and 5 of the antibiotic's central ring harbor potential for developing next-generation aminoglycosides that can evade resistance.

Chapter three revolves around the nucleotide selectivity of aminoglycoside kinases. Some APHs are ATP-specific while others are GTP-specific. APH(2'')-IVa, being dual nucleotide selective, presents an interesting opportunity to contrast ATP and GTP binding at the same active site. Crystal structures of the enzyme in complex with adenosine and guanosine demonstrate that the enzyme does not undergo conformational changes depending on which substrate is bound. Rather, distinct binding templates at the linker region anchor the purine moieties of adenosine and guanosine in different positions, thus accommodating their respective hydrogen bonding pattern preferences. In effect, while the ribose portion of each nucleoside is situated in a nearly identical location, the guanine moiety binds less deeply in the binding cleft compared to the

adenine moiety, and the resulting space in the interior of the binding cleft is occupied by a stable network of three water molecules. We subsequently undertook a residue-by-residue comparison of the active site architecture of ATP- and GTP-specific APHs based on available crystal structures, and proposed that nucleotide specificity of APH enzymes in general is controlled by at least two structural elements: the conformation of the linker loop and the identity of the gatekeeper residue.

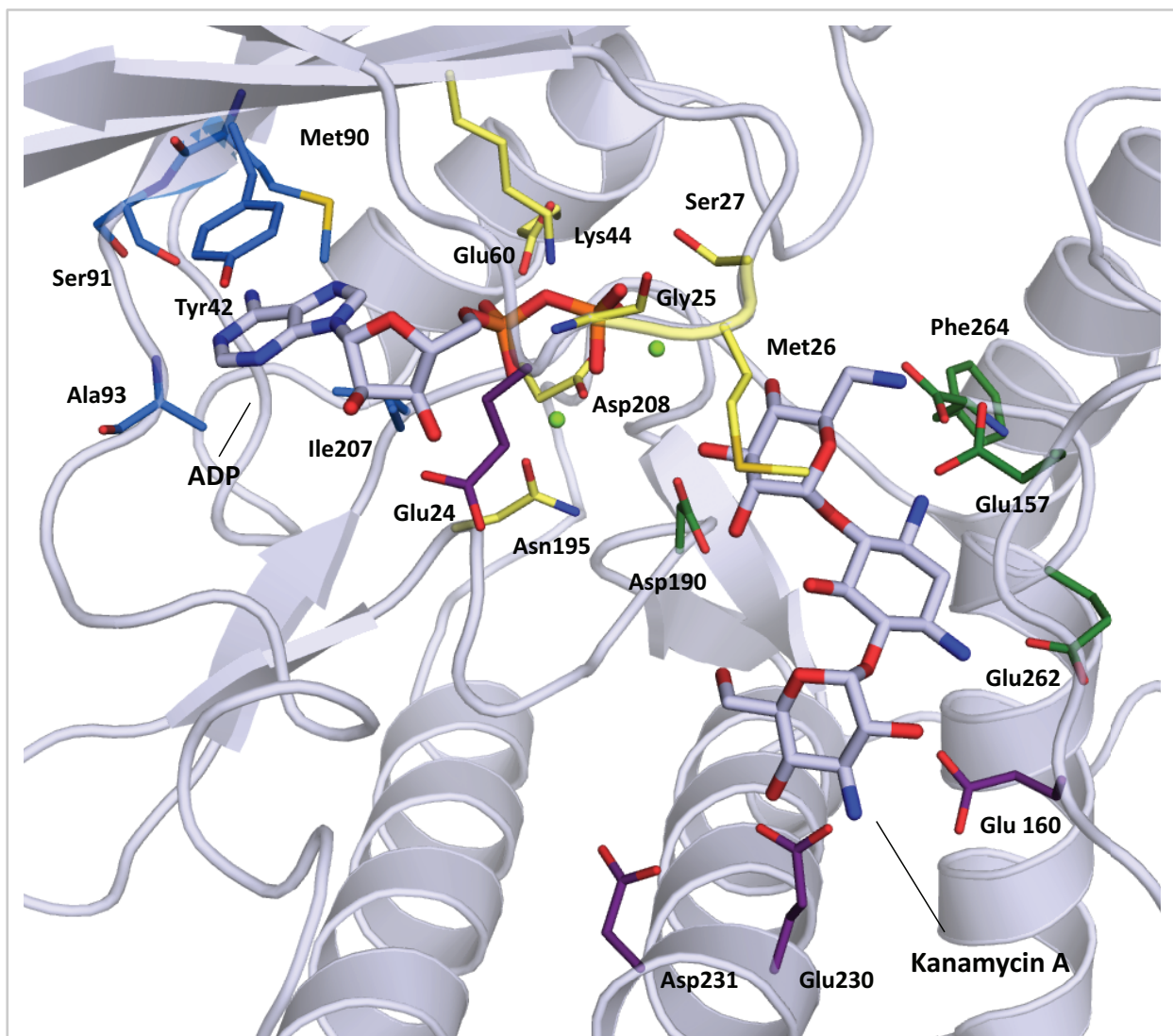


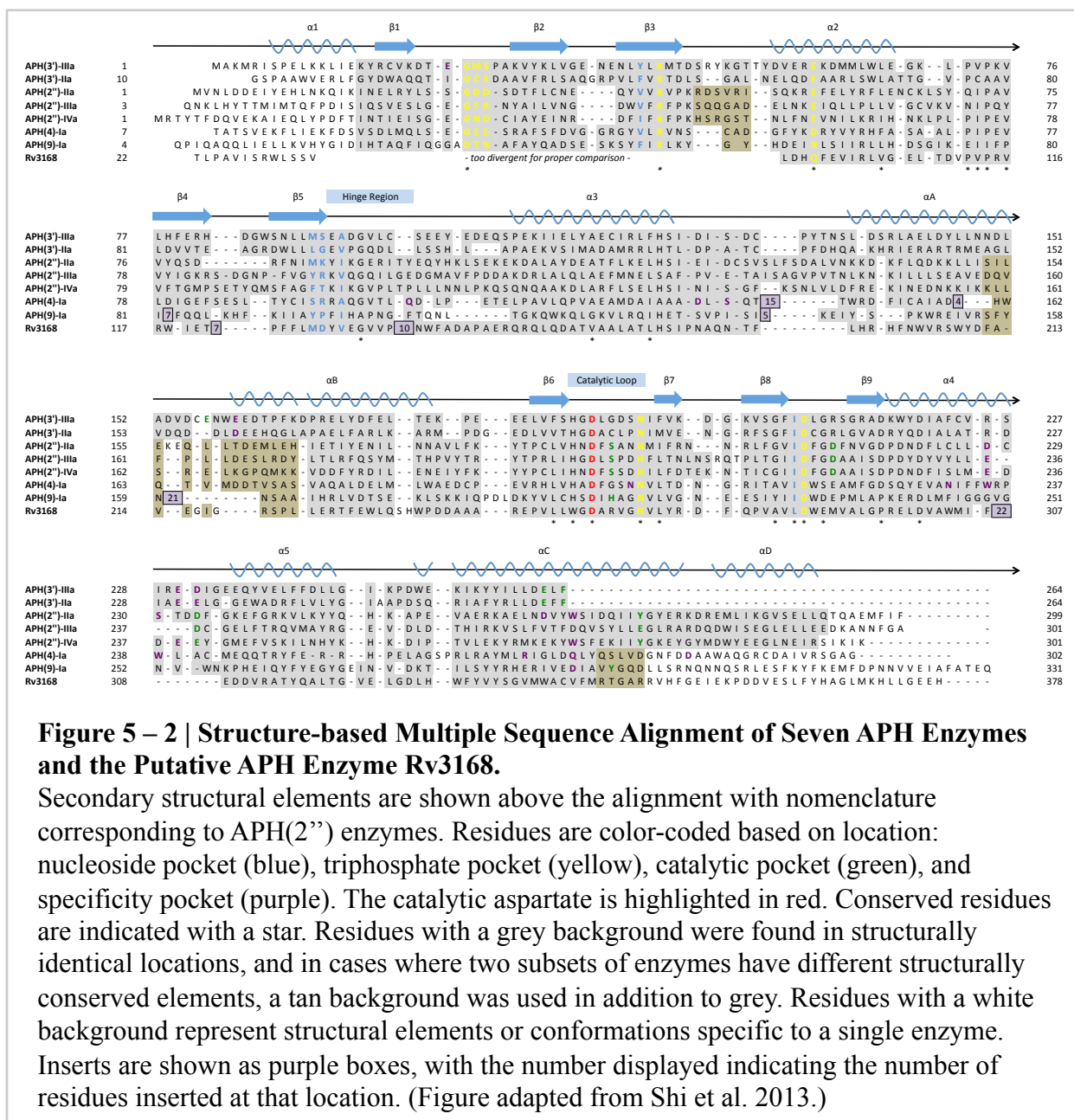
**Figure 5 – 1 | Cartoon Representation of APH(3')-IIIa (PDB Entry 1L8T) with ADP and Kanamycin A in Stick Representation.**

Residues important for substrate binding are displayed in stick representation and colored based on location: nucleoside pocket (blue), triphosphate pocket (yellow), catalytic pocket (green), and specificity pocket (purple). Two magnesium ions important for phosphate binding are shown as light green spheres. (Figure adapted from Shi et al. 2013.)

Using two mutants, we conducted a structure-activity relationship study and showed that gatekeeper residues with small side chains such as leucine or methionine favor the binding of adenosine, while bulkier residues such as tyrosine will shift the binding affinities in favor of guanosine. The impact of this residue on nucleotide specificity has recently been validated on the ATP-preferring APH(2'')-IIa, which became GTP-selective after the gatekeeper residue was mutated from a methionine to a tyrosine (Bhattacharya et al. 2013).

In the fourth chapter, we presented a nucleotide-competitive inhibitor, validated through NMR, functional assays, and X-ray crystallography. The small molecule, 4-amino-3-bromopyridine, was discovered from screening a fragment library of 254 compounds against APH(2'')-IVa. Given the small size of the compound, it is no surprise that significant inhibition was only observed at millimolar concentrations. Nevertheless, the crystal structure informed on key elements that promoted ligand binding, including a halogen interaction with the aromatic side chain of the gatekeeper residue, and led us to propose specific directions for “growing” the fragment molecule. 4-Amino-3-bromopyridine, distinct in both chemical structure and mechanism of binding compared to potential inhibitors of ATP-selective APHs, represents a novel scaffold for inhibitor development against GTP-selective aminoglycoside kinases (Fong et al. 2011; Stogios et al. 2013).

Consolidating the preceding results with crystal structures of other APH enzymes, we now have enough information to present a comprehensive picture on how this class of resistance enzyme interacts with its nucleotide and aminoglycoside substrates (Figure 5-1). The active site can be deconstructed into four distinct subsites: the nucleoside pocket, the triphosphate pocket, the catalytic pocket, and the specificity pocket. As our understanding of aminoglycoside phosphotransferases deepen, we become increasingly aware of the challenges facing the discovery of a successful APH inhibitor. Although all APHs share a similar fold, considerable sequence disparity create a plethora of slightly varying active sites, each adapted to bind a specific combination of nucleotide and aminoglycoside substrates. The intimate relationship between structure and sequence is summarized in figure 5-2, which depicts the primary sequences of all APHs with published crystals structures, generated from a manual structural alignment (Shi et al. 2013). Looking forward, it is our hope that this reservoir of information can serve as a building block in our struggle to overcome aminoglycoside resistance.



In essence, we believe that a thorough understanding of the structure and mechanism of aminoglycoside kinases, both in terms of how they are similar to as well as how they are different from eukaryotic protein kinases, is a necessary prerequisite for successful inhibitor design. Reinvigorating the potency of aminoglycosides is a small but important step in stemming the rapidly growing prevalence of antibiotic resistance that threatens the well-being of every member of society in hospital settings and beyond. We hope that our contributions will advance



the drug resistance community's progress towards the development of novel antimicrobial agents through structure-guided drug discovery.

## References

- Abbassi MS, Achour W and Hassen AB (2007) High-level gentamicin-resistance *Enterococcus faecium* strains isolated from bone marrow transplant patients: accumulation of antibiotic resistance genes, large plasmids and clonal strain dissemination. *Intl. J. Antimicrob. Agents* 29: 658.
- Aggen JB, Armstrong ES, Goldblum AA, Dozzo P, Linsell MS, Gliedt MJ, Hildebrandt DJ, Feeney LA, Kubo A, Matias RD, Lopez S, Gomez M, Wlasichuk KB, Diokno R, Miller GH and Moser HE (2010) Synthesis and spectrum of the neoglycoside ACHN-490. *Antimicrob. Agents Chemother.* 54(11): 4636.
- Alam MM, Kobayashi N, Ishino M, Sumi A, Kobayashi KI, Uehara N and Watanabe N. (2005) Detection of a novel *aph(2'')* allele (*aph[2'']-Ie* conferring high-level gentamicin resistance and a spectinomycin resistance gene *ant(9)-Ia (aad9)* in clinical isolates in Enterococci. *Microb. Drug Resist.* 11(3):239.
- Allen HK. (2014) Antibiotic resistance gene discovery in food-producing animals. *Curr. Opin. Microbiol.* 19C:25.
- Allison KR, Brynildsen MP and Collins JJ. (2011) Metabolite-enabled eradication of bacterial persisters by aminoglycosides. *Nature.* 473:216.
- Aminov RI. (2010) A brief history of the antibiotic era: lessons learned and challenges for the future. *Front. Microbiol.* 1(134): 1.
- Avent ML, Rogers BA, Cheng AC and Paterson DL. (2011) Current use of aminoglycosides: inductions, pharmacokinetics and monitoring for toxicity. *Int. Med. J.* 41: 441-8.
- Badarau A, Shi Q, Chow JW, Zajicek J, Mobashery S and Vakulenko S. (2008) Aminoglycoside 2''-phosphotransferase type IIIa from *Enterococcus*. *J. Biol. Chem.* 283:7638.
- Battistutta R, Sarno S, De Moliner E, Papinutto E, Zanotti G and Pinna L. (2000) The replacement of ATP by the competitive inhibitor emodin induces conformational modifications in the catalytic site of protein kinase CK2. *J. Biol. Chem.* 275:29618.
- Beck B and Cooper MA. (2013) Aminoglycoside antibiotics in the 21<sup>st</sup> century. *ACS Chem. Biol.* 8: 105-15.
- Bell SG. (2003) Antibiotic resistance: is the end of an era near? *Neonatal Netw.* 22(6):47.
- Bergeron P, Farthing CN, Jones, SD, Liebeschuetz JW, Lively SE, McGee LR, McKendry S, Sheppard D, and Young SC. Bisaryl-sulfonamides. *PCT Int. Appl.* WO 2006/020830 (A2), 23 Feb. 2006.
- Bhattacharya M, Toth M, Smith CA and Vakulenko SB. (2013) Bulky “gatekeeper” residue changes the cosubstrate specificity of the aminoglycoside 2''-phosphotransferase IIa. *Antimicrob. Agents Chemother.* 57(8): 3763-6.
- Blundell TL, Jhoti H and Abell C. (2002) High-throughput crystallography for lead discovery in drug design. *Nat. Rev. Drug Design.* 1:45-52.

- Boehr DD, Lane WS and Wright GD. (2001) Active site labeling of the gentamicin resistance enzyme AAC(6')-APH(2'') by the lipid kinase inhibitor wortmannin. *Chem. & Biol.* 8: 791-800.
- Boehr DD, Draker K, Koteva K, Bains M, Hancock RE and Wright GD. (2003) Broad-spectrum peptide inhibitors of aminoglycoside antibiotic resistance enzymes. *Chem. & Biol.* 10:189-96.
- Böttger EC and Springer B. (2008) Tuberculosis: drug resistance, fitness, and strategies for global control. *Eur. J. Pediatr.* 167: 141-8.
- Borovinskaya M, Pai RD, Zhang W, Schuwirth BS, Holton JM, Hirokawa G, Kaji H, Kaji A and Cate JHD. (2007) Structural basis for aminoglycoside inhibition of bacterial ribosome recycling. *Nat. Struct. Mol. Biol.* 14(8): 727-32.
- Bryan LE and Van Den Elzen HM. (1976) Streptomycin accumulation in susceptible and resistance strains of *Escherichia coli* and *Pseudomonas aeruginosa*. *Antimicrob. Agents Chemother.* 9(6): 928.
- Bryan LE and Van Den Elzen HM. (1977) Streptomycin and gentamicin accumulation by bacteria: a model for entry of streptomycin and gentamicin in susceptible and resistant bacteria. *Antimicrob. Agents Chemother.* 12(2): 163.
- Buckstein MH, He J and Rubin H. (2008) Characterization of nucleotide pools as a function of physiological state of *Escherichia coli*. *J. Bacteriol.* 190(2): 718.
- Burk DL and Berghuis AM. (2002) Protein kinase inhibitors and antibiotic resistance. *Pharmacol. Ther.* 93:10.
- Burk DL, Hon WC, Leung AK and Berghuis AM. (2001) Structural analyses of nucleotide binding to an aminoglycoside phosphotransferase. *Biochemistry.* 40:8756.
- Butler MS, Blaskovich MA and Cooper MA. (2013) Antibiotics in the clinical pipeline in 2013. *J. Antibiot.* 66: 571.
- Carbain B, Paterson DJ, Anscombe E, Campbell AJ, Cano C, Echalié A, Endicott JA, Golding BT, Haggerty K, Hardcastle IR, Jewsbury PJ, Newell DR, Noble BT, Roche C, Wang LZ and Griffin RJ. (2014) 8-Substituted *O*<sup>6</sup>-cyclohexylmethylguanine CDK2 inhibitors: using structure-based inhibitor design to optimize an alternative binding mode. *J. Med. Chem.* 57:56.
- Cater AP, Clemons WM, Brodersen DE, Morgan-Warren RJ, Wimberly BT and Ramakrishnan V. (2000) Functional insights from the structure of the 30S ribosomal subunit and its interactions with antibiotics. *Nature* 407: 340.
- Chandrakanth RK, Raju S and Patil SA. (2008) Aminoglycoside resistance mechanisms in multidrug-resistant *Staphylococcus aureus* clinical isolates. *Curr. Microbiol.* 56:558.
- Chilin A, Battistutta R, Bortolato A, Cozza G, Zanatta S, Poletto G, Mazzorana M, Zagotto G, Uriarte E, Guiotto A, Pinna LA, Meggio F and Moro S. (2008) Coumarin as attractive casein kinase 2 (CK2) inhibitor scaffold: an integrate approach to elucidate the putative binding motif and explain structure-activity relationships. *J. Med. Chem.* 51:752.

- Chow JW, Zervos MJ, Lerner SA, Thal LA, Donabedian SM, Jaworski DD, Tsai S, Shaw KJ and Clewell DB. (1997) A novel gentamicin resistance gene in *Enterococcus*. *Antimicrob. Agents Chemother.* 41(3):511.
- Chow JW. (2000) Aminoglycoside resistance in enterococci. *Clin. Infect. Dis.* 31:586.
- Clardy J, Fischbach M and Currie C. (2009) The natural history of antibiotics. *Curr. Biol.* 19(11):R437.
- Collaborative Computational Project Number 4. (1994) The CCP4 Suite: Programs for protein crystallography. *Acta Crystallogr.* D50:760.
- Daigle DM, McKay GA and Wright GD. (1997) Inhibition of aminoglycoside antibiotic resistance enzymes by protein kinase inhibitors. *J. Biol. Chem.* 272:24755-8.
- Davidson RN, den Boer M, and Ritmeijer K. (2009) Paromomycin. *Trans. R. Soc. Trop. Med. Hyg.* 103(7):653.
- Davies J, Gibert W and Gorini L. (1964) Streptomycin, suppression, and the code. *PNAS.* 51:883.
- Davies J, Anderson P and Davis BD. (1965) Inhibition of protein synthesis by spectinomycin. *Science.* 149:1096.
- Davies J. (2006) Where have all the antibiotics gone? *Can. J. Infect. Dis. Med. Microbiol.* 17(5):287.
- Davies JE. (2006) Aminoglycosides: ancient and modern. *J. Antibiot.* 59(9):532.
- Davis BD, Chen L and Tai PC. (1986) Misread protein creates membrane channels: an essential step in the bactericidal action of aminoglycosides. *Proc. Natl. Acad. Sci. USA.* 83:6164.
- Davis BD. (1987) Mechanism of bactericidal action of aminoglycosides. *Microbiol. Rev.* 51(3):341.
- De Bruin AF, Gosselink MP and van der Harst E. (2012) Local application of gentamicin-containing collagen implant in the prophylaxis of surgical site infection following gastrointestinal surgery. *Int. J. Surg.* 10:S21.
- De Stasio EA, Moazed D, Noller HF and Dahlberg AE. (1989) Mutations in 16S ribosomal RNA disrupt antibiotic – RNA interactions. *The EMBO J.* 8(4):1213.
- Dienstag J and Neu HC. (1972) In vitro studies of tobramycin, an aminoglycoside antibiotic. *Antimicrob. Agents Chemother.* 1(1):41.
- Doi Y and Arakawa Y. (2007) 16S ribosomal DNA methylation: emerging resistance mechanism against aminoglycosides. *Antimicrob. Resist.* 45:88.
- Donabedian SM, Thal LA, Hershberger E, Perri MB, Chow JW, Barlet P, Jones R, Joyce K, Rossiter S, Gay K, Johnson J, Mackinson C, Debess E, Madden J, Angulo F and Zervos MJ. (2003) Molecular characterization of gentamicin-resistant *Enterococci* in the United States: evidence of spread from animals to human through food. *J. Clin. Microbiol.* 41(3):1109.
- Durso LM and Cook KL. (2014) Impacts of antibiotic use in agriculture: what are the benefits and risks? *Curr. Opin. Microbiol.* 19:37.

- Emsley P, Lohkamp B, Scott WG and Cowtan K. (2010) Features and development of Coot. *Acta Crystallogr.* D53:2126.
- Endimiani A, Hujer KM, Hujer AM, Armstrong ES, Choudhary Y, Aggen JB and Bonomo RA. (2009) ACHN-490, a neoglycoside with potent in vitro activity against multidrug-resistant *Klebsiella pneumoniae* isolates. *Antimicrob. Agents Chemother.* 53(10):4504.
- Fong DH and Berghuis AM. (2002) Substrate promiscuity of an aminoglycoside antibiotic resistance enzyme via target mimicry. *EMBO J.* 21:2323.
- Fong DH and Berghuis AM. (2009) Structural basis of APH(3')-IIIa-mediated resistance to N1-substituted aminoglycoside antibiotics. *Antimicrob. Agents Chemother.* 53:3049.
- Fong DH, Lemke CT, Hwang J, Xiong B and Berghuis AM. (2010) Structure of the antibiotic resistance factor spectinomycin phosphotransferase from *Legionella pneumophila*. *J. Biol. Chem.* 285:9545.
- Fong DH, Xiong B, Hwang J and Berghuis AM. (2011) Crystal structures of two aminoglycoside kinases bound with a eukaryotic protein kinase inhibitor. *PLoS ONE.* 6(5):e19589.
- Forge A and Schacht J. (2000) Aminoglycoside antibiotics. *Audiol. Neurootol.* 5:3.
- Fourmy D, Recht MI and Puglisi JD. (1998) Binding of Neomycin-class aminoglycoside antibiotics to the A-site of the 16S RNA. *J. Mol. Biol.* 277:347.
- Franklin K and Clarke AJ. (2001) Overexpression and characterization of the chromosomal aminoglycoside 2'-N-acetyltransferase of *Providencia stuartii*. *Antimicrob. Agents Chemother.* 45(8):2238.
- Frase H, Toth M and Vakulenko SB. (2012) Revisiting the nucleotide and aminoglycoside substrate specificity of the bifunctional aminoglycoside acetyltransferase(6)-Ie/aminoglycoside phosphotransferase(2'')-Ia enzyme. *J. Biol. Chem.* 287(52): 43262.
- Galani I, Souli M, Daikos GL, Chrysouli Z, Poulakou G, Psychogiou M, Panagea T, Argyropoulou A, Stefanou I, Plakias G, Giamarellou H and Petrikkos G. (2012) Activity of plazomicin (ACHN-490) against MDR clinical isolates of *Klebsiella pneumoniae*, *Escherichia coli*, and *Enterobacter* spp. From Athens, Greece. *J. Chemother.* 24(4):191.
- Gatica M, Hinrichs MV, Jedlicki A, Allende CC and Allende JE. (1993) Effect of metal ions on the activity of casein kinase II from *Xenopus laevis*. *FEBS Lett.* 315:173.
- Grady, D. (2013) Deadly bacteria that resist strongest drugs are spreading. *New York Times.* March 6:A13.
- Gschwendt M, Kittstein W, Kielbassa K and Marks F. (1995) Protein kinase C  $\delta$  accepts GTP for autophosphorylation. *Biochem. Biophys. Res. Comm.* 206:614.
- Hajduk PJ and Greer J. (2007) A decade of fragment-based drug design: strategic advances and lessons learned. *Nat. Rev. Drug Design.* 6:211.
- Hammerum AM and Heuer OL. (2009) Human health hazards from antimicrobial-resistant *Escherichia coli* of animal origin. *Food Safety.* 48:916.
- Hanks SK and Hunter T. (1995) The eukaryotic protein kinase superfamily: kinase (catalytic) domain structure and classification. *FASEB J.* 9:576.

- Hon WC, McKay GA, Thompson PR, Sweet RM, Yang DSC, Wright GD and Berghuis AM. (1997) Structure of an enzyme required for aminoglycoside antibiotic resistance reveals homology to eukaryotic protein kinases. *Cell*. 89:887.
- Hopwood D, Levy S, Wenzel RP, Georgopapadakou N, Baltz RH, Bhavnani S, and Cox E. (2007) A call to arms. *Nat. Rev. Drug Discov.* 6:8.
- Hollis A and Ahmed Z. (2013) Preserving Antibiotics, rationally. *N. Eng. J. Med.* 2474.
- Howells JD, Anderson LE, Coffey GL, Senos GD, Underhill MA, Vogler DL, and Ehrlich J. (1972) Butirosin, a new aminoglycoside antibiotic complex: bacterial origins and some microbiological studies. *Antimicrob. Agents Chemother.* 2(2):79.
- Iseman MD. (1994) Evolution of drug-resistant tuberculosis: a tale of two species. *Proc. Natl. Acad. Sci. USA.* 91:2428.
- Jimenez J-M, Boyall D, Brenchley G, Collier PN, Davis, CJ, Fraysse D, Keily SB, Henderson J, Miller A, Pierard F, Settimo L, Twin HC, Bolton CM, Curnock AP, Chiu P, Tanner AJ and Young S. (2013) Design and optimization of selective protein kinase C  $\theta$  (PCK $\theta$ ) inhibitors for the treatment of autoimmune diseases. *J. Med. Chem.* 56:1799.
- Kao SJ, You I, Clewell DB, Donabedian SM, Zervos MJ, Petrin J, Shaw KJ and Chow JW. (2000) Detection of the High-Level Aminoglycoside Resistance Gene *aph(2'')-Ib* in *Enterococcus faecium*. *Antimicrob. Agents Chemother.* 44(10):2876.
- Kawaguchi H. (1976) Discovery, chemistry, and activity of amikacin. *J. Infect. Dis.* 134:S242.
- La Pietra V, La Regina G, Coluccia A, Famigliani, Pelliccia S, Plotkin B, Eldar-Finkelman H, Brancale A, Ballatore C, Crowe A, Brunden KR, Marinelli L, Novellino E and Silvestri R. (2013) Design, synthesis and biological evaluation of 1-phenylpyrazolo[3,4-*e*]pyrrolo[3,4-*g*]indolizine-4,6(1*H*,5*H*)-diones as new glycogen synthase kinase-3 $\beta$  inhibitors. *J. Med. Chem.* 56:10066.
- Laskowski RA, MacArthur MW, Moss DS and Thornton JM. (1993) PROCHECK: A program to check the stereochemical quality of protein structures. *J. Appl. Crystallogr.* 26:283.
- Lewis K. (2013) Platforms for antibiotic discovery. *Nat. Rev. Drug Design.* 12:371.
- Lu Y, Wang Y and Zhu W. (2010) Nonbonding interactions of organic halogens in biological systems: implications for drug discovery and biomolecular design. *Phys. Chem. Chem. Phys.* 12:4543.
- Macfarlane ELA, Kwasnicka A and Hancock EW. (2000) Role of *Pseudomonas aeruginosa* PhoP-PhoQ in resistance to antimicrobial cationic peptides and aminoglycosides. *Microbiol.* 146:2543.
- Marshall BM and Levy SB. (2011) Food animals and antimicrobials: impacts on human health. *Clinic. Microbiol. Rev.* 24(4):718.
- Martel A, Masson M, Moreau N and Le Goffic F. (1983) Kinetic studies of aminoglycoside acetyltransferase and phosphotransferase from *Staphylococcus aureus* RPAL. *Eur. J. Biochem.* 133:515.
- Maviglia R, Nestorini R and Pennisi M. (2009) Role of old antibiotics in multidrug resistant bacterial infections. *Curr. Drug Targets.* 10:895.

- McCollister BD, Hoffman M, Husain M and Vázquez-Torres A. (2011) Nitrite oxide protects bacteria from aminoglycosides by blocking the energy-dependent phases of drug uptake. *Antimicrob. Agents Chemother.* 55(5):2189.
- McKay B and Bauerlen V. (2014) CDC: Antibiotic overuse can be lethal. *Wall Street Journal*. <http://www.wsj.com/articles/SB10001424052702304585004579419419493198620498>.
- McKay GA, Thompson PR and Wright GD. (1994) Broad spectrum aminoglycoside phosphotransferase type III from *Enterococcus*: Overexpression, purification, and substrate specificity. *Biochemistry.* 33:6936.
- McKay GA and Wright GD. (1995) Kinetic mechanism of aminoglycoside phosphotransferase type IIIa. *J. Biol. Chem.* 270(42):24686.
- Mingeot-Leclercq MP, Glupczynski Y and Tulkens PM. (1999) Aminoglycosides: Activity and resistance. *Antimicrob. Agents Chemother.* 43:11.
- Moazed D and Noller HF. (1987) Interaction of antibiotics with functional sites in 16S ribosomal RNA. *Nature.* 327:389.
- Murshudov GN, Vagin AA and Dodson EJ. (1997) Refinement of macromolecular structures by the maximum-likelihood method. *Acta Crystallogr.* D53:2126.
- Nathan C. (2004) Antibiotics at the crossroads. *Nature.* 43:899.
- Nie Z, Perretta C, Erickson P, Margosiak S, Almasy R, Lu J, Averill A, Yager KM and Chu S. (2007) Structure-based design, synthesis, and study of pyrazolo[1,5-a][1,3,5]triazine derivatives as potent inhibitors of protein kinase CK2. *Bioorg. Med. Chem. Lett.* 17:4191.
- Niefind K, Pütter M, Guerra B, Issinger OG, and Schomburg D. (1999) GTP plus water mimic ATP in the active site of protein kinase CK2. *Nat. Struct. Biol.* 6:1100.
- Niefind K, Raaf J and Issinger OG. (2009) Protein kinase CK2 in health and disease. Protein kinase CK2: from structures to insights. *Cell Mol. Life Sci.* 66:1800.
- Noone P. (1984) Sisomicin, netilmicin and dibekacin. A review of their antibacterial activity and therapeutic use. *Drugs.* 27(6):548.
- Nurrizo D, Shewry SC, Perlin MH, Brown SA, Dholakia JN, Fuchs RL, Deva T, Baker EN and Smith, CA. (2003) The crystal structure of aminoglycoside-3'-phosphotransferase-IIa, an enzyme responsible for antibiotic resistance. *J. Mol. Biol.* 327:491.
- O'Connor S, Lam LKT, Jones ND, and Chaney MO. (1976) Apramycin, a Unique Aminocyclitol Antibiotic. *J. Org. Chem.* 41(12):2087.
- Oda T, Mori T, Kyotani Y, Nakayama M. (1971) Studies on new antibiotic lividomycins. IV. Structure of lividomycin A. *J. Antibiot. (Tokyo).* 24(10):706.
- Okachi R, Kawamoto I, Takasawa S, Yamamoto M, Sato S, Sato T and Nara T. (1974) A new antibiotic XK-62-2 (Sagamicin). I. Isolation, physicochemical and antibacterial properties. *J. Antibiot. (Tokyo).* 27(10):793.
- Olge JM, Brodrsen DE, Clemons Jr. WM, Tarry MJ, Carter AP and Ramakrishnan CV. (2001) Recognition of cognate transfer RNA by the 30S ribosomal subunit. *Science.* 292:897.

- Omoto S, Inouye S, Kojima M, and Niida T. <sup>13</sup>C-NMR studies of ribostamycin and its related compounds. *J. Antibiot. (Tokyo)*. 26(12):717.
- Otwinowski Z and Minor W. (1997) Processing of X-ray Diffraction Data Collected in Oscillation Mode. In *Methods in Enzymology* (Carter CWJ and Sweet RM Eds.) pp. 307-326, Academic Press, San Diego.
- Pettinger RC, Wolfe RN, Hoehn MM, Marks PN, Dailey WA and McGuire JM. (1953) Hygromycin I. Preliminary studies on the production and biological activity of a new antibiotic. *Antibiot. Chemother.* 3:1268.
- Poole K. (2001) Multidrug resistance in Gram-negative bacteria. *Curr. Opin. Microbiol.* 4:500.
- Qu T-T, Chen Y-C, Yu Y-S, Wei Z-Q, Zhou Z-H and Li L-J. (2006) Genotypic diversity and epidemiology of high-level gentamicin resistant *Enterococcus* in a Chinese hospital. *J. Inf.* 52:124.
- Ramirez MS and Tolmasky ME. (2010) Aminoglycoside modifying enzymes. *Drug Resis. Updates.* 13:151.
- Ramirez MS, Nikolaidis N and Tolmasky ME. (2013) Rise and dissemination of aminoglycoside resistance: the *aac(6')-Ib* paradigm. *Front. Microbiol.* 4(121):1.
- Rees, DC, Congreve M, Murray CW and Carr R. (2004) Fragment-based lead discovery. *Nat. Rev. Drug Disc.* 3:660.
- Regula G, Torriani K, Gassner B, Stucki F and Müntener CR. (2009) Prescription patterns of antimicrobials in veterinary practices in Switzerland. *J. Antimicrob. Agents Chemother.* 63:805.
- Rice LB. (2008) Federal funding for the study of antimicrobial resistance in nosocomial pathogens: no ESKAPE. *J. Infect. Dis.* 197: 1079.
- Rolston KV. (2009) The use of new and better antibiotics for bacterial infections in patients with leukemia. *Clin. Lymphoma Myeloma.* S357:63.
- Ryden R and Moore BJ. (1977) The *in vitro* activity of apramycin, a new aminocyclitol antibiotic. *J. Antimicrob. Chemother.* 3: 609.
- Schatz A, Bugie E and Waksman SA. (1944, republished in 2005) Streptomycin, a substance exhibiting antibiotic activity against gram-positive and gram-negative bacteria. *Clin. Orthop. Relat. Res.* 437:3.
- Schilling-Bartetzko S, Bartetzko A and Nierhaust KH. (1992) Kinetic and thermodynamic parameters for tRNA binding to the ribosome and for the translocation reaction. *J. Biol. Chem.* 267(7):4703.
- Schinkmann K and Blenis J. (1997) Cloning and characterization of a human STE20-like protein kinase with unusual cofactor requirements. *J. Biol. Chem.* 272:28695.
- Schuettelkopf AW and van Aalten DMF. (2004) PRODRG: A tool for high-throughput crystallography of protein-ligand complexes. *Acta Crystallogr.* D60:1355.
- Schuwirth BS, Day JM, Hau CW, Janssen GR, Dahlberg AE, Cate JHD, and Vila-Sanjurjo A. (2006) Structural analysis of kasugamycin inhibition of translation. *Nat. Struct. Mol. Biol.* 13(10):879.



- Scott DE, Coyne AG, Hudson SA, and Abell C. (2012) Fragment-based approaches in drug discovery and chemical biology. *Biochem.* 51: 4990.
- Shakya T and Wright GD. (2010) Nucleotide selectivity of antibiotic kinases. *Antimicrob. Agents Chemother.* 54:1909.
- Shakya T, Stogios PJ, Waglechner N, Evdokimova E, Ejim L, Blanchard JE, McArthur AG, Savchenko A, and Wright GD. (2011) A small molecule discrimination map of the antibiotic resistance kinome. *Chem. Biol.* 18:1591.
- Shaw KJ, Rather PN, Hare RS and Miller GH. (1993) Molecular genetics of aminoglycoside resistance genes and familial relationships of the aminoglycoside-modifying enzymes. *Microbiol. Rev.* 57:138.
- Shi K, Houston DR, and Berghuis, AM. (2011) Crystal structures of antibiotic-bound complexes of aminoglycoside 2''-phosphotransferase IVa highlight the diversity in substrate binding modes among aminoglycoside kinases. *Biochem.* 50:6237.
- Shi K and Berghuis AM. (2012) Structural basis for dual nucleotide selectivity of aminoglycoside 2''-phosphotransferase IVa provides insight on determinants of nucleotide specificity among aminoglycoside kinases. *J. Biol. Chem.* 287(16):13094.
- Shi K, Caldwell SJ, Fong DH, and Berghuis AM. (2013) Prospects for circumventing aminoglycoside kinase mediated antibiotic resistance. *Front. Cell. Inf. Microbiol.* 3(22):1.
- Sievers F, Wilm A, Dineen D, Gibson TJ, Karplus K, Li W, Lopez R, McWilliam H, Remmert M, Söding J, Thompson JD and Higgins DG. (2011) Fast, scalable generation of high-quality protein multiple sequence alignments using Clustal Omega. *Mol. Syst. Biol.* 7:539.
- Smith CA and Baker EN. (2002) Aminoglycoside antibiotic resistance by enzymatic deactivation. *Curr. Drug Targets: Infect. Disord.* 2:143.
- Smith CA, Toth M, Frase H, Byrnes, LJ and Vakulenko SB. (2012) Aminoglycoside-2'' phosphotranse-IIIa (APH(2'')-IIIa) prefers GTP over ATP: Structural templates for nucleotide recognition in the bacterial aminoglycoside-2'' kinases. *J. Biol. Chem.* 287(16):12893.
- Smith CA, Toth M, Bhattacharya M, Frase H, Vakulenko SB. (2014) Structure of the phosphotransferase domain of the bifunctional aminoglycoside-resistance enzyme AAC(6')-Ie-APH(2'')-Ia. *Acta Crystallogr. Sect. D.* 70:1561.
- Springer B, Kidan YG, Prammananan T, Ellrott K, Böttger EC and Sander P. (2001) Mechanisms of streptomycin resistance selection of mutations in the 16S rRNA gene conferring resistance. *Antimicrob. Agents Chemother.* 45(10):2877.
- Staben ST, Feng JA, Lyle K, Belvin M, Boggs J, Burch JD, Chua C-C, Cui H, DiPasquale AG, Friedman LS, Heise C, Koeppen H, Kotey A, Mintzer R, Oh A, Roberts DA, Rouge L, Rudolph J, Tam C, Wang W, Xiao Y, Young A, Zhang Y and Hoeflich KP. (2014) Backpocket flexibility provides group II p21-activated kinase (PAK) selectivity for type I 1/2 kinase inhibitors. *J. Med. Chem.* 57: 1033.
- Stogios PJ, Shakya T, Evdokimova E, Savchenko A and Wright GD. (2011) Structure and function of APH(4)-Ia, a hygromycin B resistance enzyme. *J. Biol. Chem.* 286:1966.

- Stogios PJ, Spanogiannopoulos P, Evdokimova E, Egorova O, Shakya T, Todorovic N, Capretta A, Wright GD and Savchenko A. (2013) Structure-guided optimization of protein kinase inhibitors reverses aminoglycoside antibiotic resistance. *Biochem. J.* 454:191.
- Su X-Z, Chen J, Mizushima T, Kuroda T and Tsuchiya T. (2005) AdeM, an H<sup>+</sup>-coupled *acinetobacter baumannii* multidrug efflux pump belonging to the MATE family of transporters. *Antimicrob. Agents Chemother.* 49(10):4362.
- Taber HW, Mueller JP, Miller PF and Arrow AS. (1987) Bacterial uptake of aminoglycoside antibiotics. *Microbiol. Rev.* 51(4):439.
- Tanaka N, Matsunaga K, Hirata A, Matsuhisa Y, and Nishimura T. (1983) Mechanism of action of habekacin, a novel amino acid-containing aminoglycoside antibiotic. *Antimicrob. Agents Chemother.* 24(5):797.
- Tenover FC, Tickler I, Armstrong ES, Kubo A, Lopez S, Persing DH and Miller GH. (2011) Activity of ACHN-490 against methicillin-resistant *Staphylococcus aureus* (MRSA) isolates from patients in US hospitals. *Int. J. Antimicrob. Agents.* 38:352.
- Thornsberry C, Barry AL, Jones RN, Baker CN, Badal RE, and Packer RR. (1980) Comparison of in vitro activity of Sch 21420, a gentamicin B derivative, with those of amikacin, gentamicin, netilmicin, sisomicin, and tobramycin. *Antimicrob. Agents Chemother.* 18(2):338.
- Toth M, Zajicek J, Kim C, Chow JW, Smith C, Mobashery S and Vakulenko S. (2007) Kinetic mechanism of enterococcal aminoglycoside phosphotransferase 2''-Ib. *Biochem.* 46:5570.
- Toth M, Chow JW, Mobashery S, Vakulenko SB. (2009) Source of phosphate in the enzymatic reaction as a point of distinction among aminoglycoside 2''-phosphotransferases. *J. Biol. Chem.* 284:6690.
- Toth M, Frase H, Antunes NT, Smith CA and Vakulenko SB. (2010) Crystal structure and kinetic mechanism of aminoglycoside phosphotransferase-2''-IVa. *Prot. Sci.* 19:1565.
- Toth M, Frase H, Antunes NT and Vakulenko SB. (2013) Novel aminoglycoside 2''-phosphotransferase identified in a Gram-negative pathogen. *Antimicrob. Agents Chemother.* 57(1):452.
- Tsai SF, Zervos MJ, Clewell DB, Donabedian SM, Sahm DF and Chow JW. (1998) A new high-level gentamicin resistance gene, *aph(2'')-Id*, in *Enterococcus* spp. *Antimicrob. Agents Chemother.* 42(5):1229.
- Umezawa H. (1958) Kanamycin: its discovery. *Ann. N.Y. Acad. Sci.* 76(2):27.
- Verlinde CLMJ, Fan E, Shibata S, Zhang Z, Sun Z, Deng W, Ross J, Kim J, Xiao L, Arakaki TL, Bosch J, Caruthers JM, Larson ET, LeTrong I, Napuli A, Kelly A, Mueller N, Zucker F, Van Voorhis WC, Merritt EA and Hol WGJ. (2009) Fragment-based cocktail crystallography by the medical structural genomics of pathogenic protozoa consortium. *Curr. Top. Med. Chem.* 9(18):1678.
- Vicens Q and Westhof E. (2002) Crystal structure of a complex between the aminoglycoside tobramycin and an oligonucleotide containing the ribosomal decoding A site. *Chem. Biol.* 9:747.

- Vicens Q and Westhof E. (2003) RNA as drug target: The case of aminoglycosides. *ChemBioChem*. 4:1018.
- Wachino J and Arakawa Y. (2012) Exogenously acquired 16ArRNA methyltransferases found in aminoglycoside-resistant pathogenic Gram-negative bacteria: an update. *Drug Res. Update*. 15:133.
- Waksman SA and Lechevalier HA. (1949) Neomycin, a new antibiotic active against streptomycin-resistant bacteria, including tuberculosis organisms. *Science*. 109:305.
- World Economic Forum. (2013) Global Risks 2013 – Eighth Ed. [http://www3.weforum.org/docs/WEF\\_GlobalRisks\\_Report\\_2013.pdf](http://www3.weforum.org/docs/WEF_GlobalRisks_Report_2013.pdf)
- World Health Organization. (2013) WHO Model List of Essential Medicines. 18<sup>th</sup> list. <http://www.who.int/medicines/publications/essentialmedicines/en/index.html>
- Weinstein MJ, Luedemann GM, Oden EM, Wagman GH, Rosselet JP, Marquez JA, Coniglio CT, Charney W, Herzog HL, and Black, J. (1963) Gentamicin, a new antibiotic complex from micromonospora. *J. Med. Chem.* 6(4):463.
- Weinstein MJ, Wagman JA, Marquez JA, Testa RT and Waitz JA. (1975) Verdamicin, a new broad spectrum aminoglycoside antibiotic. *Antimicrob. Agents Chemother.* 7(3):246.
- Welch KT, Virga KG, Whittermore NA, Özen C, Wright E, Brown CL, Lee RE and Serspersu EH. (2005) Discovery of non-carbohydrate inhibitors of aminoglycoside-modifying enzymes. *Bioorg. Med. Chem.* 13:6252.
- Wilcken R, Liu X, Zimmermann MO, Rutherford TJ, Fersht AR, Joerger AC and Boeckler FM. Halogen-enriched fragment libraries as leads for drug rescue of mutant p53. *J. Am. Chem. Soc.* 134:6810.
- Xu Y, Jin H, Yang Z, Zhang L, Wang Z, Li M and Zhang L. (2009) Synthesis and evaluation of novel neamine derivatives effectively targeting to RNA. *Bioorg. Med. Chem. Lett.* 19:2103.
- Xu Z, Liu Z, Chen T, Chen TT, Zheng W, Tian G, Shi J, Wang X, Lu Y, Yan X, Jiang H, Chen K, Wang S, Xu Y, Shen J and Zhu W. (2011) Utilization of halogen bond in lead optimization: a case study of rational drug design of potent phosphodiesterase type 5 (PDE5) inhibitors. *J. Med. Chem.* 54:5607.
- Yadegar A, Sattari M, Mazafari NA and Goudarzi GR. (2009) Prevalence of the genes encoding aminoglycoside-modifying enzymes and methicillin resistance among clinical isolates of *Staphylococcus aureus* in Tehran, Iran. *Microb. Drug Resist.* 15:109.
- Yde CW, Ermakova I, Issinger OG and Niefind K. (2005) Inclining the purine base-binding plane in protein kinase CK2 by exchanging the flanking side chains generates a preference for ATP as a co-substrate. *J. Mol. Biol.* 347:399.
- Yoshizawa S, Fourmy D and Puglisi JD. (1999) Recognition of the codon-anticodon helix by ribosomal RNA. *Science*. 285:1722.
- Young PG, Walanj R, Lakshmi V, Byrnes LJ, Metcalf P, Baker EN, Vakulenko SB and Smith CA. (2009) The crystal structures of substrate and nucleotide complexes of *Enterococcus faecium* aminoglycoside-2''-phosphotransferase-IIa [APH(2'')-IIa] provide insights into substrate selectivity in the APH(2'') subfamily. *J. Bacteriol.* 191:4133.

Zarrilli R, Tripodi M-F, Di Popolo A, Fortunato R, Bagattini M, Crispino M, Florio A, Triassi M and Utili R. (2005) Molecular epidemiology of high-level aminoglycoside-resistant enterococci isolated from patients in a university hospital in southern Italy. *J. Antimicrob. Chemother.* 56:827.

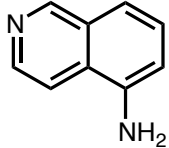
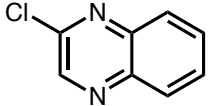
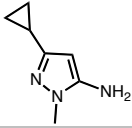
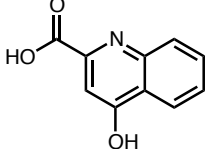
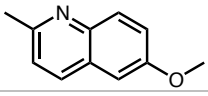
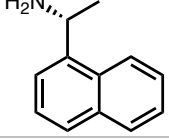
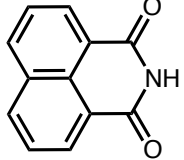
## Appendices

### Appendix A. Small Molecule Fragment Library in DMSO

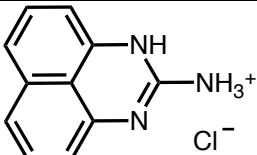
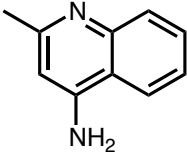
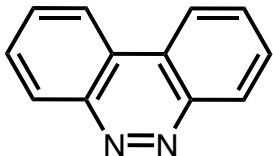
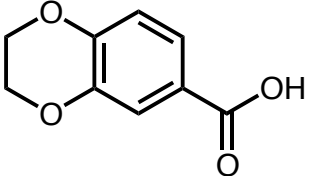
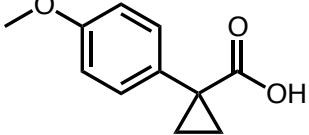
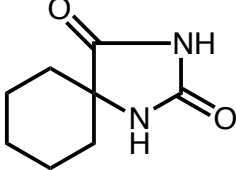
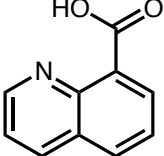
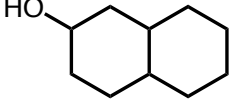
The original cocktails have been relabeled and reordered for consistency purposes according to the following conversion table.

Reordered ID used in this thesis	Original ID from source	Reordered ID used in this thesis	Original ID from source
C1	Cocktail 1	C18	Cocktail 27
C2	Cocktail 2	C19	Cocktail 28
C3	Cocktail 3	C20	Cocktail 29
C4	Cocktail 4	C21	Cocktail 34
C5	Cocktail 5	C22	Cocktail 35
C6	Cocktail 6	C23	Cocktail 36
C7	Cocktail 7	C24	Cocktail 39
C8	Cocktail 8	C25	Cocktail 41
C9	Cocktail 9	C26	Cocktail 44
C10	Cocktail 11	C27	Cocktail 48
C11	Cocktail 12	C28	Cocktail 49
C12	Cocktail 14	C29	Cocktail 53
C13	Cocktail 15	C30	Cocktail 59
C14	Cocktail 21	C31	Cocktail 60
C15	Cocktail 22	C32	Cocktail 61
C16	Cocktail 23	C33	Cocktail 63
C17	Cocktail 25	C34	Cocktail 68

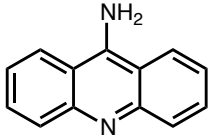
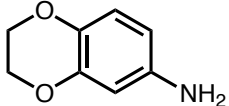
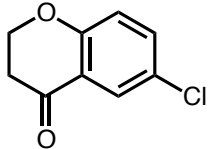
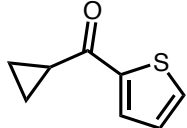
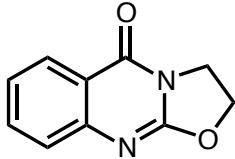
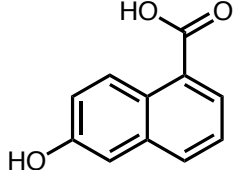
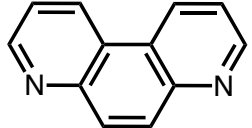
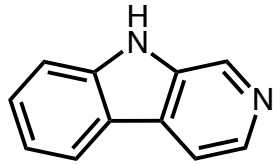
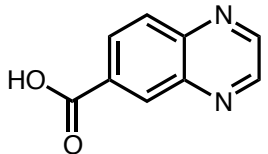
## Cocktail C1

ID	Name	CAS	[Stock]	Structure
1-1	5-AMINOISOQUINOLINE	1125-60-6	1 M	
1-2	2-CHLOROQUINOXALINE 98%	1448-87-9	0.01 M	
1-3	3-CYCLOPROPYL-1-METHYL-1H-PYRAZOL-5-AMINE	118430-74-3	0.1 M	
1-4	KYNURENIC ACID	492-27-3	0.1 M	
1-5	6-METHOXYQUINALDINE	1078-28-0	0.01 M	
1-6	(R)-(+)-Alpha-(1-NAPHTHYL)ETHYLAMINE	3886-70-2	0.01 M	
1-7	1,8-NAPHTHALIMIDE	81-83-4	0.1 M	

## Cocktail C2

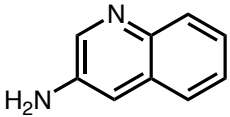
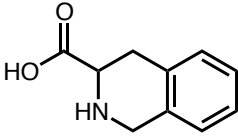
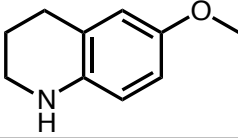
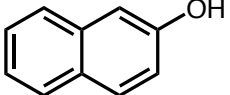
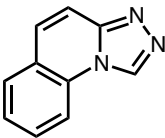
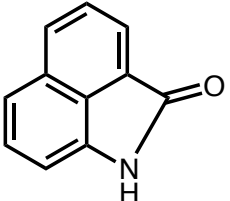
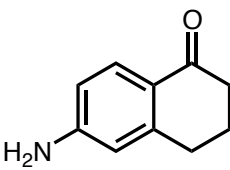
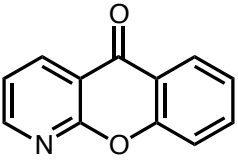
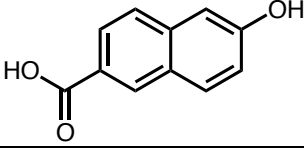
ID	Name	CAS	[Stock]	Structure
2-1	2-AMINOPERIMIDINE HYDROCHLORIDE	29416-86-2	1	
2-2	4-AMINOQUINALDINE	6628-04-2	0.1	
2-3	BENZO[C]CINNOLINE	230-17-1	0.1	
2-4	2,3-DIHYDRO-1,4- BENZODIOXINE-6-CARBOXYLIC ACID	4442-54-0	0.1	
2-5	1-(4-METHOXYPHENYL)-1- CYCLOPROPANECARBOXYLIC ACID	16728-01-1	0.1	
2-6	5,5- PENTAMETHYLENEHYDANTOI N	702-62-5	0.1	
2-7	QUINOLINE-8-CARBOXYLIC ACID	86-59-9	0.1	
2-8	DECAHYDRO-2-NAPHTHOL	825-51-4	0.1	

### Cocktail C3

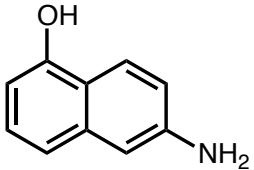
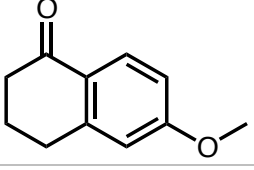
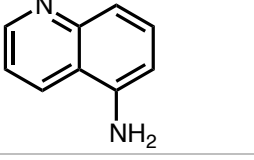
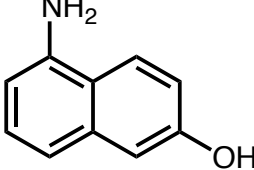
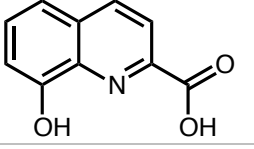
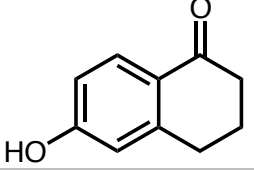
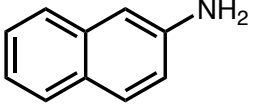
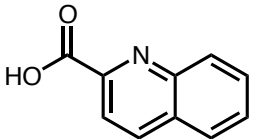
ID	Name	CAS	[Stock]	Structure
3-1	9-AMINOACRIDINE HCL SALT	90-45-9	0.1	
3-2	1,4-BENZODIOXAN-6-AMINE	22013-33-8	0.1	
3-3	6-CHLOROTHIOCHROMAN-4-ONE 98%	37674-72-9	0.1	
3-4	CYCLOPROPYL 2-THIENYL KETONE	6193-47-1	0.1	
3-5	2,3-DIHYDRO-5H-OXAZOLO[2,3- B]QUINAZOLIN-5-ONE	52727-44-3	0.1	
3-6	6-HYDROXY-1-NAPHTHOIC ACID	2437-17-4	0.1	
3-7	4,7-PHENANTHROLINE	230-07-9	0.1	
3-8	9H-PYRIDO[3,4-B]INDOLE	244-63-3	0.1	
3-9	6-QUINOXALINECARBOXYLIC ACID	6925-00-4	0.1	



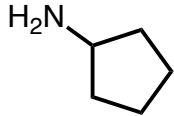
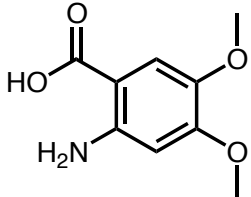
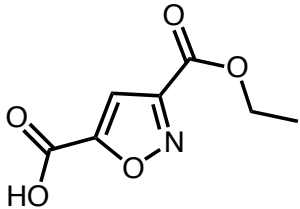
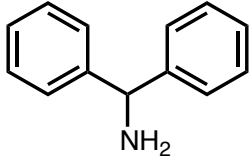
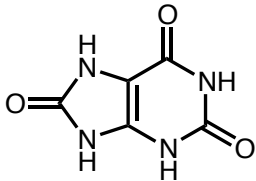
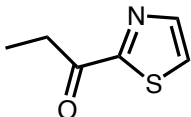
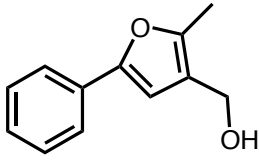
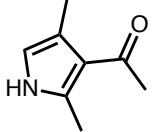
## Cocktail C4

ID	Name	CAS	[Stock]	Structure
4-1	3-AMINOQUINOLINE	580-17-6	0.1	
4-2	1,2,3,4-TETRAHYDRO-3-ISOQUINOLINECARBOXYLIC ACID HYDROCHLORIDE	74163-81-8	0.1	
4-3	6-METHOXY-1,2,3,4-TETRAHYDROQUINOLINE	120-15-0	0.1	
4-4	2-NAPHTHOL	135-19-3	0.1	
4-5	S-TRIAZOLO(4,3-A)QUINOLINE	235-06-3	0.5	
4-6	Benz[cd]indo-2(1H)-one	130-00-7	0.1	
4-7	6-AMINO-1,2,3,4-TETRAHYDRONAPHTHALEN-1-ONE	3470-53-9	0.1	
4-8	1-AZAXANTHONE	6537-46-8	0.1	
4-9	6-HYDROXY-2-NAPHTHOIC ACID	16712-64-4	0.1	

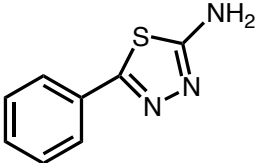
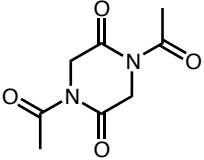
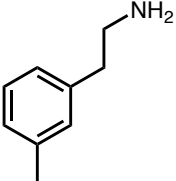
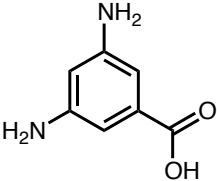
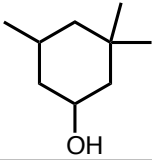
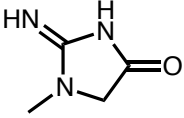
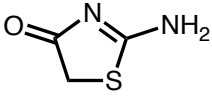
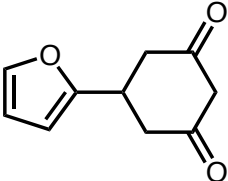
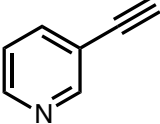
## Cocktail C5

ID	Name	CAS	[Stock]	Structure
5-1	6-AMINO-1-NAPHTHOL	23894-12-4	0.1	
5-2	6-METHOXY-1-TETRALONE	1078-19-9	0.1	
5-3	5-AMINOQUINOLINE	611-34-7	0.1	
5-4	5-AMINO-2-NAPHTHOL	86-97-5	0.1	
5-5	8-HYDROXYQUINOLINE-2-CARBOXYLIC ACID	1571-30-8	0.1	
5-6	6-HYDROXY-1-TETRALONE	3470-50-6	0.1	
5-7	2-NAPHTHYLAMINE	91-59-8	0.1	
5-8	QUINALDIC ACID	93-10-7	0.1	

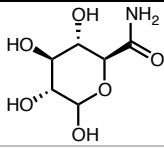
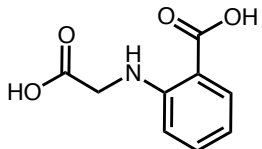
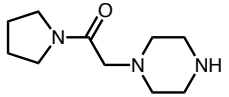
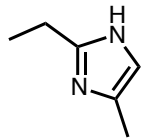
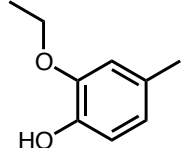
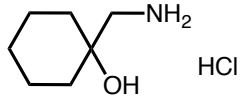
## Cocktail C6

ID	Name	CAS	[Stock]	Structure
6-1	CYCLOPENTYLAMINE	1003-03-8	0.1	
6-2	2-AMINO-4,5-DIMETHOXYBENZOIC ACID	5653-40-7	0.1	
6-3	ETHYL 5-ACETYLSOXAZOLE-3-CARBOXYLATE	104776-70-7	0.1	
6-4	AMINODIPHENYLMETHANE	91-00-9	0.1	
6-5	URIC ACID	69-93-2	0.1	
6-6	2-PROPIONYLTHIAZOLE	43039-98-1	0.1	
6-7	(2-METHYL-5-PHENYL-3-FURYL)METHANOL	111787-91-8	0.1	
6-8	3-ACETYL-2,4-DIMETHYLPYRROLE	2386-25-6	0.1	

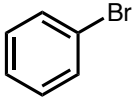
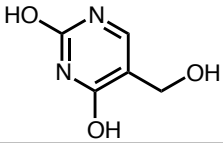
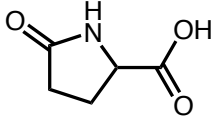
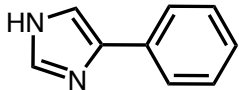
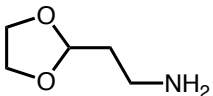
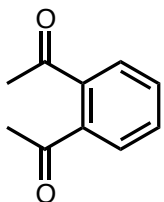
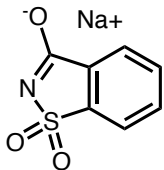
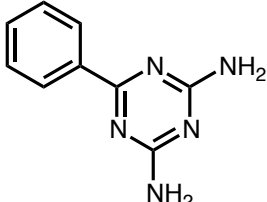
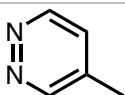
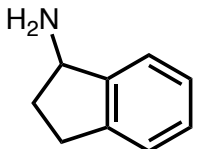
Cocktail C7

ID	Name	CAS	[Stock]	Structure
7-1	2-AMINO-5-PHENYL-[1,3,4]-THIAZOLE	2002-03-1, 312619-47-9	0.1	
7-2	N,N'-DIACETYLGLYCINE ANHYDRIDE	21827-92-9, 3027-05-2	0.1	
7-3	3-METHYLPHENETHYLAMINE	5470-40-6	0.1	
7-4	3,5-DIAMINOBENZOIC ACID	535-87-5	0.1	
7-5	3,3,5-TRIMETHYLCYCLOHEXANOL	116-02-9	0.1	
7-6	2-AMINO-1-METHYL-2-IMIDAZOLIN-4-ONE HEMISULFATE SALT	31377-28-3, 60-27-5	0.1	
7-7	PSEUDOTHIOHYDANTOIN	556-90-1	0.1	
7-8	5-(2-FURYL)CYCLOHEXANE-1,3-DIONE	1774-11-4	0.1	
7-9	3-ETHYNYLPYRIDINE	2510-23-8	0.1	

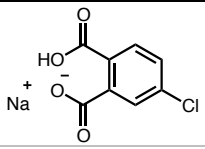
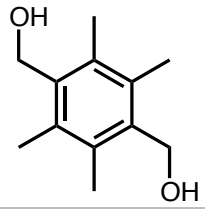
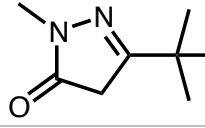
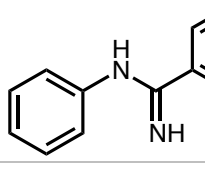
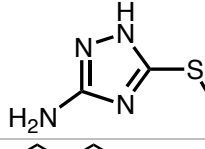
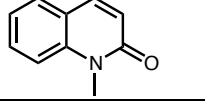
## Cocktail C8

ID	Name	CAS	[Stock]	Structure
8-1	D-GLUCURONAMIDE	3789-97-7	0.1	
8-2	N-(2-CARBOXYPHENYL)GLYCINE	612-42-0	0.1	
8-3	1-((PYRROLIDINE-1-CARBONYLMETHYL)PIPERAZINE	39890-45-4	0.1	
8-4	2-ETHYL-4-METHYLIMIDAZOLE	931-36-2	0.1	
8-5	2-ETHOXY-4-METHYLPHENOL	2563-07-7	0.1	
8-6	1-AMINOMETHYL-1-CYCLOHEXANOL HYDROCHLORIDE	19968-85-5	0.1	

## Cocktail C9

ID	Name	CAS	[Stock]	Structure
9-1	BROMOBENZENE	108-86-1	0.1	
9-2	5-(HYDROXYMETHYL)URACIL	4433-40-3	0.1	
9-3	2-PYRROLIDONE-5-CARBOXYLIC ACID	149-87-1	0.1	
9-4	4-PHENYLIMIDAZOLE	670-95-1	0.1	
9-5	2-(1,3-DIOXOLAN-2-YL)ETHANAMINE	5754-35-8	0.1	
9-6	1,2-DIACETYL BENZENE	704-00-7	0.1	
9-7	SODIUM SACCHARIN	128-44-9	0.1	
9-8	BENZOGUANAMINE	91-76-9	0.1	
9-9	4-METHYLPYRIDAZINE	1120-88-3	0.1	
9-10	1-AMINOINDAN	34698-41-4	0.1	

## Cocktail C10

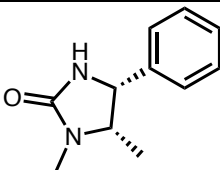
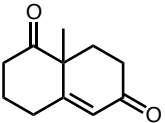
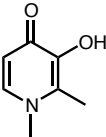
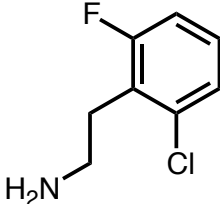
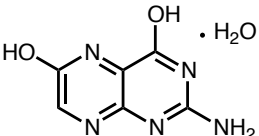
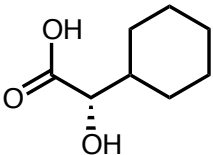
ID	Name	CAS	[Stock]	Structure
10-1	4-CHLOROPHTHALIC ACID MONOSODIUM SALT	56047-23-5	0.1	
10-2	3,6-BIS(HYDROXYMETHYL) DURENE	7522-62-5	0.1	
10-3	3-TERT-BUTYL-1-METHYL-2- PYRAZOLIN-5-ONE	87031-30-9	0.1	
10-4	N-PHENYLBENZAMIDINE	1527-91-9	0.1	
10-5	3-AMINO-5-METHYLTHIO-1H- 1,2,4-TRIAZOLE	45534-08-5	0.1	
10-6	1-METHYL-2(1H)-QUINOLINONE	606-43-9	0.1	

## Cocktail C11

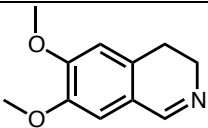
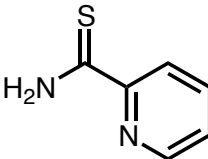
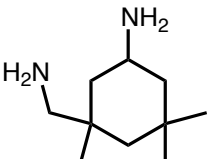
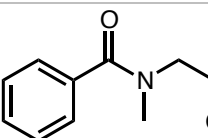
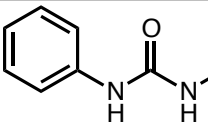
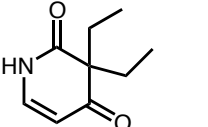
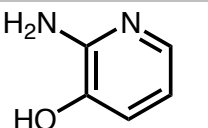
ID	Name	CAS	[Stock]	Structure
11-1	(5-FLUORO-2-METHYLPHENYL)ACETIC ACID	261951-75-1	0.1	
11-2	P-AZIDOACETOPHENONE	20062-24-2	0.1	
11-3	(2,2-DIMETHYL-2,3-DIHYDRO-1-BENZOFURAN-7-YL)METHANOL	38002-89-0	0.1	
11-4	4-CHLORO-2-(METHYLTHIO)PYRIMIDINE	49844-90-8	0.1	
11-5	CAFFEINE	58-08-2	0.1	
11-6	2-AMINOIMIDAZOLE SULFATE	1450-93-7	0.1	
11-7	3-(2-THENOYL)-PROPIONIC ACID	4653-08-1	0.1	
11-8	1,4-BIS(1-METHYL-1-HYDROXYETHYL)BENZENE	2948-46-1	0.1	



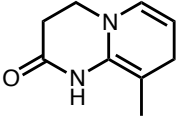
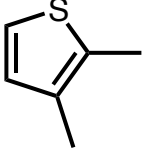
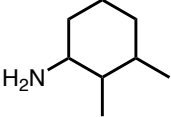
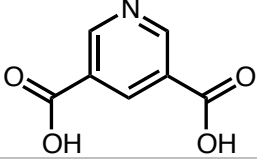
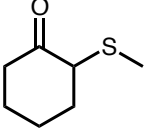
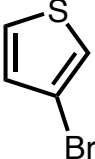
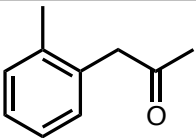
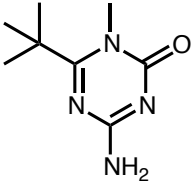
## Cocktail C12

ID	Name	CAS	[Stock]	Structure
12-1	(4R,5S)-(-)-1,5-DIMETHYL-4-PHENYL-2-IMIDAZOLIDINONE	92841-65-1	0.1	
12-2	(+/-)-3,4,8,8A-TETRAHYDRO-8A-METHYL-1,6(2H,7H)-NAPHTHALENEDIONE	20007-72-1	0.1	
12-3	3-HYDROXY-1,2-DIMETHYL-4(1H)-PYRIDONE	30652-11-0	0.1	
12-4	2-CHLORO-6-FLUOROPHENETHYLAMINE	149488-93-7	0.1	
12-5	XANTHOPTERIN MONOHYDRATE	5979-01-1	0.1	
12-6	(S)-(+)-HEXAHYDROMANDELIC ACID 98%	61475-31-8	1	

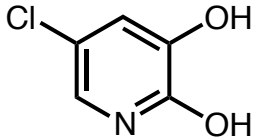
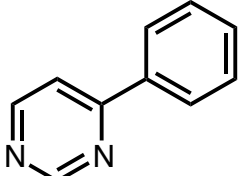
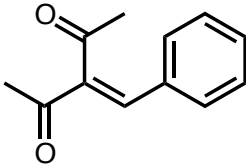
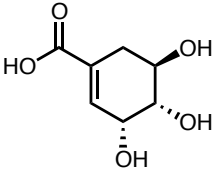
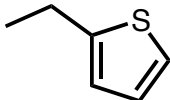
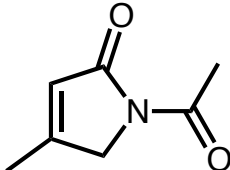
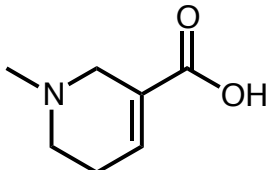
### Cocktail C13

ID	Name	CAS	[Stock]	Structure
13-1	6,7-DIMETHOXY-3,4-DIHYDROISOQUINOLINE HYDROCHLORIDE	20232-39-7	0.1	
13-2	PYRIDINE-2-THIOAMIDE	5346-38-3	0.1	
13-3	ISOPHORONEDIAMINE	2855-13-2	0.1	
13-4	(BENZOYL-METHYL-AMINO)-ACETIC ACID	2568-34-5	0.1	
13-5	1-ETHYL-3-PHENYLUREA	621-04-5	0.1	
13-6	PYRITHYLDIONE	77-04-3	0.1	
13-7	2-AMINO-3-HYDROXYPYRIDINE	16867-03-1	0.1	

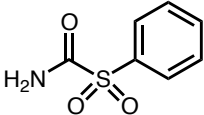
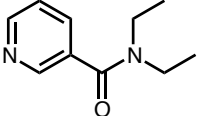
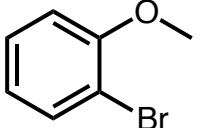
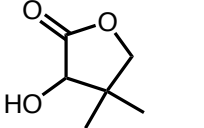
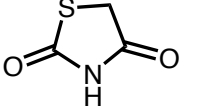
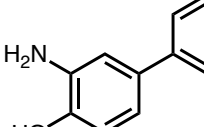
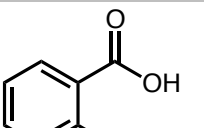
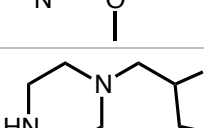
## Cocktail C14

ID	Name	CAS	[Stock]	Structure
14-1	9-METHYL-3,4-DIHYDRO-2H-PYRIDO[1,2-A]PYRIMIDIN-2-ONE	61751-44-8	0.1	
14-2	2,3-DIMETHYLTHIOPHENE	632-16-6	0.1	
14-3	2,3-DIMETHYL CYCLOHEXANAMINE	42195-92-6	0.1	
14-4	3,5-PYRIDINEDICARBOXYLIC ACID	499-81-0	0.1	
14-5	2-(METHYLTHIO) CYCLOHEXANONE	52190-35-9	0.1	
14-6	3-BROMOTHIOPHENE	872-31-1	0.1	
14-7	2-METHYLPHENYLACETONE	51052-00-7	0.1	
14-8	4-AMINO-6-(TERT-BUTYL)-1-METHYL-1,2-DIHYDRO-1,3,5-TRIAZIN-2-ONE	175204-73-6	0.1	

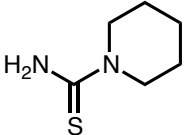
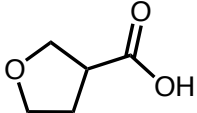
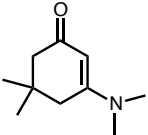
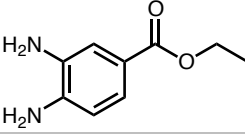
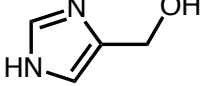
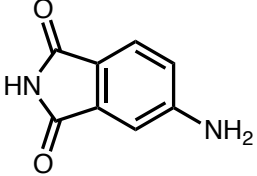
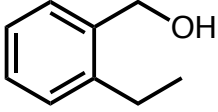
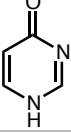
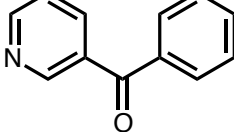
## Cocktail C15

ID	Name	CAS	[Stock]	Structure
15-1	5-CHLORO-2,3-DIHYDROXYPYRIDINE	53233-89-9	0.1	
15-2	4-PHENYLPYRIMIDINE	3438-48-0	0.1	
15-3	3-BENZYLIDENE-2,4-PENTANEDIONE	4335-90-4	0.1	
15-4	SHIKIMIC ACID	138-59-0	0.1	
15-5	2-ETHYLTHIOPHENE	872-55-9	0.1	
15-6	1-ACETYL-4-METHYL-2,5-DIHYDRO-1H-PYRROL-2-ONE	34581-92-5	0.1	
15-7	ARECAIDINE HYDROCHLORIDE	6018-28-6	0.1	

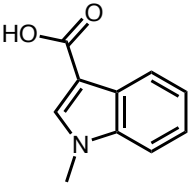
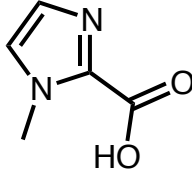
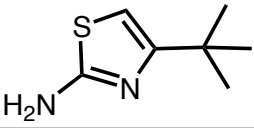
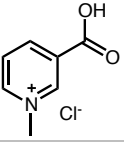
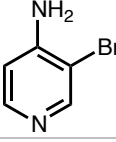
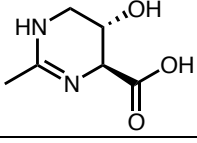
## Cocktail C16

ID	Name	CAS	[Stock]	Structure
16-1	(PHENYLSULPHONYL) ACETAMIDE	35008-50-5	0.1	
16-2	N,N-DIETHYLNICOTINAMIDE	59-26-7	0.1	
16-3	2-BROMOANISOLE	578-57-4	0.1	
16-4	DL-PANTOLACTONE	79-50-5	0.1	
16-5	2,4-THIAZOLIDINEDIONE	2295-31-0	0.1	
16-6	2-AMINO-4-PHENYLPHENOL	1134-36-7	0.1	
16-7	2-METHOXYNICOTINIC ACID	16498-81-0	0.1	
16-8	1-TETRAHYDRO-FURFURYLPIPERAZINE	82500-35-4	0.1	

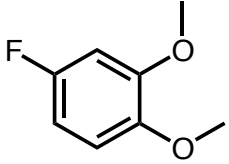
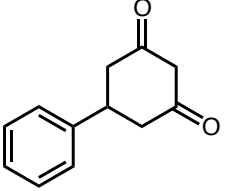
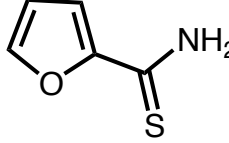
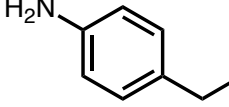
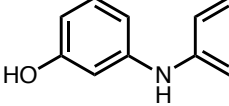
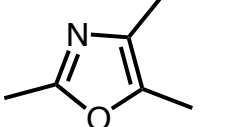
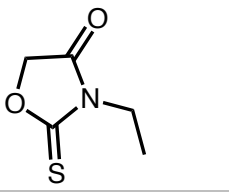
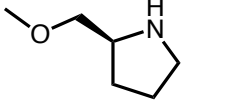
Cocktail C17

ID	Name	CAS	[Stock]	Structure
17-1	1-PIPERIDINECARBOTHIOAMIDE	14294-09-8	0.1	
17-2	TETRAHYDRO-3-FUROIC ACID	89364-31-8	0.1	
17-3	3-(DIMETHYLAMINO)-5,5-DIMETHYL-2-CYCLOHEXEN-1-ONE	31039-88-0	0.1	
17-4	ETHYL 3,4-DIAMINOBENZOATE	37466-90-3	0.1	
17-5	4-(HYDROXYMETHYL)IMIDAZOLE HYDROCHLORIDE	32673-41-9, 822-55-9	0.1	
17-6	4-AMINOPHTHALIMIDE	3676-85-5	0.1	
17-7	2-ETHYLBENZYL ALCOHOL	767-90-8	0.1	
17-8	4(3H)-PYRIMIDINONE	4562-27-0	0.1	
17-9	3-BENZOYLPYRIDINE	5424-19-1	0.1	

## Cocktail C18

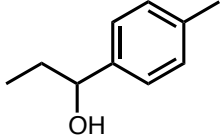
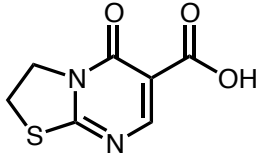
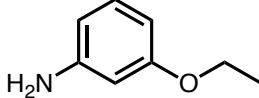
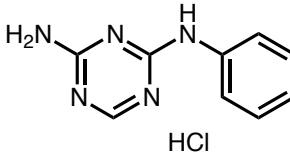
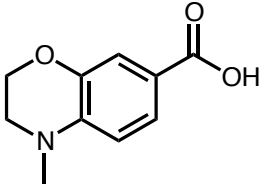
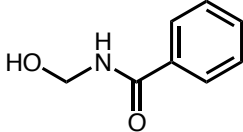
ID	Name	CAS	[Stock]	Structure
18-1	1-METHYL-3-INDOLEACETIC ACID	1912-48-7	0.5	
18-2	1-METHYLIMIDAZOLE-2-CARBOXYLIC ACID, LITHIUM SALT	20485-43-2	0.1	
18-3	2-AMINO-4-TERT-BUTYLTHIAZOLE	74370-93-7	0.1	
18-4	TRIGONELLINE HYDROCHLORIDE	6138-41-6	0.1	
18-5	4-AMINO-3-BROMOPYRIDINE	13534-98-0	1	
18-6	HYDROXYECTOINE	165542-15-4	0.1	

Cocktail C19

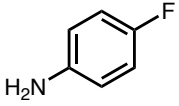
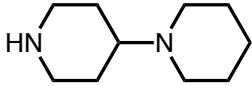
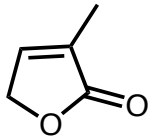
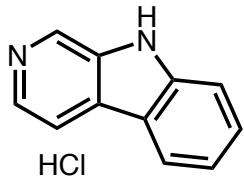
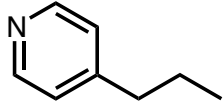
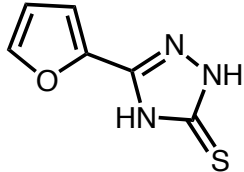
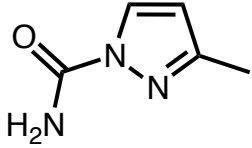
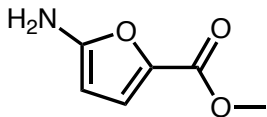
ID	Name	CAS	[Stock]	Structure
19-1	4-FLUOROVERATROLE	398-62-9	0.1	
19-2	5-PHENYLCYCLOHEXANE-1,3-DIONE	493-72-1, 35376-44-4	0.1	
19-3	FURAN-2-CARBOTHIOAMIDE	17572-09-7	0.1	
19-4	4-AMINOBENZYL ALCOHOL	623-04-1	0.1	
19-5	3-HYDROXYDIPHENYLAMINE	101-18-8	0.1	
19-6	2,4,5-TRIMETHYLOXAZOLE	20662-84-4	0.1	
19-7	3-ETHYL-2-THIOXO-4-OXAZOLIDINONE	10574-66-0	0.1	
19-8	(S)-(+)-2-(METHOXYMETHYL)PYRROLIDINE	63126-47-6	0.1	



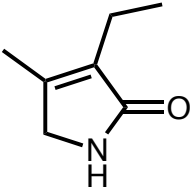
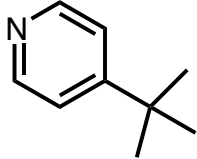
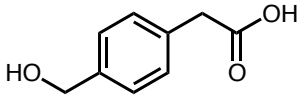
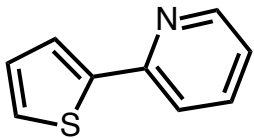
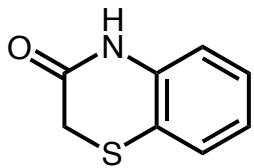
## Cocktail C20

ID	Name	CAS	[Stock]	Structure
20-1	1-(4-METHYLPHENYL)-1-PROPANOL	25574-04-3	0.1	
20-2	5-OXO-2,3-DIHYDRO-5H-PYRIMIDO[2,1-B][1,3]THIAZOLE-6-CARBOXYLIC ACID	32084-55-2	0.1	
20-3	3-ETHOXYANILINE	621-33-0	0.1	
20-4	2-AMINO-4-ANILINO-1,3,5-TRIAZINE HYDROCHLORIDE	6011-10-5	0.1	
20-5	4-METHYL-3,4-DIHYDRO-2H-1,4-BENZOXAZINE-7-CARBOXYLIC ACID	90563-93-2	0.1	
20-6	N-(HYDROXYMETHYL) BENZAMIDE	6282-02-6	0.1	

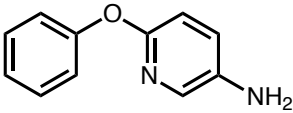
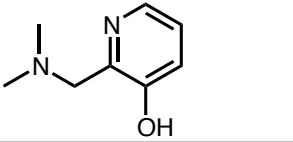
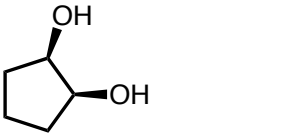
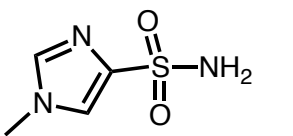
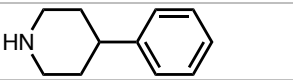
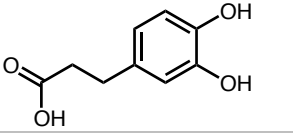
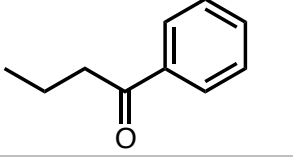
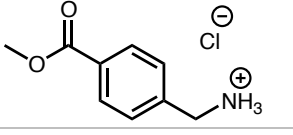
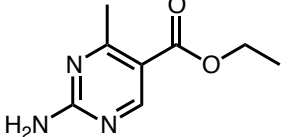
## Cocktail C21

ID	Name	CAS	[Stock]	Structure
21-1	4-FLUOROANILINE	371-40-4	0.1	
21-2	4-PIPERIDINOPIPERIDINE	4897-50-1	0.1	
21-3	3-METHYL-2(5H)-FURANONE	22122-36-7	0.1	
21-4	NORHARMANE HYDROCHLORIDE	7259-44-1, 244-63-3	0.1	
21-5	4-PROPYLPYRIDINE	1122-81-2	0.1	
21-6	5-(2-FURYL)-2,4-DIHYDRO-[1,2,4]- TRIAZOLE-3-THIONE	35771-65-4	0.1	
21-7	3-METHYLPYRAZOLE-1- CARBOXAMIDE	873-50-7	0.1	
21-8	METHYL 5-AMINO-2-FUROATE	22600-30-2	0.1	

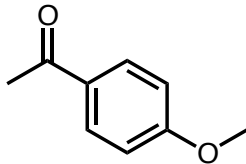
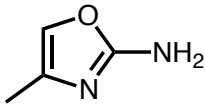
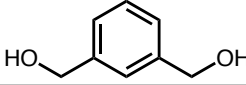
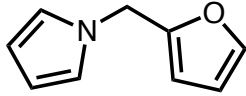
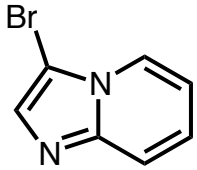
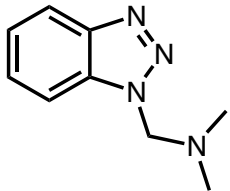
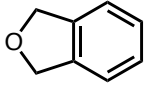
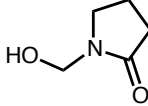
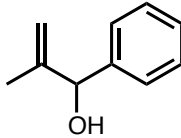
## Cocktail C22

ID	Name	CAS	[Stock]	Structure
22-1	3-ETHYL-4-METHYL-3-PYRROLIN-2-ONE	766-36-9	0.1	
22-2	4-TERT-BUTYLPYRIDINE	3978-81-2	0.1	
22-3	4-(HYDROXYMETHYL)PHENYLACETIC ACID	73401-74-8	0.1	
22-4	2-(2-THIENYL)PYRIDINE	3319-99-1	0.1	
22-5	(2H)1,4-BENZOTHAZIN-3(4H)-ONE	5325-20-2	0.1	

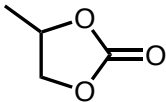
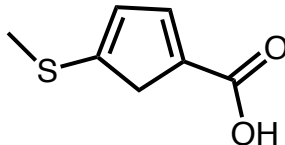
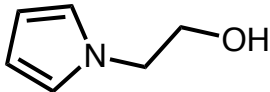
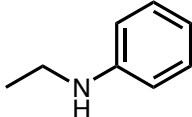
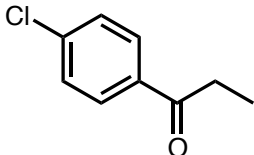
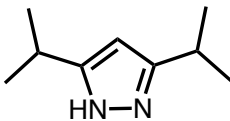
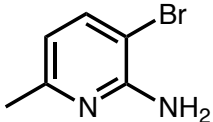
## Cocktail C23

ID	Name	CAS	[Stock]	Structure
23-1	6-PHENOXY-3-PYRIDINAMINE	25194-67-6	0.1	
23-2	2-(DIMETHYLAMINOMETHYL)-3-HYDROXYPYRIDINE	2168-13-0	0.1	
23-3	CIS-1,2-CYCLOPENTANEDIOL	5057-98-7	0.1	
23-4	1-METHYL-1H-IMIDAZOLE-4-SULFONAMIDE	111124-90-4	0.1	
23-5	4-PHENYLPYPERIDINE	771-99-3	0.1	
23-6	3-(3,4-DIHYDROXYPHENYL)PROPIONIC ACID	1078-61-1	0.1	
23-7	BUTYROPHENONE	495-40-9	0.1	
23-8	METHYL 4(AMINOMETHYL)BENZOATE HYDROCHLORIDE	6232-11-7	0.1	
23-9	ETHYL 2-AMINO-4-METHYLPYRIMIDINE-5-CARBOXYLATE	81633-29-6	0.1	

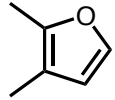
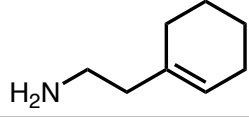
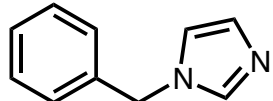
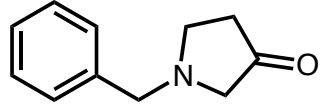
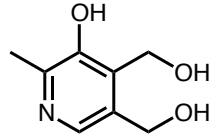
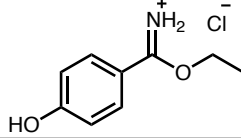
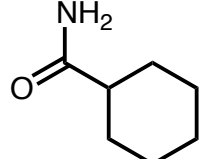
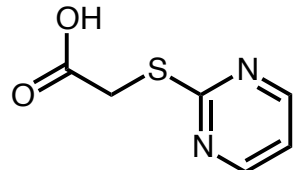
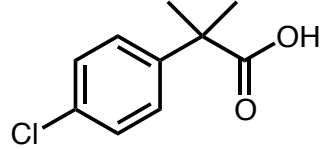
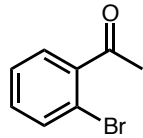
## Cocktail C24

ID	Name	CAS	[Stock]	Structure
24-1	4'-METHOXYACETOPHENONE	100-06-1	0.1	
24-2	4-METHYL-1,3-OXAZOL-2-AMINE	35629-70-0	0.1	
24-3	1,3-BENZENEDIMETHANOL	626-18-6	0.1	
24-4	1-FURFURYLPIRROLE	1438-94-4	0.1	
24-5	3-BROMOIMIDAZO[1,2-A]PYRIDINE	4926-47-0	0.1	
24-6	N,N-DIMETHYLBENZOTRIAZOLE-METHANAMINE	57684-30-7	0.1	
24-7	PHTHALAN	496-14-0	0.1	
24-8	1-(HYDROXYMETHYL)-2-PYRROLIDINONE	15438-71-8	0.1	
24-9	2-METHYL-1-PHENYL-2-PROPEN-1-OL	4383-08-8	0.1	

## Cocktail C25

ID	Name	CAS	[Stock]	Structure
25-1	PROPYLENE CARBONATE	108-32-7	0.1	
25-2	5-(METHYLTHIO)THIOPHENE-2-CARBOXYLIC ACID	20873-58-9	0.1	
25-3	1-(2-HYDROXYETHYL)PYRROLE	6719-02-4	0.1	
25-4	N-ETHYLANILINE	103-69-5	0.1	
25-5	4'-CHLOROPROPIOPHENONE	6285-05-8	0.1	
25-6	3,5-DIISOPROPYLPYRAZOLE	17536-00-4	0.1	
25-7	2-AMINO-3-BROMO-6-METHYLPYRIDINE	126325-46-0	0.1	

## Cocktail C26

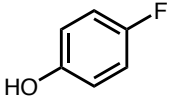
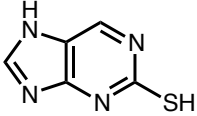
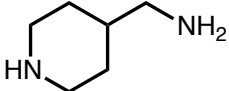
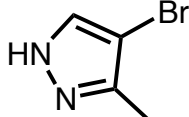
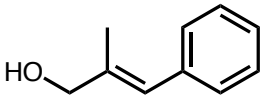
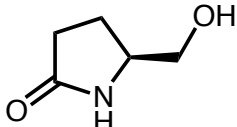
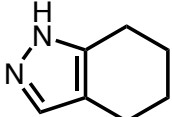
ID	Name	CAS	[Stock]	Structure
26-1	2,3-DIMETHYLFURAN	14920-89-9	0.1	
26-2	2-(1-CYCLOHEXENYL)ETHYLAMINE	3399-73-3	0.1	
26-3	1-BENZYLIMIDAZOLE	4238-71-5	0.1	
26-4	1-BENZYL-3-PYRROLIDINONE	775-16-6	0.1	
26-5	PYRIDOXINE	65-23-6	0.1	
26-6	ETHYL 4-HYDROXYBENZIMIDATE HYDROCHLORIDE	54998-28-6	0.1	
26-7	CYCLOHEXANECARBOXAMIDE	1122-56-1	0.1	
26-8	2-(CARBOXYMETHYLTHIO)PYRIMIDINE	88768-45-0	0.1	
26-9	2-(4-CHLOROPHENYL)-2-METHYLPROPIONIC ACID	6258-30-6	0.1	
26-10	2'-BROMOACETOPHENONE	2142-69-0	0.1	

## Cocktail C27

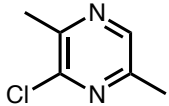
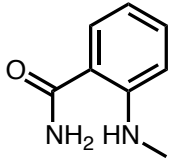
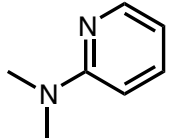
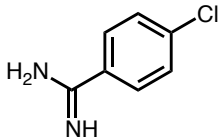
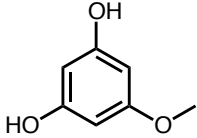
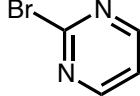
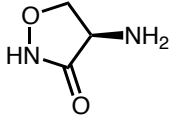
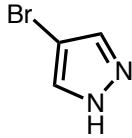
ID	Name	CAS	[Stock]	Structure
27-1	6-METHYL-3(2H)-PYRIDAZINONE	13327-27-0	0.1	
27-2	5-METHOXY-2-BENZIMIDAZOLINONE	2080-75-3	0.1	
27-3	3-BENZYL-1,3-OXAZOLIDINE	13657-16-4	0.1	
27-4	2,2'-BIPYRIMIDINE	34671-83-5	0.1	
27-5	3-BROMOPHENOL	591-20-8	0.1	
27-6	2-(PHENYLSULFONYL)ETHANOL	20611-21-6	0.1	
27-7	4-FLUOROPHENYLUREA	659-30-3	0.1	
27-8	METHYL 4-OXO-3-PIPERIDINECARBOXYLATE HYDROCHLORIDE	71486-53-8	0.1	
27-9	3-(2-HYDROXYPROPYL)-5-METHYL-2-OXAZOLIDINONE	3375-84-6	0.1	
27-10	3-BROMOBENZYLAMINE	10269-01-9	0.1	



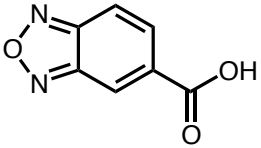
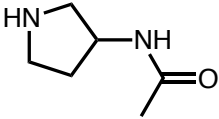
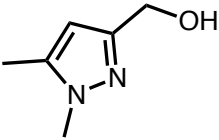
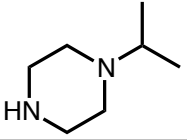
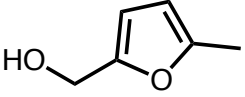
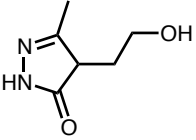
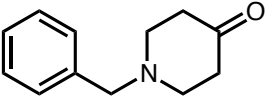
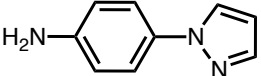
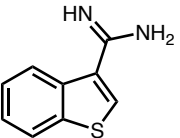
## Cocktail C28

ID	Name	CAS	[Stock]	Structure
28-1	4-FLUOROPHENOL	371-41-5	0.1	
28-2	2-MERCAPTOPURINE	28128-19-0	0.1	
28-3	4-(AMINOMETHYL)PIPERIDINE	7144-05-0	0.1	
28-4	4-BROMO-3-METHYLPYRAZOLE	13808-64-5	0.1	
28-5	2-METHYL-3-PHENYL-2-PROPEN-1-OL	1504-55-8	0.1	
28-6	(S)-(+)-5-(HYDROXYMETHYL)-2-PYRROLIDINONE	17342-08-4	0.1	
28-7	4,5,6,7-TETRAHYDROINDAZOLE	2305-79-5	0.1	

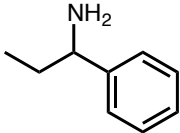
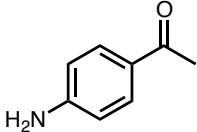
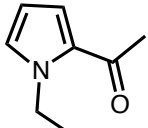
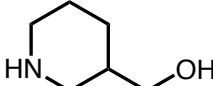
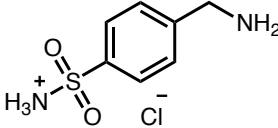
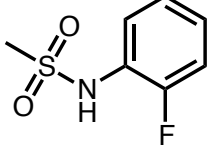
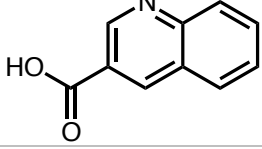
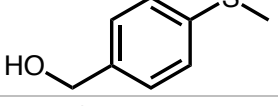
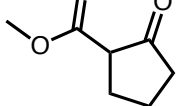
Cocktail C29

ID	Name	CAS	[Stock]	Structure
29-1	3-CHLORO-2,5-DIMETHYLPYRAZINE	95-89-6	0.1	
29-2	2-(METHYLAMINO)BENZAMIDE	7505-81-9	0.1	
29-3	2-DIMETHYLAMINOPYRIDINE	5683-33-0	0.1	
29-4	4-CHLOROBENZENE-1-CARBOXIMIDAMIDE HYDROCHLORIDE	115297-57-9	0.1	
29-5	5-METHOXYRESORCINOL	2174-64-3	0.1	
29-6	2-BROMOPYRIMIDINE	4595-60-2	0.1	
29-7	D-CYCLOSERINE	68-41-7	0.1	
29-8	4-BROMOPYRAZOLE	2075-45-8	0.1	

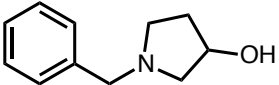
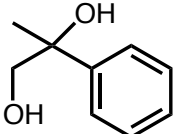
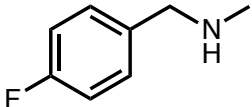
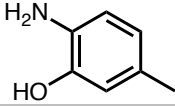
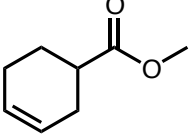
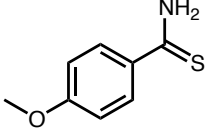
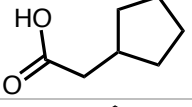
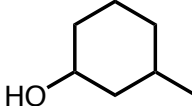
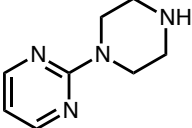
### Cocktail C30

ID	Name	CAS	[Stock]	Structure
30-1	BENZOFURAZAN-5-CARBOXYLIC ACID	19155-88-5	0.1	
30-2	N-(3-PYRROLIDINYL)ACETAMIDE	79286-74-1	0.1	
30-3	(1,5-DIMETHYL-1H-PYRAZOL-3-YL)METHANOL	153912-60-8	0.1	
30-4	1-ISOPROPYL-PIPERAZINE	4318-42-7	0.1	
30-5	(5-METHYL-2-FURYL)METHANOL	3857-25-8	0.1	
30-6	4-(2-HYDROXYETHYL)-3-METHYL-2-PYRAZOLIN-5-ONE	7721-54-2	0.1	
30-7	1-BENZYL-4-PIPERIDONE	3612-20-2	0.1	
30-8	4-(1H-PYRAZOL-1-YL)ANILINE	17635-45-9	0.1	
30-9	1-BENZOTHIOPHENE-3-CARBOXIMIDAMIDINE HYDROCHLORIDE HYDRATE	465515-36-0	0.1	

### Cocktail C31

ID	Name	CAS	[Stock]	Structure
31-1	(S)-(-)-1-PHENYLPROPYLAMINE	2941-20-0	0.1	
31-2	4'-AMINOACETOPHENONE	99-92-3	0.1	
31-3	2-ACETYL-1-ETHYLPYRROLE	39741-41-8	0.1	
31-4	3-PIPERIDINEMETHANOL	4606-65-9	0.1	
31-5	HOMOSULFAMINE HYDROCHLORIDE	138-37-4	0.1	
31-6	N-(2-FLUOROPHENYL) METHANESULFONAMIDE	98611-90-6	0.1	
31-7	QUINOLINE-3-CARBOXYLIC ACID	6480-68-8	0.1	
31-8	4-(METHYLTHIO) BENZYL ALCOHOL	3446-90-0	0.1	
31-9	METHYL 2-CYCLOPENTANONE CARBOXYLATE	10472-24-9	0.1	

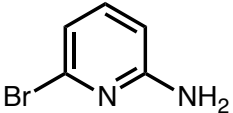
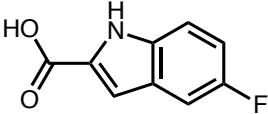
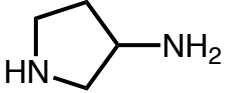
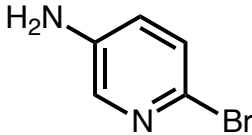
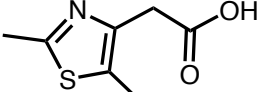
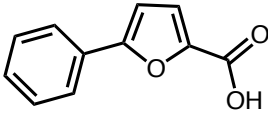
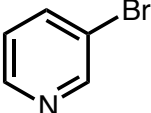
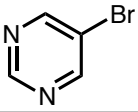
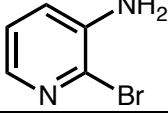
### Cocktail C32

ID	Name	CAS	[Stock]	Structure
32-1	1-BENZYL-3-PYRROLIDINOL	775-15-5, 10472-24-9	0.1	
32-2	2-PHENYL-1,2-PROPANEDIOL	4217-66-7	0.1	
32-3	(4-FLUORO-BENZYL)-METHYL-AMINE	405-66-3	0.1	
32-4	6-AMINO-M-CRESOL	2835-98-5	0.1	
32-5	3-CYCLOHEXENE-1-CARBOXYLIC ACID METHYL ESTER	6493-77-2	0.1	
32-6	4-METHOXYTHIOBENZAMIDE	2362-64-3	0.1	
32-7	CYCLOPENTYLACETIC ACID	1123-00-8	0.1	
32-8	3-METHYLCYCLOHEXANOL	591-23-1	0.1	
32-9	2-(1-PIPERAZINYL)PYRIMIDINE	20980-22-7	0.1	

### Cocktail C33

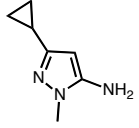
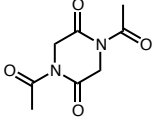
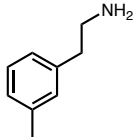
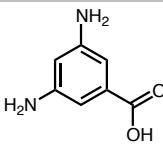
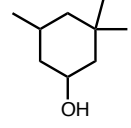
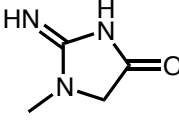
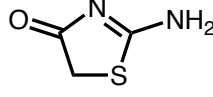
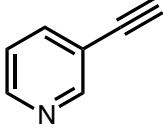
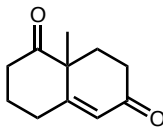
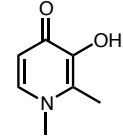
ID	Name	CAS	[Stock]	Structure
33-1	2-(4-CHLOROPHENYL) ETHANETHIOAMIDE	17518-48-8	0.1	
33-2	1,3-DIMETHYL-3,4,5,6- TETRAHYDRO-2(1H)- PYRIMIDINONE	7226-23-5	0.1	
33-3	3-HYDROXYPHENETHYL ALCOHOL	13398-94-2	0.1	
33-4	1,1-DIMETHYL-4- PHENYLPYPERAZINIUM IODIDE	54-77-3	0.1	
33-5	(4-CHLOROPHENYL) METHANOL	873-76-7	0.1	
33-6	2-CYCLOHEXYLETHANOL	4442-79-9	0.1	
33-7	3-BROMO-N- METHYLANILINE	66584-32-5	0.1	
33-8	N-METHYL-N- PHENYLTHIOUREA	4104-75-0	0.1	
33-9	(1S,2S)-2- METHOXYCYCLOHEXANOL	2979-24-0, 134108-92-2	0.1	
33-10	METHYL 3- AMINOTHIOPHENE-4- CARBOXYLATE HYDROCHLORIDE	39978-14-8	0.1	

### Cocktail C34

ID	Name	CAS	[Stock]	Structure
34-1	2-AMINO-6-BROMOPYRIDINE	19798-81-3	0.1	
34-2	5-FLUOROINDOLE-2-CARBOXYLIC ACID	399-76-8	0.1	
34-3	3-AMINOPYRROLIDINE	116183-82-5	0.1	
34-4	5-AMINO-2-BROMOPYRIDINE	13534-97-9	0.1	
34-5	2-(2,5-DIMETHYL-1,3-THIAZOL-4-YL)ACETIC ACID	306937-38-2	0.1	
34-6	5-PHENYL-2-FUROIC ACID	52938-97-3	0.1	
34-7	3-BROMOPYRIDINE	626-55-1	0.1	
34-8	5-BROMOPYRIMIDINE	4595-59-9	0.1	
34-9	3-AMINO-2-BROMOPYRIDINE	39856-58-1	0.1	

## Appendix B. Small Molecule Fragment Library in Water

### Cocktail KS1

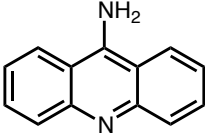
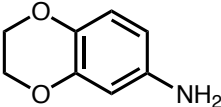
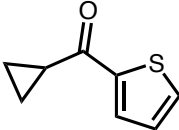
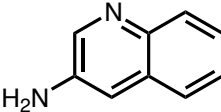
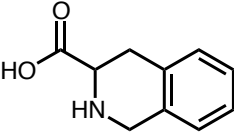
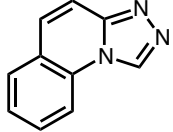
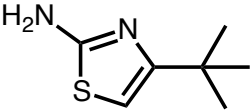
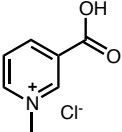
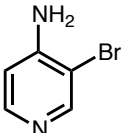
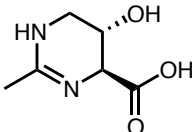
New ID	Old ID	Compound	CAS	[Stock]	Structure
KS1-1	1-4	3-Cyclopropyl-1-methyl-1H-pyrazol-5-amine	118430-74-3	100 mM	
KS1-2	7-2	N,N'-diacetylglycine anhydride	21827-92-9, 3027-05-2	20 mM	
KS1-3	7-3	3-Methylphenethylamine	5470-40-6	20 mM	
KS1-4	7-4	3,5-Diaminobenzoic acid	535-87-5	5 mM	
KS1-5	7-5	3,3,5-Trimethylcyclohexanol	116-02-9	20 mM	
KS1-6	7-6	2-Amino-1-methyl-2-imidazolin-4-one hemisulfate salt	31377-28-3, 60-27-5	100 mM	
KS1-7	7-7	Pseudothiohydantoin	556-90-1	10 mM	
KS1-8	7-9	3-Ethynylpyridine	2510-23-8	10 mM	
KS1-9	12-2	(+/-)-3,4,8,8A-Tetrahydro-8A-methyl-1,6(2H,7H)-naphthalenedione	20007-72-1	20 mM	
KS1-10	12-3	3-Hydroxy-1,2-dimethyl-4(1H)-pyridone	39652-11-0	50 mM	



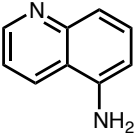
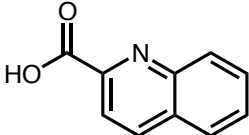
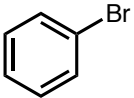
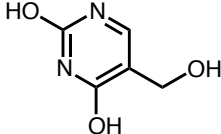
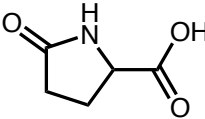
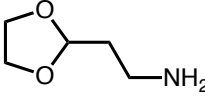
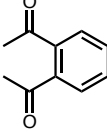
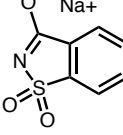
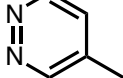
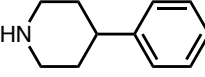
## Cocktail KS2

New ID	Old ID	Compound	CAS	[Stock]	Structure
KS2-1	2-10	Decahydro-2-naphthol	825-51-4	100 mM	
KS2-2	14-3	9-Methyl-3,4-dihydro-2H-pyrido[1,2-A]-pyrimidin-2-one	61751-44-8	20 mM	
KS2-3	14-5	2,3-Dimethylcyclohexanamine	42195-92-6	20 mM	
KS2-4	14-7	2-(Methylthio)cyclohexanone	52190-35-9	5 mM	
KS2-5	14-9	2-Methylphenylacetone	51052-00-7	20 mM	
KS2-6	16-1	(Phenylsulphonyl)Acetamide	35008-50-5	100 mM	
KS2-7	16-2	N,N-Diethylnicotinamide	59-26-7	10 mM	
KS2-8	16-4	DL-Pantolactone	79-50-5	10 mM	
KS2-9	16-5	2,4-Thiazolidinedione	2295-31-0	20 mM	
KS2-10	16-9	1-Tetrahydrofurfuryl-piperazine	82500-35-4	50 mM	

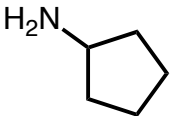
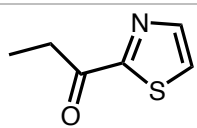
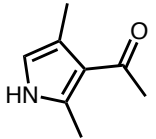
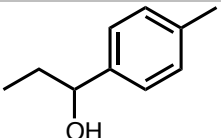
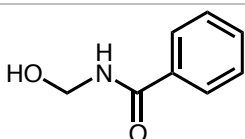
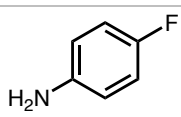
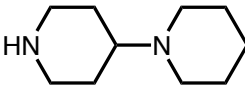
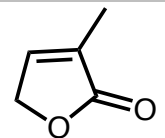
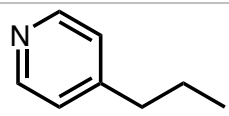
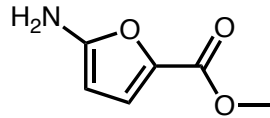
## Cocktail KS3

New ID	Old ID	Compound	CAS	[Stock]	Structure
KS3-1	3-1	9-Aminoacridine hydrochloride	90-45-9	25 mM	
KS3-2	3-2	1,4-Benzodioxan-6-amine	22013-33-8	25 mM	
KS3-3	3-4	Cyclopropyl-2-thienyl ketone	6193-47-1	20 mM	
KS3-4	4-1	3-Aminoquinoline	580-17-6	20 mM	
KS3-5	4-2	1,2,3,4-Tetrahydro-3-isoquinolinecarboxylic acid hydrochloride	74163-81-8	5 mM	
KS3-6	4-5	S-Triazolo(4,3-A)-quinoline	235-06-3	5 mM	
KS3-7	18-4	1-Methylimidazole-2-carboxylic acid, lithium salt	20485-43-2	100 mM	
KS3-8	18-7	Trigonelline hydrochloride	6138-41-6	100 mM	
KS3-9	18-8	4-Amino-3-bromopyridine	13534-98-0	10 mM	
KS3-10	18-9	Hydroxyectoine	165542-15-4	100 mM	

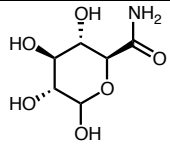
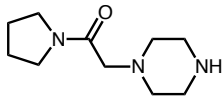
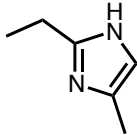
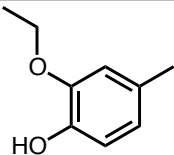
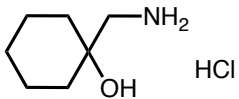
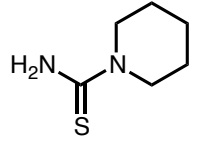
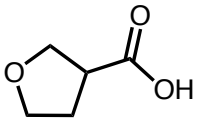
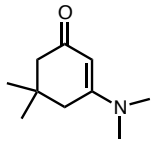
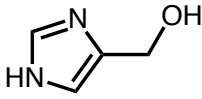
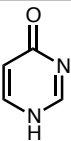
## Cocktail KS4

New ID	Old ID	Compound	CAS	[Stock]	Structure
KS4-1	5-3	5-Aminoquinoline	611-34-7	20 mM	
KS4-2	5-8	Quinaldic Acid	93-10-7	20 mM	
KS4-3	9-1	Bromobenzene	108-86-1	20 mM	
KS4-4	9-2	5-(Hydroxymethyl)-uracil	4433-40-3	10 mM	
KS4-5	9-3	2-Pyrrolidone-5-carboxylic acid	149-87-1	10 mM	
KS4-6	9-5	2-(1,3-Dioxolan-2-yl)-ethanamine	5754-35-8	100 mM	
KS4-7	9-6	1,2-Diacetylbenzene	704-00-7	10 mM	
KS4-8	9-7	Sodium saccharin	128-44-9	20 mM	
KS4-9	9-9	4-Methylpyridazine	1120-88-3	100 mM	
KS4-10	23-6	4-Phenylpiperidine	771-99-3	5 mM	

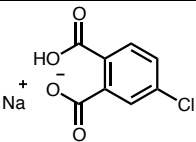
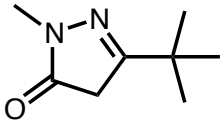
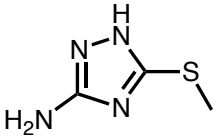
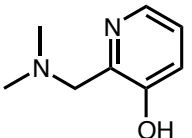
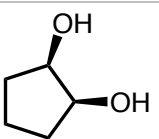
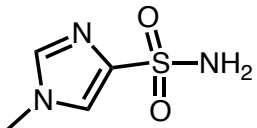
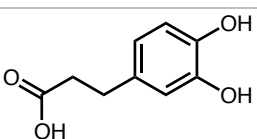
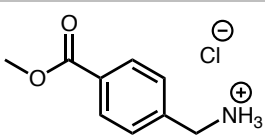
## Cocktail KS5

New ID	Old ID	Compound	CAS	[Stock]	Structure
KS5-1	6-1	Cyclopentylamine	1003-03-8	100 mM	
KS5-2	6-6	2-Propionylthiazole	43039-98-1	100 mM	
KS5-3	6-8	3-Acetyl-2,4-dimethylpyrrole	2386-25-6	5 mM	
KS5-4	20-1	1-(4-Methylphenyl)-1-propanol	25574-04-3	20 mM	
KS5-5	20-7	N-(Hydroxymethyl)benzamide	6282-02-6	5 mM	
KS5-6	21-1	4-Fluoroaniline	371-40-4	100 mM	
KS5-7	21-2	4-Piperidinopiperidine	4897-50-1	20 mM	
KS5-8	21-3	3-Methyl-2(5H)-furanone	22122-36-7	100 mM	
KS5-9	21-5	4-Propylpyridine	1122-81-2	20 mM	
KS5-10	21-9	Methyl-5-amino-2-furoate	22600-30-2	10 mM	

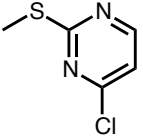
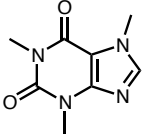
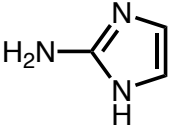
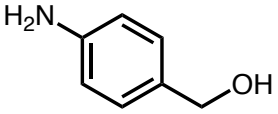
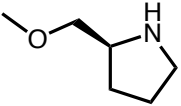
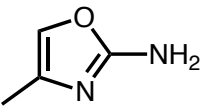
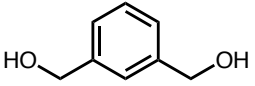
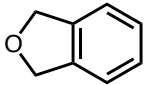
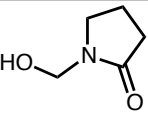
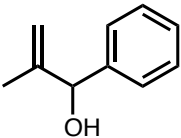
## Cocktail KS6

New ID	Old ID	Compound	CAS	[Stock]	Structure
KS6-1	8-1	D-Glucuronamide	3789-97-7	10 mM	
KS6-2	8-3	1-((Pyrrolidine-1-carbonyl)methyl)-piperazine	39890-45-4	10 mM	
KS6-3	8-4	2-Ethyl-4-methylimidazole	931-36-2	50 mM	
KS6-4	8-5	2-Ethoxy-4-methylphenol	2563-07-7	10 mM	
KS6-5	8-6	1-Aminomethyl-1-cyclohexanol hydrochloride	19968-85-5	50 mM	
KS6-6	17-2	1-Piperidinecarbothioamide	14294-09-8	5 mM	
KS6-7	17-3	Tetrahydro-3-furoic acid	89364-31-8	50 mM	
KS6-8	17-4	3-(Dimethylamino)-5,5-dimethyl-2-cyclohexen-1-one	31039-88-0	20 mM	
KS6-9	17-6	4-(Hydroxymethyl)imidazole hydrochloride	32673-41-9, 822-55-9	50 mM	
KS6-10	17-9	4(3H)-Pyrimidinone	4562-27-0	50 mM	

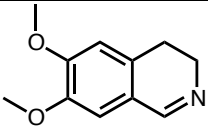
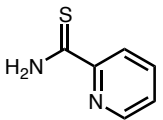
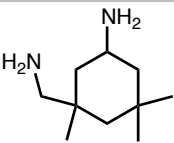
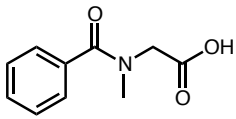
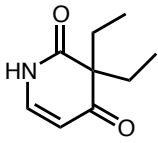
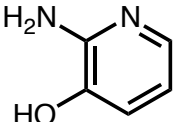
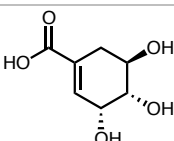
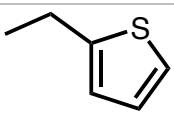
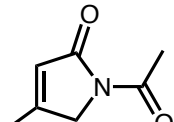
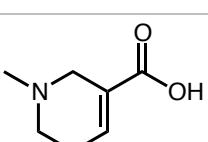
## Cocktail KS7

New ID	Old ID	Compound	CAS	[Stock]	Structure
KS7-1	10-1	4-Chlorophthalic acid monosodium salt	56047-23-5	20 mM	
KS7-2	10-4	3-Tert-butyl-1-methyl-2-pyrazolin-5-one	87031-30-9	20 mM	
KS7-3	10-6	3-Amino-5-methylthio-1H-1,2,4-triazole	45534-08-5	10 mM	
KS7-4	23-2	2-(Dimethylamino-methyl)-3-hydroxy-pyridine	2168-13-0	10 mM	
KS7-5	23-4	Cis-1,2-cyclopentane-diol	5057-98-7	100 mM	
KS7-6	23-5	1-Methyl-1H-imidazole-4-sulfonamide	111124-90-4	5 mM	
KS7-7	23-7	3-(3,4-Dihydroxyphenyl) propionic acid	1078-61-1	10 mM	
KS7-8	23-9	Methyl-4(aminomethyl)-benzoate hydrochloride	6232-11-7	20 mM	

## Cocktail KS8

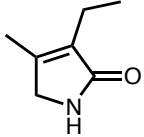
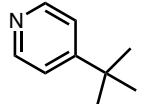
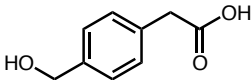
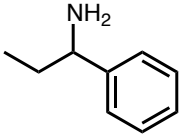
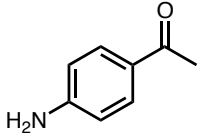
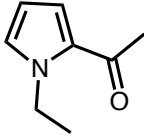
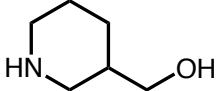
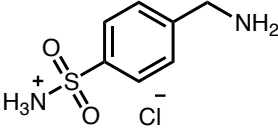
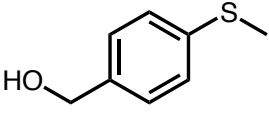
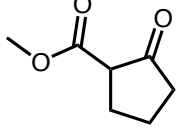
New ID	Old ID	Compound	CAS	[Stock]	Structure
KS8-1	11-5	4-Chloro-2-(methylthio)pyrimidine	49844-90-8	20 mM	
KS8-2	11-6	Caffeine	58-08-2	50 mM	
KS8-3	11-8	2-Aminoimidazole sulfate	1450-93-7	50 mM	
KS8-4	19-5	4-Aminobenzyl alcohol	623-04-1	50 mM	
KS8-5	19-9	(S)-(+)-2-(Methoxymethyl)pyrrolidine	63126-47-6	50 mM	
KS8-6	24-2	4-Methyl-1,3-oxazol-2-amine	35629-70-0	50 mM	
KS8-7	24-3	1,3-Benzenedimethanol	626-18-6	10 mM	
KS8-8	24-7	Phthalan	496-14-0	20 mM	
KS8-9	24-8	1-(Hydroxymethyl)-2-pyrrolidinone	15438-71-8	10 mM	
KS8-10	24-9	2-Methyl-1-phenyl-2-propen-1-ol	4383-08-8	20 mM	

## Cocktail KS9

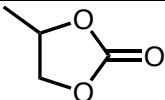
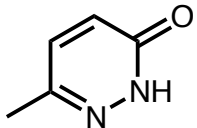
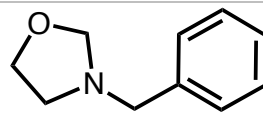
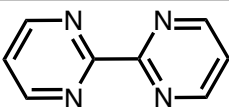
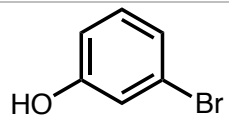
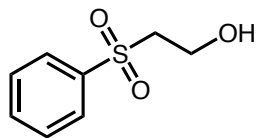
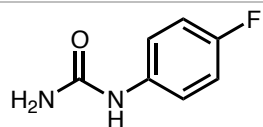
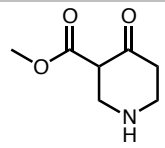
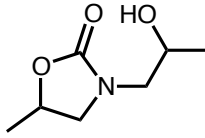
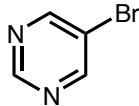
New ID	Old ID	Compound	CAS	[Stock]	Structure
KS9-1	13-1	6,7-Dimethoxy-3,4-dihydroisoquinoline hydrochloride	20232-39-7	20 mM	
KS9-2	13-3	Pyridine-2-thioamide	5346-38-3	5 mM	
KS9-3	13-6	Isophoronediamine	2855-13-2	20 mM	
KS9-4	13-7	(Benzoyl-methyl-amino)-acetic acid	2568-34-5	20 mM	
KS9-5	13-9	Pyrithyldione	77-04-3	10 mM	
KS9-6	13-10	2-Amino-3-hydroxypyridine	16867-03-1	50 mM	
KS9-7	15-5	Shikimic acid	138-59-0	20 mM	
KS9-8	15-6	2-Ethylthiophene	872-55-9	50 mM	
KS9-9	15-7	1-Acetyl-4-methyl-2,5-dihydro-1H-pyrrol-2-one	34581-95-2	5 mM	
KS9-10	15-9	Arecaidine hydrochloride	6018-28-6	50 mM	



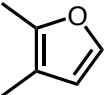
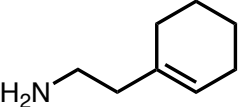
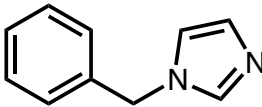
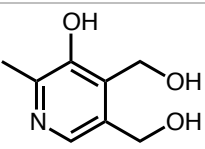
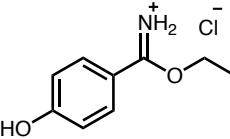
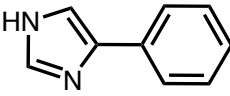
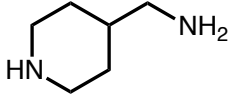
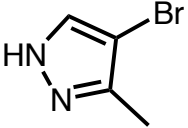
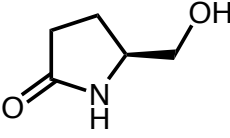
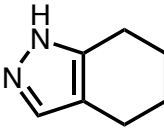
## Cocktail KS10

New ID	Old ID	Compound	CAS	[Stock]	Structure
KS10-1	22-1	3-Ethyl-4-methyl-3-pyrrolin-2-one	766-36-9	10 mM	
KS10-2	22-2	4-Tert-butylpyridine	3978-81-2	20 mM	
KS10-3	22-5	4-(Hydroxymethyl)phenylacetic acid	73401-74-8	5 mM	
KS10-4	31-1	(S)-(-)-1-Phenylpropylamine	2941-20-0	20 mM	
KS10-5	31-2	4-Aminoacetophenone	99-92-3	10 mM	
KS10-6	31-3	2-Acetyl-1-ethylpyrrole	39741-41-8	20 mM	
KS10-7	31-4	3-Piperidinemethanol	4606-65-9	100 mM	
KS10-8	31-5	Homosulfamine hydrochloride	138-37-4	100 mM	
KS10-9	31-8	4-(Methylthio)-benzylalcohol	3446-90-0	20 mM	
KS10-10	31-9	Methyl-2-cyclopentanone carboxylate	10472-24-9	100 mM	

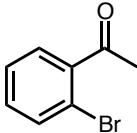
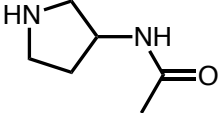
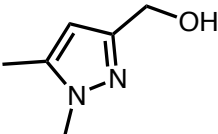
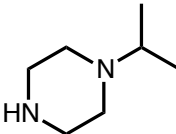
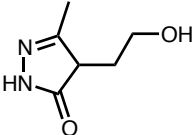
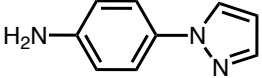
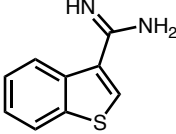
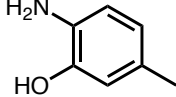
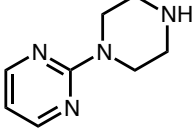
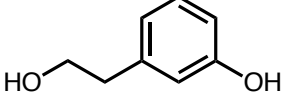
## Cocktail KS11

New ID	Old ID	Compound	CAS	[Stock]	Structure
KS11-1	25-1	Propylene carbonate	108-32-7	100 mM	
KS11-2	27-1	6-Methyl-3(2H)-pyridazinone	13327-27-0	20 mM	
KS11-3	27-3	3-Benzyl-1,3-oxazolidine	13657-16-4	20 mM	
KS11-4	27-4	2,2'-Bipyrimidine	34671-83-5	20 mM	
KS11-5	27-5	3-Bromophenol	591-20-8	50 mM	
KS11-6	27-6	2-(Phenylsulfonyl)-ethanol	20611-21-6	100 mM	
KS11-7	27-7	4-Fluorophenylurea	659-30-3	5 mM	
KS11-8	27-8	Methyl-4-oxo-3-piperidinecarboxylate hydrochloride	71486-53-8	50 mM	
KS11-9	27-9	3-(2-Hydroxypropyl)-5-methyl-2-oxazolidinone	3375-84-6	100 mM	
KS11-10	34-9	5-Bromopyrimidine	4595-59-9	20 mM	

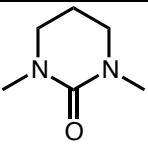
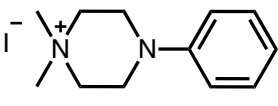
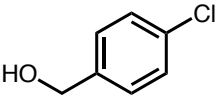
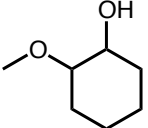
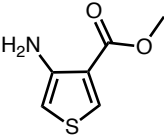
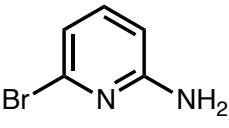
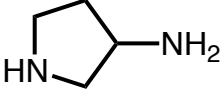
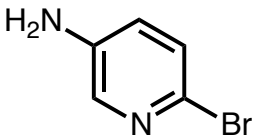
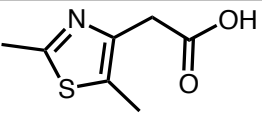
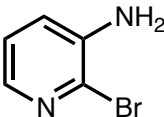
## Cocktail KS12

New ID	Old ID	Compound	CAS	[Stock]	Structure
KS12-1	26-1	2,3-Dimethylfuran	14920-89-9	20 mM	
KS12-2	26-2	2-(1-Cyclohexenyl)-ethylamine	3399-73-3	50 mM	
KS12-3	26-3	1-Benzylimidazole	4238-71-5	25 mM	
KS12-4	26-5	Pyridoxine	65-23-6	50 mM	
KS12-5	26-6	Ethyl-4-hydroxybenzimidate hydrochloride	54998-28-6	50 mM	
KS12-6	9-4	4-Phenylimidazole	670-95-1	3 mM	
KS12-7	28-3	4-(Aminomethyl)-piperidine	7144-05-0	50 mM	
KS12-8	28-4	4-Bromo-3-methylpyrazole	13808-64-5	5 mM	
KS12-9	28-8	(S)-(+)-5-(Hydroxymethyl)-2-pyrrolidinone	17342-08-4	100 mM	
KS12-10	28-9	4,5,6,7-Tetrahydroindazole	2305-79-5	20 mM	

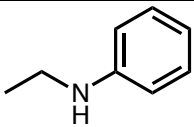
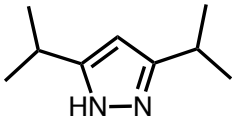
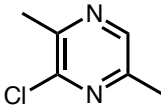
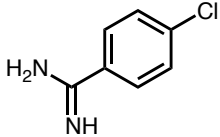
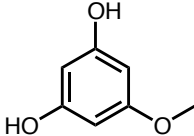
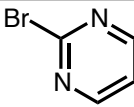
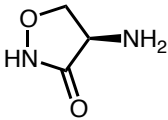
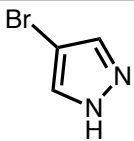
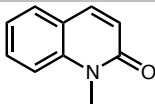
## Cocktail KS13

New ID	Old ID	Compound	CAS	[Stock]	Structure
KS13-1	26-10	2'-Bromoacetophenone	2142-69-0	20 mM	
KS13-2	30-2	N-(3-Pyrrolidiny)-acetamide	79286-74-1	100 mM	
KS13-3	30-3	(1,5-Dimethyl-1H-pyrazol-3-yl)-methanol	153912-60-8	20 mM	
KS13-4	30-4	1-Isopropyl-piperazine	4318-42-7	100 mM	
KS13-5	30-7	4-(2-Hydroxyethyl)-3-methyl-2-pyrazolin-5-one	7721-54-2	50 mM	
KS13-6	30-9	4-(1H-Pyrazol-1-yl)-aniline	17635-45-9	20 mM	
KS13-7	30-10	1-Benzothiophene-3-carboximidamide hydrochloride hydrate	465515-36-0	20 mM	
KS13-8	32-4	6-Amino-M-cresol	2835-98-5	5 mM	
KS13-9	32-10	2-(1-Piperazinyl)-pyrimidine	20980-22-7	50 mM	
KS13-10	33-3	3-Hydroxyphenethyl alcohol	13398-94-2	20 mM	

## Cocktail KS14

New ID	Old ID	Compound	CAS	[Stock]	Structure
KS14-1	33-2	1,3-Dimethyl-3,4,5,6-tetrahydro-2(1H)-pyrimidinone	7226-23-5	100 mM	
KS14-2	33-4	1,1-Dimethyl-4-phenylpiperazinium iodide	54-77-3	50 mM	
KS14-3	33-5	(4-chlorophenyl)-methanol	873-76-7	10 mM	
KS14-4	33-9	(1S,2S)-2-Methoxycyclohexanol	2979-24-0, 134108-92-2	100 mM	
KS14-5	33-10	Methyl-3-aminothiophene-4-carboxylate hydrochloride	39978-14-8	10 mM	
KS14-6	34-1	2-Amino-6-bromopyridine	19798-81-3	10 mM	
KS14-7	34-3	3-Aminopyrrolidine	116183-82-5	100 mM	
KS14-8	34-5	5-Amino-2-bromopyridine	13534-97-9	10 mM	
KS14-9	34-6	2-(2,5-Dimethyl-1,3-thiazol-4-yl)-acetic acid	306937-38-2	50 mM	
KS14-10	34-10	3-Amino-2-bromopyridine	39856-58-1	20 mM	

## Cocktail KS15

New ID	Old ID	Compound	CAS	[Stock]	Structure
KS15-1	25-5	N-Ethylaniline	103-69-5	20 mM	
KS15-2	25-7	3,5-Diisopropylpyrazole	17536-00-4	5 mM	
KS15-3	29-1	3-Chloro-2,5-dimethylpyrazine	95-89-6	50 mM	
KS15-4	29-4	4-Chlorobenzene-1-carboximidamide hydrochloride	115297-57-9	50 mM	
KS15-5	29-5	5-Methoxyresorcinol	2174-64-3	100 mM	
KS15-6	29-6	2-Bromopyrimidine	4595-60-2	10 mM	
KS15-7	29-7	D-Cycloserine	68-41-7	5 mM	
KS15-8	29-8	4-Bromopyrazole	2075-45-8	50 mM	
KS15-9	10-8	1-Methyl-2(1H)-quinolinone	606-43-9	10 mM	
KS15-10	28-1	4-Fluorophenol	371-41-5	50 mM	